

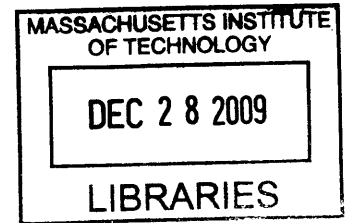
A FULLY IMPLANTABLE INTRACOCHELEAR DRUG DELIVERY DEVICE: DEVELOPMENT AND CHARACTERIZATION

BY

ERIN E. LEARY SWAN

M.S., BIOMEDICAL ENGINEERING
BOSTON UNIVERSITY, 2004

B.S., AEROSPACE ENGINEERING
THE PENNSYLVANIA STATE UNIVERSITY, 1998



SUBMITTED TO THE DEPARTMENT OF MECHANICAL ENGINEERING IN PARTIAL FULFILLMENT OF THE REQUIREMENTS FOR THE DEGREE OF

DOCTOR OF SCIENCE IN MECHANICAL ENGINEERING
AT THE
MASSACHUSETTS INSTITUTE OF TECHNOLOGY

ARCHIVES

SEPTEMBER 2009

© 2009 ERIN E. LEARY SWAN. ALL RIGHTS RESERVED.

THE AUTHOR HEREBY GRANTS TO MIT PERMISSION TO REPRODUCE AND TO DISTRIBUTE PUBLICALLY PAPER AND ELECTRONIC COPIES OF THIS THESIS DOCUMENT IN WHOLE OR IN PART IN ANY MEDIUM NOW KNOWN OR HEREAFTER CREATED.

SIGNATURE OF AUTHOR: _____
DEPARTMENT OF MECHANICAL ENGINEERING
SEPTEMBER 1, 2009

CERTIFIED BY: _____
ROGER D. KAMM
GERMESHUSEN PROFESSOR OF MECHANICAL AND BIOLOGICAL ENGINEERING
THESIS SUPERVISOR

CERTIFIED BY: _____
MARK J. MESCHER
PRINCIPAL MEMBER OF THE TECHNICAL STAFF, CHARLES STARK DRAPER LABORATORY
RESEARCH SUPERVISOR

ACCEPTED BY: _____
DAVID E. HARDT
RALPH E. AND ELOISE F. CROSS PROFESSOR OF MECHANICAL ENGINEERING
CHAIRMAN, COMMITTEE ON GRADUATE STUDENTS

A FULLY IMPLANTABLE INTRACOCHLEAR DRUG DELIVERY DEVICE: DEVELOPMENT AND CHARACTERIZATION

BY

ERIN E. LEARY SWAN

SUBMITTED TO THE DEPARTMENT OF MECHANICAL ENGINEERING ON SEPTEMBER 1, 2009
IN PARTIAL FULFILLMENT OF THE REQUIREMENTS FOR THE DEGREE OF

DOCTOR OF SCIENCE IN MECHANICAL ENGINEERING

ABSTRACT

In a collaborative effort with the Massachusetts Eye and Ear Infirmary, Draper Laboratory is developing an implantable microfluidic drug delivery system for long-term treatment of inner ear disorders and prevention of sensorineural hearing loss. This versatile device is envisioned to deliver multiple therapies and control the sequence and rate of drug dosing. Such a system could have an immediate application in the treatment of ototoxic and inflammatory conditions affecting the inner ear, including autoimmune inner ear disease and cisplatin-induced ototoxicity. Current efforts include ongoing refinement of the design, miniaturization of components, and testing in an in vivo guinea pig model.

This thesis focuses on the interactions between the device and inner ear, including the investigation of drug transport due to convective diffusion in the cochlea during drug delivery. A lumped-parameter model was implemented in an electrical circuit simulator after converting mechanical variables to their electrical analogues. A flow module described the output of the microfluidic system and used storage and loss elements to represent cochlear anatomy contributing to the flow profile. In the other portion of the model, a transport module solved for the drug concentration profile within the cochlea resulting from diffusion and convection. The model was validated using a bench-top fluorescent flow study and was compared to in vivo animal drug delivery studies.

Additionally, mechanical and biological interactions related to protein and tissue biofouling were investigated. The protein composition of the endogenous fluid of the inner ear was analyzed using a mass-spectrometry approach, and in vitro flow experiments were implemented to quantify biofouling in the device due to protein build-up and determine the impact of biofouling on microfluidic device performance. The effects of tissue build-up on the implanted system were studied through the use of histology preparation of the cochlea after long-term implantation. Further work included the fabrication and testing of microfluidic components, diaphragm-based capacitive elements and manual valves, for integration into the device. Through this research, both the impact of this device on the animal and the result of implantation on the device were more fully characterized.

THESIS SUPERVISOR: ROGER D. KAMM

TITLE: GERMESHAUSEN PROFESSOR OF MECHANICAL AND BIOLOGICAL ENGINEERING

RESEARCH SUPERVISOR: MARK J. MESCHER

TITLE: PRINCIPAL MEMBER OF THE TECHNICAL STAFF, CHARLES STARK DRAPER LABORATORY

ACKNOWLEDGMENT

September 1, 2009

This thesis was prepared at The Charles Stark Draper Laboratory, Inc., under the National Institutes of Health grant 5 R01 DC 006848-02 and internally sponsored research funding.

Publication of this thesis does not constitute approval by Draper or the sponsoring agency of the findings or conclusions contained herein. It is published for the exchange and stimulation of ideas.

Erin E. Leary Swan

ASSIGNMENT

Draper Laboratory Report Number T-1646

In consideration for the research opportunity and permission to prepare my thesis by and at The Charles Stark Draper Laboratory, Inc., I hereby assign my copyright of the thesis to The Charles Stark Draper Laboratory, Inc., in Cambridge, Massachusetts.

Erin E. Leary Swan

8/1/09

Date

PERSONAL ACKNOWLEDGMENT

This thesis would not have been possible without generous support of C.S. Draper Laboratory through the Draper Fellow program. I am sincerely grateful to my thesis advisor, Mark Mescher, whose guidance, expertise, and support enabled me to complete the research contained in this thesis.

I appreciate the efforts of my thesis supervisor, Roger Kamm, and thesis committee members, William Sewell, Anette Hosoi, and Ioannis Yannas. Their input and experience were valuable in the shaping and execution of this project.

I would like to acknowledge several people who are deeply involved in the inner ear delivery project and who all freely offered their knowledge and assistance throughout the course of my work. Members of the group include Jeffrey Borenstein, Mark Mescher, Jason Fiering, Sarah Tao, and Maria Holmboe at Draper and Sharon Kujawa, William Sewell, Michael McKenna, Zhiqiang Chen, Brian Murphy, and Marcello Peppi at the Massachusetts Eye and Ear Infirmary.

Josh Alper and Jeff Palmer deserve my thanks for their assistance as study partners in preparation for qualifying exams. I would not have passed without them.

My parents, David and Judy Leary, have unflinching offered their love and encouragement in all my endeavors. For that, I am eternally grateful.

My fiancé, George Pararas-Carayannis, has provided the foundation of support and understanding I have relied upon to complete this thesis. His kindness, patience, and love have not wavered. I owe him my deepest gratitude. Σ' αγαπώ Γεωργίος.

TABLE OF CONTENTS

1.0 INTRODUCTION	13
1.1 SPECIFIC AIMS	14
1.2 REFERENCES	16
2.0 BACKGROUND	17
2.1 INTRODUCTION	17
2.2 ANATOMY AND PHYSIOLOGY	18
2.3 PHARMACOKINETICS	22
2.4 INNER EAR DRUG DELIVERY APPLICATIONS	26
2.5 INNER EAR DRUG DELIVERY METHODS	38
2.6 CONCLUDING REMARKS	51
2.7 REFERENCES	51
3.0 DRUG DELIVERY MODELING AND EXPERIMENTATION	67
3.1 DESCRIPTION OF THE DEVICE	67
3.2 DESCRIPTION OF A PREVIOUS COCHLEAR DELIVERY SIMULATOR	71
3.3 GOVERNING EQUATIONS	72
3.4 LUMPED PARAMETER MODELING	75
3.5 COMPARISON OF THE MODEL TO DIFFUSION-ONLY ANALYTIC SOLUTION	88
3.6 DRUG TRANSPORT MODELING IN A GLASS CAPILLARY TUBE	89
3.7 MODELING OF DRUG DELIVERY IN THE GUINEA PIG COCHLEA	100
3.8 COMPARISON OF THE MODEL TO EXPERIMENTAL DATA	113
3.9 LIMITATIONS OF THE MODEL	115
3.10 ADAPTATION OF THE MODEL FOR HUMANS	116
3.11 CONCLUSION	116

3.12 REFERENCES	116
4.0 PROTEIN COMPOSITION AND DEVICE INTERACTION	119
4.1 PROTEIN COMPOSITION ANALYSIS	119
4.2 PROTEIN BIOFOULING	128
4.3 TISSUE BIOFOULING	134
4.4 CONCLUSION	139
4.5 REFERENCES	140
5.0 MICROFLUIDIC COMPONENTS: FABRICATION AND TESTING	147
5.1 INTRODUCTION	147
5.2 FABRICATION METHODS	148
5.3 MEMBRANE CAPACITOR	153
5.4 MANUAL SCREW VALVE	158
5.5 CONCLUSION	162
5.6 REFERENCES	162
6.0 CONCLUSION	165
6.1 CONCLUDING REMARKS	165
6.2 FUTURE DIRECTIONS	165

1.0 INTRODUCTION

In recent years, a great deal of effort has been applied to molecular biology approaches to the prevention and reversal of sensorineural hearing loss. Additionally, researchers are addressing clinical opportunities related to the long-term delivery of compounds to regenerate sensory cells in the inner ear [1]. As these treatments become reality, a barrier exists in supplying the compounds to the necessary sites in the inner ear.

Many inner ear disorders are not adequately treated by current methods. Systemic drug delivery is limited by the existence of a blood-labyrinth barrier, similar to the blood-brain barrier, which serves as an impediment for many charged or large molecules entering the inner ear [2]. Existing techniques for direct delivery of drugs into the inner ear are extremely limited due to challenges specific to the inaccessibility and sensitivity of cochlear structures.

Local delivery methods are constrained in their ability to precisely deliver drugs into the cochlea for extended periods. Delicate inner ear structures are extremely sensitive to changes in pressure or volume associated with bolus or perfusion-type delivery. Distribution of drug to the inner ear via diffusion from the middle ear has been used in a variety of applications such as Menière's disease and sudden sensorineural hearing loss. Variations include placing a drug-filled gel or foam in the middle ear or utilizing wicks extending from the tympanic membrane [3-5]. These passive systems rely on diffusion through the round window for access to the inner ear fluids and are inefficient due to loss of drug through the Eustachian tube and to lack of dosing control [5]. Other groups have used small osmotic drug pumps with catheters entering the middle or inner ear. These micropumps are passive and operate only for short durations [6]. They operate at only a single infusion rate. Finally, research is being conducted to combine drug delivery capabilities with the electrodes used for cochlear implants [7]. These, however, are not being tested in ears with normal hearing. Currently, there are no available devices for extended perfusion of drugs directly into the inner ears of hearing humans.

To address the need for precise, well-controlled drug delivery directly to the inner ear, a collaboration between Draper Laboratory and the Massachusetts Eye and Ear Infirmary (MEEI) is developing a fully implantable long-term microelectromechanical system (MEMS)-based delivery device [8, 9]. This microfluidic system incorporates microfabricated components with electrical controls and appropriate packaging for implantation behind the ear, and it utilizes a novel single-lumen based reciprocating approach with no net volume increase in the cochlea over time.

The critical elements of the device consist of an overall size consistent with surgical placement within a small cavity behind the ear, a pumping element capable of infusing drug into recirculating perilymph, a valve-controlled drug reservoir, and integration with sensors for control of flow rate. Ultimately, an integrated drug delivery device with sensors for flow, concentration and bioactivity would provide customized therapy based on individual responses to treatment. The device would infuse highly-concentrated solution into the cochlea over a few seconds. The same volume of less concentrated fluid would then be withdrawn back into the device over minutes. This process would be repeated at sufficient time intervals, and with delivery occurring through diffusive and convective transport in the inner ear.

Immediate applications of this system in the treatment of otologic disorders include delivery of otoprotective drugs during chemotherapy and radiation and delivery of therapeutics for autoimmune inner ear disease. Future applications based on regenerative approaches will provide powerful clinical tools in the treatment and prevention of hearing loss.

1.1 SPECIFIC AIMS

This thesis focused on investigating various aspects of interactions between the device and the animal. System design must incorporate factors originating from the mechanical-biological interface. The device must adequately deliver drugs to optimal effect and must provide stable performance in the biological environment. Research for this thesis was divided into three specific aims.

Aim 1: Characterize drug transport within the cochlea using computer modeling and in vivo experimental data

A lumped-parameter model was constructed to characterize the diffusive and convective drug transport in the cochlea from the delivery device. Mechanical and biological aspects of the device-cochlea system were converted to electrical analogues. A circuit simulation was implemented and solved using MicroCap software.

The model was validated in a bench-top environment using fluorescence delivery to a glass tube to track transport of the molecules along the tube length. Experimental data was compared to modeled results from the circuit simulator.

In vivo drug delivery experiments utilizing the microfluidic device implanted into guinea pigs were undertaken. Hearing responses were measured to infer the drug delivery profile, and these results and model output were compared.

Minimal changes to the lumped-parameter model would allow for its use in predicting drug delivery in human applications of the device. Because pharmacokinetic studies in the cochlea meet with great difficulty, this model would be useful in the development of the device and of novel drugs for inner ear applications.

Aim 2a: Investigate the impact of protein biofouling on the microfluidic system using bench-top testing

A mass-spectrometry-based proteomics analysis of perilymph, endogenous inner ear fluid, was performed to identify the major proteins. Various proteins impact both the delivery system and the drugs delivered. Some, such as albumin, may adsorb to material surfaces and cause flow restrictions and lead to changes in device flow profiles. Additionally, many proteins may bind to drug molecules or change their composition limiting drug effectiveness and availability.

A bench-top flow study of protein solution was undertaken to compare protein build-up on several device materials. The study was meant to mimic perilymph flow through the channels of the delivery device.

Aim 2b: Examine in vivo cellular and tissue biofouling of system using histology

A guinea pig was implanted with a functioning device for 30 days, and the cochlea, with the embedded cannula, was processed for histological evaluation. After sectioning, the cannula was examined microscopically for evidence of cellular ingrowth or other occlusion. Also, surrounding tissue was examined for evidence of immunological response.

Aim 3: Fabricate and test microfluidic components

In order to miniaturize the delivery system and move to a more fully-integrated platform, device components were fabricated from polymer laminate sheets using a micromachining tool. A diaphragm-based capacitive membrane replaced a long length of compliant tubing used to tune the device delivery profile. A membrane-based manual valve was constructed to enable flow control, and a 5-valve

manifold assembly allowed for filling, purging, and drug loading of the device. These fluidic components were tested for their flow characteristics including compliance and fluidic resistance.

In this thesis, Chapter 2 contains a literature review of the current state of inner ear drug delivery for auditory applications including delivery methods and current and horizon applications. Drug transport modeling and experimentation are covered in Chapter 3. The following chapter describes a protein composition analysis and studies to examine biofouling of the device. Chapter 5 includes information on the fabrication and testing of two microfluidic components, a membrane capacitor and a manual valve, that were developed for integration in the delivery system.

1.2 REFERENCES

1. Holley, M.C., *The auditory system, hearing loss and potential targets for drug development*. Drug Discovery Today, 2005. **10**(19): p. 1269-1282.
2. Inamura, N. and A.N. Salt, *Permeability changes of the blood-labyrinth barrier measured in vivo during experimental treatments*. Hearing Research, 1992. **61**: p. 12-18.
3. Hoffmann, K.K. and H. Silverstein, *Inner ear perfusion: indications and applications*. Curr Opin Otolaryngol Head Neck Surg, 2003. **11**: p. 334-339.
4. Silverstein, H., *Use of a new device, the MicroWick, to deliver medication to the inner ear*. Ear Nose Throat J, 1999. **78**(8): p. 595-600.
5. Jackson, L.E. and H. Silverstein, *Chemical perfusion of the inner ear*. Otolaryngol Clin North Am, 2002. **35**: p. 639-653.
6. Brown, J.N., et al., *Osmotic pump implant for chronic infusion of drugs into the inner ear*. Hear Res, 1993. **70**: p. 167-172.
7. Shepherd, R.K. and J. Xu, *A multichannel scala tympani electrode array incorporating a drug delivery system for chronic intracochlear infusion*. Hear Res, 2002. **172**: p. 92-98.
8. Chen, Z., et al., *Inner Ear drug delivery via a reciprocating perfusion system in the guinea pig*. J Control Release, 2005. **110**: p. 1-19.
9. Fiering, J., et al., *Local drug delivery with a self-contained, programmable, microfluidic system*. Biomedical Microdevices, 2009. **11**(3): p. 571-578.

2.0 BACKGROUND

2.1 INTRODUCTION

The inner ear provides a unique opportunity for local drug delivery. Access to the inner ear is limited by the presence of a blood-cochlear barrier, which is anatomically and functionally similar to the blood-brain barrier [1, 2]. Due to tight junctions between cells, substances in systemic circulation encounter substantial physical barriers to entry, preventing many molecules with potentially therapeutic effect from gaining access to their inner ear targets. Additionally, the cochlea is a closed space, and cochlear function is sensitive to small changes in fluid volume. Therefore, delicate approaches are required to avoid possible damage from the delivery method itself.

Otologic practice requires drug delivery to the inner ear, but current methods of delivery utilize inefficient routes. Drugs are commonly delivered systemically, with the expectation that they will reach their intended inner ear targets in the necessary form and concentration, and without deleterious side effects. Systemic corticosteroids, for example, are used in the otologic management of sudden sensorineural hearing loss (SSNHL) and autoimmune inner ear disease (AIED) [3-5]. Their clinical usefulness, however, is limited by undesirable side effects arising from the high systemic doses required to achieve therapeutic concentration in the cochlea [6].

Additional applications include otoprotection from a variety of sources toxic to the inner ear. An active area of research is focused on preventing hearing loss due to cisplatin chemotherapy, radiation for cancer treatments and aminoglycoside antibiotics. Noise induced hearing loss (NIHL) affects millions of people and represents another target for local therapy.

Recent advances in the pharmacology and molecular biology of hearing have revealed new possibilities for preventing or minimizing hearing loss. Sensorineural hearing loss results from death of the cochlear sensory and neural cells. In humans, these cells do not regenerate, and loss is often followed by secondary degeneration of auditory neurons. Scientists and clinicians are making progress in understanding the molecular mechanisms associated with cochlear and auditory nerve degenerative processes [7] and in finding agents that can minimize degeneration and facilitate repair [8, 9]. These insights offer the potential for development of novel and precise drug treatments. Moreover, the extraordinary progress that has been made in defining genes and protein activities offers hope for gene transfer and cell-based approaches to treat these diseases [10, 11].

For current applications and new therapies based on these discoveries to be clinically relevant, it is necessary to develop safe and reliable mechanisms for the direct delivery of compounds into the inner ear. Methods for local delivery can be categorized as either intratympanic or intracochlear approaches.

Intratympanic delivery can be accomplished via perfusion of the middle ear with the goal of diffusion through the round window membrane (RWM) into the fluid spaces of the inner ear. This method, introduced over 50 years ago [12], remains in common use in the treatment of inner ear diseases. Technological advances beyond the simple middle ear injection method include the use of hydrogels, nanoparticles, and microcatheter systems. These systems aim to maintain therapeutic levels of drug on the round window for extended periods of time.

Direct intracochlear drug delivery involves placement of drugs within cochlear perilymphatic spaces via a cochleostomy in the surrounding bone or RWM [13, 14]. This mode of delivery allows drugs to reach their intended targets more directly than with systemic delivery. Molecules perfused into a perilymph compartment (ideally the scala tympani) have direct access to the cells of the inner ear [15]. Methods of delivery include direct perfusion using micropumps and osmotic pumps. Research is being conducted on modifying the electrodes of cochlear prostheses to integrate drug delivery components, while yet others are developing novel implantable delivery devices [16-19].

In this review, we provide a brief overview of the anatomy and physiology of the inner ear as it relates to local drug delivery. Current and horizon applications for conditions that may be treated via direct inner ear delivery are discussed. Finally, methods to locally deliver drugs to the inner ear for both clinical and research applications are presented. These approaches are categorized by the location of delivery and by the passive versus active mode of distribution.

2.2 ANATOMY AND PHYSIOLOGY

The inner ear, which contains both the organ of hearing, the cochlea, and the organ of balance, the vestibular system, is embedded deep within the skull near the brainstem in the petrous bone, one of the hardest bones in the body. The extreme inaccessibility of the cochlea, coupled with its very small size, creates unique though tractable problems for cochlear drug delivery. The complexity of the cochlear structures and their extreme sensitivity to the changes in fluid volume also must be considered.

The cochlea can be thought of as a long coiled tube, 31-33 mm in human, [20] looking much like the snail shell from which it derives its name. It varies in diameter along its length from apex to base.

Stretched across the middle of the tube is the organ of Corti, which is the highly organized basilar membrane that contains the mechano-sensory cells of the inner ear. The basilar membrane moves in response to sound waves that enter the inner ear. The structure of the organ of Corti is tonotopically organized so that high frequency sounds produce the greatest motion in the base of the tube and low frequency sounds move the organ most at the apex.

The mechano-sensory cells of the ear are called hair cells because early microscopists considered the stereocilia at the apical surfaces to look like tiny hairs. Hair cells are organized into rows that run the length of the coil from its base to its apex and are organized tonotopically in their response to sound. There are two types of hair cells: a single row of inner hair cells responds to sound by releasing a neurotransmitter to excite afferent auditory neurons, and three rows of outer hair cells serve to amplify the sound-evoked motion of the basilar membrane to more effectively deliver frequency-specific stimulation to the inner hair cells.

If one looks at a cross section through the cochlea, as shown in Figure 1, a distinctive feature is the presence of three relatively large fluid-filled compartments. These three compartments coil up the cochlea along with the organ of Corti. The middle compartment is the scala media, which is filled with endolymph (discussed below). The scala media forms a border of the organ of Corti, and the apical surfaces of cells in the organ of Corti, including the hair cells, project into the scala media. The lower and upper fluid compartments respectively are the scala tympani and scala vestibuli, both of which are filled with perilymph. These two compartments communicate with each other at the apex of the cochlea through the helicotrema. There are two orifices in the surface of the cochlear bone, both of which are located at the base of the cochlea. The round window is a membranous opening in the bone within the scala tympani. It sits at the base of the scala tympani and is very compliant, capable of bulging into the middle ear. It separates perilymph from the middle ear space. The oval window, in the scala vestibuli, contains the footplate of the stapes, one of the middle ear bones, that transmits acoustic vibrations from eardrum to the inner ear.

Perilymph is the primary fluid of the cochlea. It bathes most of the cells within the cochlea including the basolateral surfaces of the sensory cells, the neurons, and most of the other specialized structures within the cochlea. Perilymph is similar to cerebrospinal fluid (CSF), with which it is diffusional continuity, though some studies have shown that protein concentration in perilymph is significantly (10 to 20 times) higher than in CSF [21-26]. The volume of perilymph in the human cochlea is about 70 μL , with around 40 μL in the scala tympani [26].

The scala media is filled with endolymph, about 8 μL in human, which has an ionic composition similar to the intracellular environment, high in potassium and low in sodium. The fluid space provides a highly unique environment for the apical surface of the hair cells. The cells that form the borders of the scala media are all connected by tight junctions. The primary function of the scala media is to provide an electrochemical environment that supports the hair cells' ability to transduce mechanical motion into electrical potentials. It contains a relatively large (100 mV) positive electrical potential. This unique electrochemical environment is created by a structure called the stria vascularis, which is, as its name implies, highly vascularized. It runs along the outside of the scala media and extracts energy from the blood that is needed to create the electrochemical battery of the scala media.

The cochlea can be viewed as a set of membranous tubes within a coiled bony tunnel with the organ of Corti, containing the hair cells, stretched across the middle, the scala media providing the electrochemical battery for transduction forming the apical border of the organ of Corti, and tubes containing perilymph and bathing most of the cochlear structures on either side of the organ of Corti and scala media. The stria vascularis runs along the outside of the scala media. Finally, the coil of the cochlea winds around the modiolus, into which are packed the cell bodies of the auditory neurons, appropriately termed the spiral ganglion neurons (SGN). These bipolar neurons send dendrites to the inner hair cells and axons to the brain.

Airborne sound passes through the external auditory canal and moves the tympanic membrane. Motion of the membrane by the sound waves is transmitted through the ossicles (3 tiny bones: the malleus, the incus, and the stapes) to transfer the airborne sound into the movement of the footplate of the stapes, which is inserted in the oval window of the inner ear. The piston-like motion of the stapes transfers a pressure wave to the fluid-filled space of the inner ear behind the oval window. Thus the middle ear functions to match the acoustic impedance of the airborne sound to that of fluid environment of the inner ear.

Motion of the basilar membrane ultimately produces movement of the stereocilia at the apical surfaces of the hair cells. As the stereocilia move, mechanically sensitive ion channels on the stereocilia open and shut in synchrony with the motion. As a result, the hair cells depolarize and repolarize with an electrical waveform that is similar to the mechanical motion. The outer hair cells possess resonance properties that are tonotopically organized to correspond to the maximum sensitivity of the basilar membrane, so that they in essence amplify the motion of the basilar membrane over a narrow range of frequencies, enhancing the frequency discrimination of the system. The inner hair cells respond to the

outer hair cell-enhanced basilar membrane motion by releasing neurotransmitter from the base of the hair cell. This release activates the auditory nerve fibers.

There are a number electrophysiological parameters one can monitor to assess cochlear function, and some of these (distortion product otoacoustic emissions (DPOAEs) and auditory brainstem responses (ABRs)) are often used clinically. Current flowing through the transduction channels in the hair cells will generate a cochlear microphonic (CM) potential that mimics the acoustic waveform. One can record the CM potential to get an indication of hair cell function or to assess the effects of drugs on the hair cells. The CM is dominated by response of the outer hair cells. Another monitor of hair cell function, DPOAEs, takes advantage of the mechanical motion induced in the basilar membrane by the outer hair cell resonance. This mechanical response by the outer hair cell is propagated back out through the middle ear as an acoustic signal that can be measured in the auditory canal. This mechanical response is inherently nonlinear and will generate distortion products that can be detected noninvasively in the ear canal. The distortion product corresponding to a particular frequency is quite robust and is commonly used as a metric of cochlear function, and in particular, outer hair cell function.

Responses of the auditory neurons can be monitored individually with microelectrodes, but it is also feasible to monitor the synchronous activity of groups of nerve fibers. The compound action potential (CAP) is measured with a ball electrode placed near the RWM in response to a click or a tone pip. In this case, a group of fibers discharge synchronously in response to the stimulus, producing a signal large enough to measure even at a distance. Tone pips of varying frequency allow the investigator to assess specific regions along the length of the cochlea, e.g. responses to high frequency tone pips are generated in the basal portion of the organ of Corti. This measure is surgically invasive but useful in animal experiments. Clinically, it is possible to monitor these responses with electrodes placed on the surface of the scalp by averaging responses to a large number of stimuli. These ABRs are clinically useful in providing objective assessment of cochlear function noninvasively.

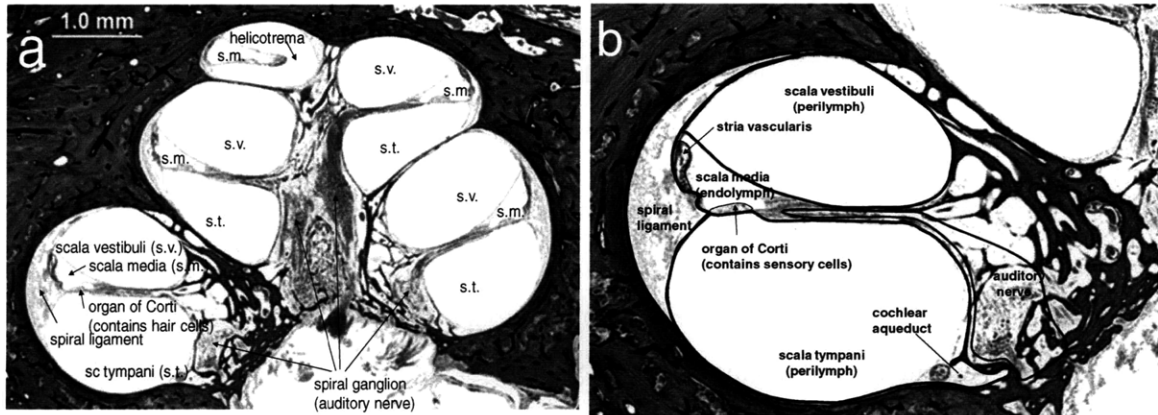


Figure 2.1 (a) A mid-modiolar section from a human temporal bone indicates the coiled structure of the cochlea as it winds around a central modiolus, which contains the spiral (auditory) ganglion and its associated auditory nerve fibers. (b) Each segment contains 3 fluid filled structures, the scala tympani (s.t.), scala media (s.m.), and scala vestibuli (s.v.). The organ of Corti, which contains the sensory cells of the cochlea (hair cells), separates the scala media and the scala tympani with the apical surface of the epithelium facing the fluid space of the scala media and all other cell surfaces bathed in perilymph of the scala tympani. The scala vestibuli is the fluid space at the upper portion of each turn. The outer edge of each turn is occupied by the spiral ligament, which is in diffusional continuity with perilymph. The outer edge of the scala media is bordered by the stria vascularis. The scala tympani and scala vestibuli are joined at the apical extreme of the cochlea at the helicotrema. The cochlear aqueduct connects the fluid space of the scala tympani with the cerebrospinal fluid space.

2.3 PHARMACOKINETICS

2.3.1 Absorption

2.3.1.1 Fluid compartments

Most of the structures of the cochlea are protected from the systemic circulation by the presence of a blood-cochlear barrier (or blood-labyrinthine barrier), similar to the blood-brain barrier. The extracellular fluid spaces of the ear can be considered pharmacologically as comprising four components: (1) the systemic circulation - largely confined to the stria vascularis and to fluid contained within the blood vessels and capillaries; (2) perilymph, a fluid similar in composition to CSF that provides a favorable milieu for sensory cell and neuronal function; (3) endolymph, a fluid high in potassium ions which provides the electrochemical drive for sensory cell function; and (4) the extracellular fluid of cochlear bone, which seems to be a transitional region between the systemic circulation and the perilymph.

A small portion of the inner ear, the stria vascularis, is readily accessible from the systemic circulation. It is surrounded by cells connected with tight junctions, which provide a part of the blood-cochlear barrier [27]. Drugs that act in the stria vascularis can be administered systemically, and the most likely action is a reduction of the endocochlear potential. Because the endocochlear potential is the battery that drives the cochlear transduction process, a reduction in the endocochlear potential will decrease hearing capability. The vascularization of the rest of the cochlea is relatively sparse, though the modiolus and walls of the scala tympani are exceptions [28]. The endothelial cells that line the vasculature are connected with tight junctions and no fenestrations [27, 29], and this network of tightly coupled endothelial cells is the dominant component of the blood-cochlear barrier.

Perilymph, the primary fluid of the inner ear, is in diffusional continuity with CSF via the cochlear aqueduct in most animals, though the transfer of fluid between the two spaces is limited [30]. In humans, the aqueduct is usually not patent [31], though diffusional continuity is achieved via other pathways, most notably the spaces around and within the auditory nerve [32].

Perilymph is primarily produced locally via the vascular supply to the cochlea (reviewed in [33, 34]), though a minor contribution from the CSF is possible. The site of production of perilymph is not known, though the vascular supply to the modiolus and walls of the scala tympani have been suggested [32, 35]. Perilymph resembles CSF in composition, and this similarity likely arises from a similar mode of production of perilymph and CSF.

Endolymph, the highly specialized extracellular fluid that fills the scala media, bathes the apical surfaces of the sensory cells. Endolymph is primarily produced in the stria vascularis and is secreted by the marginal cells of the stria vascularis, which face the endolymph. Endolymph contains high concentrations of potassium, low concentrations of sodium, and very low concentrations of calcium. The scala media is lined with cells that contain tight junctions. The tight junctions help the scala media retain its unusual electrical potential – around +100 mV, called the endocochlear potential. The endocochlear potential and the high potassium concentration of the scala media provide the electrochemical drive to the hair cells to allow their transduction of mechanical motion.

The cochlea is surrounded by petrous bone. This bone normally does not remodel and is very poorly vascularized. The bone is accessible to perilymph via lacuna canaliculi which are canals or holes in the bone in free communication with the scala tympani [32, 36, 37]. However, the bone is also

accessible to the systemic circulation via fenestrated blood vessels. The bone has not been characterized with regard to its presence in or out of the blood-cochlear barrier.

2.3.1.2 Barrier mechanisms

The prime component of the blood-cochlear barrier is a continuous capillary endothelium lining blood vessels in the cochlea. The endothelial cells are connected with tight junctions and no fenestrations [27]. Thus drugs entering the perilymph from the systemic circulation must either be transported across, or dissolve into and out of, the capillary endothelia.

The scala media is also surrounded by cells connected by tight junctions. Chemicals entering the scala media from the vasculature must either enter via the marginal cells of the stria vascularis, or by first entering the perilymph. Either way, the drugs must be transported across the cell lining to enter the scala media. Because the scala media has a relatively high positive charge due to the endocochlear potential, the charge a drug carries will be a significant factor in its ability to enter the scala media, with positively charged drugs at a disadvantage.

As with the blood-brain barrier, there are other elements of the barrier as well. The relatively high protein content of perilymph [23, 24, 38] will tend to bind drugs that do enter, buffering the concentration of such drugs. There are also likely to be other components to the blood-cochlear barrier, such as enzymes and cellular uptake systems that can reduce the concentration of chemicals that enter the cochlea, but these are not well characterized in the cochlea.

2.3.1.3 Properties of drugs that can cross the barrier

As with the blood-brain barrier, drugs that are large or highly charged have difficulty crossing passively. Drugs with high lipid solubility cross more readily. Drugs with high protein binding are less likely to cross. The unusual positive potential in the scala media poses an additional constraint for drug entry. Drugs that are positively charged tend not to enter the scala media since the electrical gradient works against them.

2.3.2 Distribution

Once a drug enters the cochlear fluids, its distribution is governed by many of the same pharmacokinetic variables seen in the bloodstream. Most of the structures of the cochlea are in diffusional continuity with the perilymph. Thus a drug placed into the perilymph can diffuse into the

organ of Corti, which contains hair cells, neuronal terminals, and other specialized cells. The perilymph is also in diffusional continuity with the spiral ganglion and structures within the modiolus of the cochlea. Access to structures in the modiolus is enhanced by the presence of numerous lacuna canaliculi on the surface of the osseous spiral lamina [37]. These perforations are on the order of 0.2 to 23 microns in diameter [36]. Finally, the spiral ligament and spiral limbus are also in diffusional continuity with perilymph.

Cochlear structures that are not accessible from the perilymph include the stria vascularis and the scala media, and thus the surfaces of cells that line the scala media. Both of the structures are lined with cells that are connected via tight junctions [27].

The protein composition of perilymph in the human has a number of elements in common with that of blood, though perilymph concentrations are lower [23], and protein interactions with drugs are as important in the perilymph as in blood. Albumin levels are high and can bind acidic drugs, and acid glycoproteins can bind basic drugs. Partition coefficients of drugs with these proteins will determine free concentration of the drug. These proteins can provide a reservoir for accumulation of the drug in perilymph over time.

The distribution of drugs within the inner ear is dependent upon the point of entry of the agents. There are 3 practical entry points: through or near the RWM (at the base of the cochlea on the scala tympani side), through or near the oval window (at the base of the cochlear on the scala vestibuli side), or through the bone of the cochlea via application in the middle ear.

The cochlea is a long set of coiled tubes. The perilymph of the scala tympani can be thought of as beginning at the base of the cochlea near the RWM, continuing apically to the end of the tube where it then connects with the perilymph of the scala vestibuli and continues back down to the base to the oval window, where the footplate of the stapes is located. Drug transport via simple diffusion along the length of the perilymphatic space, because of the large length relative to cross section would require very long times (hours to days) for significant drug distribution throughout the cochlea.

Salt, Plontke, and colleagues have extensively modeled the distribution of drugs applied at the RWM [39, 40]. They suggest that in addition to diffusion along the length of the cochlea, diffusion through the tissue of the cochlea from one scala to another must be considered as well [41, 42]. The magnitude of the interscalar distribution will be highly dependent upon the drug [43]. Highly lipid

soluble drugs, like steroids, will have a greater component of its distribution through tissue than would a drug with a high rate of cellular uptake via carrier systems.

Many drugs are delivered into the middle ear space with the hope that they will diffuse through the RWM into the scala tympani of the basal turn. The round window is an Achilles heel in the blood-cochlear barrier. It is permeable to water and many drugs [44, 45]. The major problems with this mode of entry from a pharmacokinetic perspective are that it relies on simple diffusion to pass drug from the middle to the inner ear, and once in the scala tympani, the only mode of distribution is simple diffusion in a fluid space with little turnover. Using implanted electrodes and tracer ions, the longitudinal volume flow in the scala tympani was determined to be negligible, approximately 1.6 nL/min directed apically [46]. The RWM can vary greatly in thickness [44] which can lead to variability in absorption of drug into the scala tympani.

Delivery of agent into the scala vestibuli does not provide as favorable access to the structures of the organ of Corti as application via the scala tympani. In theory, access to the auditory neurons should be possible via canal perforantes in the scala vestibuli portion of the osseous spiral lamina [32]. Also, there are possible diffusion pathways to the scala tympani via entry into and exit from the modiolus as well as into and out of the spiral ligament.

2.3.3 Metabolism and clearance

Issues of metabolism and clearance of drugs are specific for each drug. Some of the same barriers that limit drug entry, e.g. tight junctions, will also limit exit of drugs once they enter. Uptake systems to remove agents from the perilymph and either metabolize or transport agents to the systemic circulation will be important. Plasma has enzymes, such as esterases, which are likely to be present in perilymph as well and can alter the structure of drugs that enter the perilymph.

2.4 INNER EAR DRUG DELIVERY APPLICATIONS

Current applications for inner ear drug delivery are grouped into three main categories, otoprotection, SSNHL, and AIED. The sensory cells of the cochlea must be protected from noise and surgical trauma, ototoxic drugs such as cisplatin and aminoglycoside antibiotics, and head and neck radiation. In addition, drugs are used to minimize or reverse hearing loss due to sudden events of unknown nature and to immune reactions within the cochlea.

Future application research is focused on maintenance of spiral ganglion cells after hearing loss, and regeneration of hair cells. A variety of techniques including gene transfer and stem cell transplantation are being explored.

2.4.1 Current applications

2.4.1.1 Noise induced hearing loss

Hearing loss is associated with both acute and chronic noise exposure. The overwhelming of the natural antioxidant system by the formation of free radicals is a hypothesized cause of NIHL [47]. Many types of steroids, antioxidants, and nerve and growth factors have been studied to protect the ear from trauma or to minimize or reverse damage [48].

The effectiveness of steroids in reducing hearing loss due to noise has been inconclusive. In one study, dexamethasone was administered intracochlearly in a manner using an osmotic pump, and the animal was exposed to noise trauma on day four. A dose dependent reduction in outer hair cell loss was seen seven days after exposure, and the highest dose tested, 100 ng/mL, resulted in less ABR shifts than control [49]. Using a different methodology, Sendowski et al. directly infused methylprednisone for seven days into the cochlea after exposing the guinea pig to impulse noise trauma. The steroid accelerated the recovery of temporary hearing shifts during the period and reduced hair cell loss. However, the drug did not limit permanent threshold shifts [50]. Both cyclosporine A and immunosuppressant, FK506, delivered intraperitoneally immediately prior to sound exposure showed decreased ABR threshold shift after both one and two weeks [51]. Steroids, if proven effective, may be excellent candidates for local delivery as patients can experience significant side effects when given at high doses systemically. High doses are likely necessary to achieve a therapeutic concentration within the cochlea.

Other researchers have used antioxidants such as D-methionine and N-acetylcysteine to prevent NIHL [52-54]. Caroverine, a glutamate antagonist and antioxidant, was delivered to counteract excess glutamate and reactive oxygen species released during noise trauma. An osmotic pump was implanted to deliver subcutaneously, and the guinea pig was pretreated for 48 hours prior to noise exposure. The protective properties of the caroverine resulted in 5-10dB shifts after four weeks compared to 30dB shifts seen in the controls [55].

A variety of new therapies, such as growth factors and peptides, are being introduced to combat the effects of NIHL. Insulin-like growth factor-1 (IGF-1) applied in a hydrogel to the RWM reduced ABR shifts and outer hair cell loss at seven and thirty days post noise exposure [56]. Likewise, neurotrophic factor-3 (NT-3) protected the inner ear from noise induced damage, but brain-derived neurotrophic factor (BDNF) showed no protection [57]. Researchers attempting to inhibit the apoptotic cascade initiated by noise trauma have met with promising results using AM-111 and D-JNKI-1 peptides, among others [58-60]. Large and complex molecules such as peptides will likely require local delivery to the inner ear as they may have difficulty in traversing the blood-cochlear barrier or may be quickly inactivated by enzymes.

2.4.1.2 Cisplatin ototoxicity

Cisplatin, a chemotherapy agent commonly used in cancer treatment, is ototoxic, and compounds such as antioxidants and platinum binders are being investigated for co-administration to mitigate the hearing loss associated with cisplatin treatment [61, 62]. A study of the dose dependency of cisplatin ototoxicity in guinea pigs revealed that a sudden drop in CAP of 40 dB occurred from one to five days after cisplatin was administered, depending on dose, which varied from 3 to 300 µg/mL [63]. The drug resulted in loss of outer hair cells, especially in the basal turn of the cochlea. Cisplatin generates reactive oxygen species by activating the NOX-3 enzyme, unique in the cochlea, and leads to apoptosis of outer hair cells [64]. With damage occurring first at high frequency, some reports show hearing thresholds elevated in 75-100% of patients taking cisplatin. Ototoxicity is both dose and age dependent with elderly and children affected to a greater extent [61, 65].

Antioxidants, such as methionine, are useful in scavenging free radicals from the inner ear [66]. When delivered with cisplatin, hearing loss is reduced [67]. Unfortunately, a study where L-methionine was delivered systemically with the cisplatin resulted in hearing protection but also made the cisplatin ineffective [68]. Locally delivered, antioxidants may protect hair cells without inactivating the chemotherapy treatment. Two studies have proven inconclusive, though. D-methionine was delivered to the RWM via osmotic pump in combination with systemic cisplatin. Chemotherapy was given for five days, and the D-methionine treated ears had better DPOAEs on days 3 and 4. The threshold shifts were not significant by days 5 and 6 [69]. A different antioxidant, thiourea was also investigated by delivering it directly through a cochleostomy via osmotic pump. Five days after starting thiourea, cisplatin was started. The study resulted in less outer hair cell loss but threshold shifts were not affected [70].

Thiols neutralize cisplatin since the sulfur has a high affinity for the platinum. However, sodium thiosulfate (STS), if administered systemically, will inactivate the cisplatin and reduced its anti-tumor activity [71]. In order to utilize the otoprotective aspects of STS, it must be contained within the inner ear, making it an excellent candidate for local delivery. Wang, et al. used an osmotic pump for intracochlear delivery and showed that six days after cisplatin the thiol protected 93% of inner and outer hair cells [72]. Guinea pigs were treated with STS, half via osmotic pump in the middle ear and half via daily injections into the middle ear. Cisplatin was started two days later, and both delivery methods resulted in less hearing loss [73].

2.4.1.3 Aminoglycoside ototoxicity

Another possible application for inner ear drug delivery is in the prevention of aminoglycoside antibiotic ototoxicity due to the generation of oxygen free radicals [74]. Some reports show the incidence of hearing loss associated with these antibiotics is as high as 33% [61, 65]. There is a dose dependent effect, and patients experience high frequency hearing loss due to the loss of outer hair cells in the basal turn. Hypotheses that reactive oxygen species leading to apoptosis are involved have led to testing protective agents such as antioxidants and iron chelators. The assumptions are that the antioxidants scavenge free radicals, and the iron chelators bind iron in the cochlea so it cannot react with aminoglycosides to generate reactive oxygen species [61, 65]. A study by Sergi et al. showed that antioxidants delivered with gentamicin resulted in less hearing loss [67].

Steroids have also been tested for their otoprotective attributes during antibiotic treatment. The intracochlear infusion of dexamethasone before and after kanamycin delivery protected hearing. More outer hair cells survived, and shifts in ABR were decreased [75].

2.4.1.4 Radiation ototoxicity and trauma

Hearing loss due to head and neck radiation and intracochlear surgical trauma represents a possible area that would benefit from local delivery of otoprotective agents. During radiation treatment of head and neck tumors, the cochlea is often exposed. Hearing loss is dependent on both dose and tumor site and can result in sudden or progressive hearing loss [76]. This side effect occurs in approximately one third of patients and results from loss of hair cells, degeneration of the stria vascularis, and loss of spiral ganglion cells [77]. Patients are commonly given steroids to reduce inflammation, but local delivery would reduce the side effects associated with systemic steroid treatment. Inflammation often results from inner ear surgical trauma, as well. The application of

corticosteroid by syringe following cochleostomy enhanced the recovery of CAP thresholds over four weeks [78].

2.4.1.5 Sudden sensorineural hearing loss

SSNHL is defined as the loss of more than 30 dB of hearing in three consecutive frequencies in less than three days [79]. There are two hypothesized causes: viral infections and vascular events resulting in a local decrease in blood flow [80]. Steroids have some effectiveness in treating SSNHL, and the best indicators of treatment success are the severity of hearing loss and the time before treatment is started [80].

This disorder is an excellent candidate for local delivery because the high systemic doses of steroids needed for treatment cause significant side effects. The Microwick, a device for facilitating diffusion through the RWM has been utilized as one method of local delivery [81, 82]. In a human study of ten patients treated intratympanically, hearing improved in 80% of participants [83]. Often, patients who have failed to tolerate systemic steroids or could not take them have been treated locally. Dexamethasone or methylprednisone delivered intratympanically has shown varied success [84, 85]. Hearing improvement in 44% to 75% of patients has been reported [86-88].

Results of treatment have varied, and some studies point to a strong correlation between success and time to commencing treatment [89]. A retrospective study of a single intratympanic injection of dexamethasone showed no improvement if treatment began more than 36 days after SSNHL onset. If begun sooner, 40% of patients show improvement [90]. Battista reported no significant hearing recovery for 25 patients given dexamethasone intratympanically. The mean time until treatment was 28 days, but there was evidence of improvement for those patients whose treatment started within eleven days [91].

2.4.1.6 Autoimmune inner ear disease

AIED results in the loss of hearing when the immune regulation system is compromised [92]. Treatment results from high dose systemic steroids and locally delivered steroids have been inconclusive [81, 93]. Encouraging results have been shown with methotrexate [94]. Ryan et al. suggested a treatment of high dose prednisone with the addition of methotrexate if relapse occurred when the steroid was tapered [8]. Improvements in treatment may be facilitated by local delivery for both SSNHL and AIED.

2.4.2 Horizon Applications

Hearing loss is associated with progressive degeneration of the cochlea, loss of the sensory hair cells, and their associated neural connections. In the human, hair cells and neurons do not regenerate spontaneously after they have been lost. Thus, clinical treatments to date have focused mainly on functional improvement, such as cochlear implants. While cochlear implantation can provide sensory function for individuals with impairment, the effectiveness of application inherently depends upon the residual function of surviving sensory cells and neurons. As a first pass effort, the ability to preserve existing sensory cells and their functions can be used to enhance therapeutic efficacy of cochlear prostheses. However, with a better understanding of the inner ear cell cycle machinery, emphasis can also be placed on discovering therapies for the regeneration of new sensory hair cells, and ultimately a clinical treatment for restoring functional hearing. Ideally, concurrent advances in therapeutic development and drug delivery technologies to the auditory system will be developed in order to realize a clinically relevant treatment of progressive hearing loss.

2.4.2.1 Neurotrophin therapy

The loss of hair cells in hearing loss is followed by the degeneration of spiral ganglion cells. This degeneration can be attributed to the loss of hair cell activity as well as survival factors, such as neurotrophins. Neurotrophic factors have the ability to influence cell growth, differentiation, division, and survival. Application of neurotrophic factors as a clinical therapeutic for hearing loss has been limited due to their short half-life *in vivo*, as well as poor pharmacokinetics, proteolytic degradation, and the potential side-effects of high-dose, systemic delivery. However, the advent of novel drug delivery systems, as described below, has allowed for localized neurotrophin delivery to the inner ear and the decrease in chances of non-specific and undesirable side-effects.

Neurotrophins can be delivered to the inner ear by direct injection or longer-term continuous delivery by methods such as polymer release, cannula microinfusion systems, or osmotic pump [95]. Delivery of exogenous neurotrophic factors to the inner ear has been shown to preserve both hair cells and SGN. The neurotrophic factors NT-3, glial cell-derived neurotrophic factor (GDNF), BDNF, and fibroblast growth factor (FGF) have all been shown to protect hair cells from cell death in models of ototoxicity [95-99]. Nerve growth factor, NT-3, BDNF, GDNF, and ciliary neurotrophic factor promote SGN survival in numbers similar to pre-deafened states, individually and in combination [95, 100-102]. BDNF and NT-3, in particular, have been implicated as the principal neurotrophins involved in the

neuronal development of the cochlea, and consequently, the *in vivo* survival and rescue of adult auditory neurons [11]. More recently, it has been shown that rescue can occur even after delayed neurotrophin delivery. Miller et al. [102] examined the effects of chronic infusion of BDNF and FGF initiated 4 days, 3 weeks, and 6 weeks after de-afferentiation from deafening and found that maintenance and regrowth of spiral ganglion cells could occur with delayed treatment out to 6 weeks. However, relatively little is known about the longevity of effects after treatment is withdrawn. There is evidence that SGN survival is maintained well after cessation of neurotrophin administration [103]. However, it has also been demonstrated that as early as 2 weeks after cessation of BDNF treatment, a rapid decline in neuron survival could be seen in that the number surviving was not significantly different from deafened, untreated cochleae [104, 105]. Furthermore, the rate of neuronal degeneration after cessation of treatment was more rapid than in the deafened, untreated cochleae. The exact mechanism behind loss of survival effects is unclear. It is thought that this accelerated degeneration may be due to the loss of direct trophic support to the auditory neurons from BDNF, plus a loss of endogenous survival factors from supporting cells that were also preserved by BDNF. It has also been shown that BDNF increases nitric oxide synthase expression, leading to an increase in nitric oxide production, which can initiate a neurotoxic cascade. Furthermore, the reaction of NO with superoxide radicals associated with certain ototoxic agents leads to the formation of even stronger oxidative agent, which accumulates and only elicits a response after BDNF withdrawal [104].

However, the effect of neurotrophins can be enhanced when administered in combination with other forms of therapy, such as electrical stimulation. *In vivo* studies have demonstrated enhanced SGN survival in deafened cochleae treated with concurrent exogenous neurotrophin delivery and electrical stimulation [10, 106]. More importantly, continued chronic electrical stimulation after cessation of neurotrophin delivery significantly reduced the rate of SGN loss, although this effect was localized to the region of the cochlea proximal to the electrode array [105]. Therefore, a system which can provide electrical stimulation as well as concurrent delivery of antioxidants would be synergistic to continuous exogenous neurotrophin treatment.

2.4.2.2 Gene Therapy

Gene therapy is the addition or transfer of a segment of genetic material into a cell that results in expression of transgenic protein, and ultimately a change in the function or behavior of the cell. Although the development of gene therapy for the human ear to date has been limited due to technical and ethical issues, it still remains a promising technique for treating both genetic and acquired forms of

hearing loss [107, 108]. In the inner ear, gene therapy is generally targeted at three main application areas: the introduction of protective factors to enhance spiral ganglion and hair cell survival, the regeneration of functional hair cells by transdifferentiation of supporting cells, and the treatment of hereditary disease by insertion of a functional wild-type gene.

Local delivery to the inner ear of genes that can express therapeutic products is an alternative to the delivery of exogenous molecules for spiral ganglion and hair cell protection and survival. Transfer of BDNF [11, 109], GDNF [110, 111], or NT-3 [112] genes in the cochlea gave comparable outcomes to conventional exogenous delivery of neurotrophic factors in terms of SGN and hair cell survival in the injured inner ear. Gene therapy to deliver GDNF in conjunction with chronic electrical stimulation has also been applied. Individually, both treatments exhibited significant rescue of SGN compared with deafened controls, with GDNF being more effective than chronic electrical stimulation [10]. However, as with exogenous neurotrophin delivery, combining treatments was significantly more effective than either treatment alone. Aside from long term delivery of neurotrophins, gene therapy has also been used to provide overexpression of antioxidants. Overexpression of catalase and manganese superoxide dismutase was able to protect hair cells and hearing thresholds in a guinea pig aminoglycoside ototoxicity model [113]. The overexpression of antioxidant genes may prove beneficial in protecting the cochlea against oxidative stress due to other forms of ototoxicity, such as noise, as well as aging.

Because the mature cochlear sensory epithelium has only sensory hair cells and non-sensory supporting cells, regeneration in the inner ear sensory epithelium must depend on the transdifferentiation of one cell type to another. Many of the genes and factors which determine cell fate in the inner ear have been identified. By re-expressing these developmental genes in the injured tissue, supporting cells could potentially be forced into a hair cell phenotype. One such gene is *Atoh1* (also known as *Math1*, or the human homolog *Hath1*). *Atoh1* is a basic helix-loop-helix transcription factor which is necessary to induce cell differentiation in the epithelial ridge of the developing organ of Corti. *Atoh1* has also been shown to be successful in transdifferentiation of supporting cells into new hair cells in the deafened adult guinea pig by demonstration of increased hair cell counts and lower thresholds on ABR relative to untreated, deafened controls [114, 115].

Genes whose dysfunction or mutation is associated with hearing loss are also possible targets for inner ear gene therapy. Advances in molecular biology and genetics have enabled the identification of over 75 different genes contributing to hereditary hearing loss; each of these is a potential target for gene therapy [116, 117]. The largest proportion of hereditary sensorineural hearing loss cases are due to

mutations in the GJB2 gene, which encodes the gap junction channel protein connexin 26 (cx26). Connexins are transmembrane proteins that assemble to form the gap junction channel of a cell, which in turn regulates intracellular signaling. In the inner ear, cx26 is widely expressed throughout non-sensory epithelial and connective tissue cells, allowing these cells to communicate in regulating fluid and ion balance. Potassium ions are transported by gap junctions to maintain high levels of the endocochlear potential for hair cell excitation [118, 119]. Alterations in cx26 cause a disturbance in potassium homeostasis by preventing potassium ions from being recycled by the hair cells back to the endolymph, ultimately leading to hair cell death by potassium intoxication. However, because GJB2 knockout mice are embryonic-lethal, the pathogenesis of deafness due to mutations of this gene has been difficult to examine. Therefore, several groups are working towards viable mouse models to study the pathological role of GJB2 [118, 120, 121]. Relevant mouse models for studying abnormalities of GJB2 in the pathogenesis of deafness will be needed before clinical applications of gene therapy can be considered for such cases of hereditary hearing loss.

The final common pathway in any case, acquired or genetic hearing loss, and inner ear dysfunction, is hair cell injury and loss. By targeting hair cells, supporting cells, or neurons, gene therapy can be used to change cellular phenotype for preservation, rescue, and even regeneration of hair cells. The various cell types of the inner ear can be selectively transfected by viral vectors, including adenovirus, adeno-associated virus, herpes simplex virus, vaccinia virus, lentivirus, and nonviral cationic liposomes. However, cytotoxicity and short-term expression of gene products remain problematic. Reviews regarding the practicality of utilizing these transfer agents can be found in the literature [117, 122, 123].

The ear itself is considered a particularly attractive target organ for the study and potential application of gene therapy. The bony housing of the sensory epithelium isolates the organ system, thereby limiting unwanted systemic diffusion of transfer agents. However, delivery of vectors into the inner ear requires increasingly sophisticated methods of delivery. Although liposomes and some viral vectors can follow pathways for small molecules, such as diffusion across the RWM, most vectors cannot. Therefore, efforts in delivery of transfer agents have focused on delivery to the basal turn of the cochlea through a cochleostomy, or by injection directly through the RWM. Vector delivery can also be achieved by accessing the inner ear through the stapes footplate or the semicircular canal [123]. However, similar to the delivery of other therapeutic agents to the inner ear, diffusion of vectors through the cochlea shows a gradient of transfection with the greatest at the site of injection.

Therefore, one important consideration in moving towards clinical applications will be determining a method to provide the uniform distribution of transfer throughout the entire cochlea. Another consideration will be the duration of expression of the transgene. Currently, expression is often short-lived, lasting only days to months. A method of delivery which ensures continued expression of the therapeutic gene over an extended period of time will also be crucial in the successful applications of gene therapy.

2.4.2.3 RNA Interference

In certain situations, it is desirable to decrease or eliminate the expression and function of a particular gene. Studies on mouse cochleae have shown that a large number of negative cell growth genes are upregulated in later development, including cyclin-dependant kinase inhibitors (p27kip1 and p19inkd) [124] and tumor suppressor genes (pRb) [125]. Their expression coincides with cell cycle exit, as well as establishment and maintenance of the quiescent status of cochlear sensory epithelia. Certain genes may also be upregulated as a result of injury. For example, ototoxic insult from aminoglycosides, cisplatin, and noise can all lead to a common cascade of cell death genes leading to cell cycle arrest and apoptosis. Potential targets in this cascade include caspases, the Bcl-2 family of proteins, p53, and the c-jun NH2-terminal kinases [126].

The effects of these genes have been well characterized by creating null cells in culture and in knockout animal models. Targeted inhibition of gene expression can be carried out utilizing homologous recombination, antisense vectors, ribozymes, and DNAzymes. However, recently, a new method of gene manipulation known as RNA interference (RNAi) has shown to be a promising therapeutic approach in shutting off gene expression. RNAi is a method used to silence gene expression post-transcriptionally through the introduction of double stranded RNA. The double stranded RNA induces the sequence-specific degradation of complementary messenger RNA. RNAi provides a rapid means to assess the loss of gene. However, double stranded RNA longer than 30 base pairs provokes the antiviral/interferon pathway in mammals and results in the global shutdown of protein synthesis. Therefore, the use of RNAi as a clinical therapy did not become apparent until the advent of chemically synthesized small interfering RNAs (siRNAs) of 21-22 nucleotides, which could be used to target mammalian genes by RNAi while evading the interferon response [127, 128].

In order to realize RNAi as a therapeutic modality for gene silencing, several obstacles need to be addressed. SiRNAs are relatively small and are rapidly excreted when administered through the

blood stream. They are also relatively unstable in a serum environment with a half-life of approximately 0.8 hours, and can be degraded by RNase activity within a short window of time [129]. As with other molecules, when administered systemically, a nonspecific distribution occurs, which in turn decreases the local concentration at the site of action. Even at the target site, cellular uptake requires efficient endocytosis of the double stranded siRNA. The duration of siRNA effects is also limited, lasting only 3-5 days in rapidly proliferating cells and up to three weeks in non-dividing cells [129]. To increase stability, techniques to chemically modify siRNA oligonucleotides are being explored including changes in backbone structure, replacement of nucleotides with analogs, and addition of conjugates. Both viral and non-viral carrier systems are also being examined as a means to efficiently transfect cells. However, the development of systems for local delivery will be highly dependent on the accessibility of the target tissue.

Several siRNA-based drug candidates are in pre-clinical commercial development for applications in the inner ear, and recently, lipocomplexed siRNA has been effectively delivered intact by Gelfoam to the RWM in rats with successful silencing in the cochlea [130]. Also, siRNA complexes perfused directly to the scala media of the guinea pig have shown uptake in stria cells along the length of the cochlea [131]. However, before a clinical development program can be initiated for siRNA in the inner ear, basic information such as residence time of siRNA in the inner ear cells and duration of therapeutic effect will need to be examined. With long-term expression of siRNAs, RNAi may become a potential therapeutic strategy to preserve hearing.

2.4.2.4 Cell-Based Therapy

Recent advances have also made possible the potential for cell-based approaches to preserve hearing as well as for regeneration [122, 132, 133]. Cells have been transplanted to the inner ear as an answer to the need for long term stable delivery of neurotrophins, which is not possible with current methods of exogenous neurotrophin delivery and gene transfection. Fibroblasts transduced with BDNF transgene have been encapsulated in a matrix of agarose and delivered via a modified electrode through a cochleostomy site [134]. These cells were shown to express transgene and secrete BDNF *in vivo*. The BDNF-excreting electrodes were also able to preserve significantly more spiral ganglion cells than control electrodes, though this effect decreased with distance from the basal turn. Although, this approach combines the electrode stimulation with a possible method for long term growth factor delivery, a method would need to be set in place to ensure that these transplanted cells would not proliferate, invade or obliterate the cochlea. Another cell-based method for neurotrophin delivery is the

transplantation of neural stem cells [135]. Neural stem cells injected by infusion pump into the lateral semicircular canal were found attached to the cochlea in every turn after 28 days. Most of these cells expressed markers for glial cells and were positive for GDNF, while approximately 50% of the cells were positive for BDNF. If injected at the time of cochlear implant surgery, the spontaneous production of neurotrophin by these transplant cells could provide an effective mechanism for spiral ganglion preservation.

Although these neural stem cells are able to survive in the inner ear environment, they have not been found to migrate into the sensory epithelium in normal ears, but have had limited success in migration and transdifferentiation into hair cells in ears subjected to traumatic injury. Parker et al. [136] found that neuronal stem cells from a clonal cell line were able to migrate as well as receive signals from the microenvironment to upregulate genetic cell fate programs expressed by local endogenous cells - either neural, glial, hair cell or supporting cell types. Therefore, though the inner ear cannot regenerate sensory cells from its own endogenous population, it is still able to influence stem cell differentiation among particular cochlear phenotypes.

The cell type with the greatest capacity for differentiation into multiple cell types is the pluripotent embryonic stem cell. Survival of embryonic stem cells in the inner ear after transplantation has been well documented, and migration can occur in the auditory nerve fibers of the rat cochlea [137-140]. However, undifferentiated cells grafted into the inner ear also showed no potential to differentiate into hair cell phenotype [140]. Embryonic stem cells can, however, be directed by applying cues such as in normal development. It has been shown that, from embryonic stem cells, it is possible to enrich a population of inner ear progenitor cells which express marker genes that define the developing inner ear by culture in the presence of endothelial growth factor and IGF-1 [141]. Injection of these cells into chick embryonic ear resulted in integration into cochlear sensory epithelia and a hair cell phenotype. Recently it has been shown that endogenous stem cells exist and can be isolated from the adult ear and expanded as neurospheres *in vitro* in the presence of mitogenic factors to obtain sufficient numbers of cells for transplantation [142, 143]. Injection of these inner ear progenitor cells into the chick inner ear resulted in similar results to the injection of embryonic stem cell derived progenitors in terms of survival, integration, and differentiation into hair cells.

Another option for cell regeneration is bone-marrow derived cells, which can be obtained from the recipient patient, enabling autologous transplant [144, 145]. When introduced into the chinchilla inner ear without selection for inner ear progenitors, the cells showed the upregulation of neural and

glial markers [145]. However, the number is limited, and a method to induce neuronal differentiation would be needed in order to induce regeneration of SGN from transplants.

Stem cell therapy is a promising step in the regeneration of sensory cells in the inner ear and the restoration of hearing. However, it is difficult to predict how this technology can be translated into clinical practice. Functional restoration will depend not only on the introduction of new cells, but also differentiation of cells to the correct phenotype, and the formation of appropriate three-dimensional tissue structures. This will rely heavily on the ability to control the local microenvironment of the cells once transplanted. The derived cells and tissues will also need to be mechanically and structurally compliant with the native tissue, and able to integrate into the host without immunological rejection. Before stem cells can be considered for therapeutic applications, these issues of sustainability and functionality must be addressed. In this relatively young field, it is currently unclear what environment is needed to induce functional cells and tissues of the inner ear. It is possible that a treatment for hearing loss does not exist in any one therapy, and the ability to restore hearing will ultimately rely on an intricate combination of drug treatment, gene manipulation, as well as transplantation in conjunction with implanted devices, such as integrated delivery systems and cochlear prostheses.

2.5 INNER EAR DRUG DELIVERY METHODS

Inner ear drug delivery methods can be divided into two main categories based on the location of entry of the drug. Intratympanic delivery involves depositing the therapeutic agent in the middle ear, relying primarily on diffusion through the RWM for access to the scala tympani. The second method, intracochlear, depends on a cochleostomy with direct delivery into the inner ear space, completely bypasses the middle ear.

Intratympanic delivery must rely solely on diffusion through the round window and for dispersion throughout the scala tympani. Therefore, access to the apical regions of the scala tympani can be limited, and large concentration gradients may develop. Also, the RWM presents a physical barrier to delivery. A great deal of variability of condition and thickness of the membrane across population has been observed [146, 147], limiting dosage control from patient to patient. Alzamil reports, for example, round window niche obstruction in a third of human ears [148]. Also, due to the anatomy of the round window, substances may be more or less likely to transverse the membrane based on size and constitution [45, 149]. Because it is applied in the middle ear, drug can be lost through the Eustachian tube, which leads from the middle ear to the pharynx. These factors, along with

the inability to control specific delivery parameters, combine for a lack of precise control of dosage in intratympanic delivery. This method of delivery does offer less opportunity for surgical trauma or damage than the intracochlear method, and the middle ear is relatively easy to access. Many of these implantation procedures do not require general anesthesia.

Intracochlear delivery provides direct access to neural and sensory cells and does not necessarily rely solely on diffusion for drug distribution. Fluid flow may augment diffusion which could provide access to more apical regions of the cochlea. Because drug is deposited directly into the perilymph, the types of molecules and/or particles are not limited by RWM transit. While dosage may be precisely controlled, a greater possibility of surgical trauma exists. Additionally, indwelling devices are at risk of biofouling due to tissue growth and protein build-up in the scala tympani.

Both intratympanic and intracochlear delivery offer opportunities for inner ear drug delivery and can be utilized as required for optimal delivery parameters.

2.5.1 Intratympanic drug delivery

For intratympanic delivery, multiple passive and active drug delivery approaches are being explored, with applications ranging from protection from NIHL to delivery of regenerative compounds aimed at arresting sensorineural hearing loss. This research is often aimed at establishing extended release profiles with controllable and predictable kinetics using compounds within the middle ear. In the following, examples of passive drug delivery to the cochlea will be described for several principal approaches: biodegradable polymers, hydrogel-based systems, and nanoparticles. In addition, examples of active intratympanic delivery are described using a variety of components and devices, including microcatheters, microwicks, and osmotic pumps. Here, we define active as any device used for intratympanic dosing of therapeutics, although in some cases, these devices by themselves do not provide a mechanism for changing dosing.

2.5.1.1 Passive intratympanic delivery

Passive drug delivery systems are designed to deliver drug compounds with specific kinetic profiles using local triggers for release, such as hydrolysis in the *in vivo* environment, or in response to local stimuli such as temperature or pH. Drug may be dispersed within a matrix or contained within a reservoir encapsulated by a shell of bulk polymer, depending upon the specific application.

2.5.1.1.1 Biodegradable polymer intratympanic delivery

Early biodegradable polymer drug delivery systems, developed for a wide range of therapeutic applications, were based upon poly (lactic) co-glycolic acid (PLGA), and this approach has also been employed for the inner ear. Biodegradable polymer delivery has been successfully employed for a number of clinical applications, including implantation of wafers to treat glioblastoma multiforme, depot systems for contraception and treatments for endometriosis or estrogen replacement therapy, and inserts for patients with glaucoma. Biodegradable polymer devices for delivery may take the form of degradable microparticles or nanoparticles, hydrogels or larger microfabricated structures with specific release profiles.

Sustained release structures based on siloxane have been investigated as fast- and slow-release vehicles for delivery of compounds of interest for inner ear disease therapies and tinnitus. Release rates for devices on the order of 1 mm in dimension ranged from 15 – 50 µg/day, and were filled with glucocorticoid or beclomethasone and placed on the RWM to study effects on hearing over the 28 day duration of the guinea pig studies. Monitoring of auditory function via ABR, assays of perilymph following delivery, and histology were all conducted. Histology appeared normal in the guinea pig cochleae, and assays demonstrated the presence of beclomethasone in the perilymph of the scala tympani of virtually all implanted animals. Auditory function over a range of frequencies from 3 – 12 kHz was altered as monitored by ABR thresholds, and by day 28 there were significant differences in hearing for all but the placebo groups [150].

The specific nature of the biodegradable polymer delivery vehicle can determine whether efficacious therapy is achieved, such as in the targeting of SGN [95]. Meniere's disease patients have been treated using a biodegradable gelatin polymer matrix known as Gelfoam, with high success rates for elimination of vertigo and tinnitus following gentamicin-soaked Gelfoam material placement on the RWM [151]. When Gelfoam was applied in an animal model as a means to reverse hearing loss and promote SGN survival in deafened guinea pigs, however, there was no evidence of enhanced response. Specifically, SGN survival was not observed when neurotrophin-soaked Gelfoam was administered to deafened guinea pigs, in spite of the fact that radiolabeling confirmed that release of the drug was sustained. When alginate polymer was substituted for Gelfoam, SGN survival was maintained in the implanted ear, suggesting that the kinetics and maintenance of drug concentration is dependent upon the specific polymer chemistry and degradation characteristics of the delivery vehicle [152].

2.5.1.1.2 Hydrogel-based intratympanic delivery

Hydrogel-based delivery for therapeutic applications can enable precise targeting of tissues and organs through the use of triggering mechanisms. These triggers may be chemical, including pH or other ionic factors or the presence of specific molecular species, or may be physical, such as temperature, pressure or electrical potential. Triggering will cause the hydrogel to swell and release its payload of drug in a controlled fashion. Many of the investigations of hydrogel-based delivery for treatment of inner ear diseases have employed biodegradable hydrogels, often with a hyaluronic acid-based chemistry. In one such study, a rescue agent was delivered locally onto the RWM following impulse noise trauma. The JNK inhibitor AM-111 was prepared in a hyaluronic acid gel formulation and applied to the RWM in a chinchilla, following exposure to acute acoustic trauma. The gel-based delivery approach was observed to provide significant and rapid recovery from the original insult, presumably due to fast degradation of the gel and subsequent transport of the drug across the RWM and into the cochlea [58].

Cochlear protection from NIHL has also been investigated using IGF. In one study, recombinant human insulin-like growth factor -1 (rhIGF-1) was loaded into a biodegradable hydrogel produced by glutaraldehyde cross-linking of collagen, and delivered by placement on the RWM. Auditory response was monitored using ABR measurements following noise exposure, and immunostaining was conducted to monitor outer hair cell degeneration. These evaluations concluded that significant protective benefit to the outer hair cells was conferred by the biodegradable hydrogel treatment with rhIGF-1 [56].

In another set of studies, BDNF was delivered to assess protection of auditory neurons, using the same biodegradable hydrogel carrier. Concentrations of BDNF in the perilymph were seen to be much higher in the cochleae of guinea pigs from the hydrogel group than in either control animals or a group that received an injection through the RWM. Analysis using ELISA confirmed sustained delivery of growth factor for periods of 7 days after placement of the hydrogel on the RWM [153-155].

2.5.1.1.3 Nanoparticle delivery

Nanoparticle delivery to the inner ear has emerged as a promising new avenue for delivering compounds to the cochlea in a sustained and controllable manner. The nanoparticles may be comprised of biodegradable or nondegradable materials, depending upon the application and the desired pharmacokinetic profile. In one study, Tamura et al. [156] encapsulated traceable fluorescent dye into PLGA nanoparticles and compared delivery profiles with transport of the unencapsulated rhodamine

molecule in a guinea pig model. Nanoparticles with diameter of roughly 150 nm were prepared using a 50/50 ratio of lactic / glycolic acid and with rhodamine B contained within the matrix. For both systemic application and placement on the RWM, nanoparticles containing rhodamine B produced significant levels of rhodamine in the cochlea, as assessed by counting of fluorescent particles. The presence of rhodamine was not observed in the cochlea following either systemic application or RWM placement of the free molecule.

Nanoparticles have been investigated as an alternative to viral vector systems, which have shown promise for treatment of inner ear diseases but carry concerns about safety as well as precision of targeting of specific cells and tissues [157]. As a model system, Praetorius and co-workers delivered silica nanoparticles labeled with the fluorescent cyanine dye, Cy3, to the cochlea by placement on the RWM of mice. The silica particles had a diameter of 20 nm and their transport was observed via immunohistochemistry and histology, accompanied by ABR testing to ensure that hearing thresholds were not altered. No evidence of cytotoxicity was observed, and silica nanoparticles were observed in inner hair cells, vestibular hair cells and in the spiral ganglia. An interesting observation stemming from this work was the occurrence of retrograde axonal transport [157].

In another study, PLGA nanoparticles were prepared with a uniform dispersion of superparamagnetic iron oxide nanoparticles within the PLGA matrix and delivered in a chinchilla. The PLGA nanoparticles ranged from 100 – 300 nm in diameter, while the embedded magnetic materials were in the 5 – 15 nm range. Nanoparticles were placed upon the RWM for duration of 40 minutes. Either with or without magnetic field exposure, magnetite and PLGA-coated nanoparticles were observed throughout all turns of the cochlea, within the perilymph and within the inner and outer hair cells, as well as in the stria vascularis and the spiral ligament [158]. It is well known that low molecular weight compounds such as gentamicin can cross the RWM quite readily [44], either through tight junctions or via an intracellular pathway. The application of magnetic fields and modulation of degradation profiles of the PLGA can provide additional levels of control over long-term drug delivery to the inner ear structures.

Liposomes represent another particle-based mode for delivery to the inner ear, and these vehicles have been explored as a means for gene therapy. Cationic liposomes can be mixed with DNA for transfection of numerous cell types, and introduced into the cochlea via microinjection. In one such study, Wareing et al. [159] reported that 14 days of transgene expression was observed with an absence of toxicity or inflammatory response. Guinea pigs were treated with either injection or an osmotic

pump delivery of cationic liposomes containing DNA complexes, and tissue sections were evaluated using immunohistochemistry and PCR analysis. From the base to the apex, beta-galactosidase was observed in virtually all tissue types, with highest concentrations in the spiral ligament; PCR-based assays confirmed these observations. Persistence of the transgene expression for two weeks was observed for both microinjection and osmotic pump infusion; however the osmotic pump delivery was associated with local trauma and inflammatory responses [159]. This suggests that liposome delivery is a viable approach for intratympanic delivery but that the means to transport the liposomes to the cochlea is a critical element of the strategy.

2.5.1.2 Active intratympanic drug delivery

Active intratympanic drug delivery was explored at least as early as the 1950's for streptomycin ablation treatment of vertigo associated with Meniere's disease [160]. This study showed that vestibular function could be attenuated, but a majority of test cases lost all cochlear function. It appears that interest in intratympanic drug delivery did not substantially accelerate until the 1990's, although there were earlier large-scale efforts underway, e.g. Sakata's study of dexamethasone treatment for tinnitus [161]. Intratympanic delivery is now the most frequently used first-line treatment for the vertigo of Meniere's disease [82]. The methods for and uses of intratympanic drug delivery are sufficiently numerous that review articles have been dedicated to the topic [43, 79, 82, 162]. Treatments have expanded beyond those initially performed for vertigo, and now include perfusion methods to treat SSNHL, AIED, tinnitus, and the hearing loss associated with Meniere's Disease. The compounds tested are numerous and include aminoglycosides, corticosteroids, glutamate receptor antagonists, protease inhibitors, antioxidants, and neurotrophins [95, 163]. The specific methods for intratympanic infusion are varied. Direct infusion via syringe was successfully used to treat patients 3-5 times per day in a study where gentamicin resolved vertigo in Meniere's Disease as long as 25 years after therapy started in greater than 90% of cases [164]. The residence time of drugs delivered by this method of direct infusion can be increased by placing Gelfoam [162], fibrin glue [165], or other compounds at the round window, thereby increasing the likelihood of sustained diffusion into the cochlea across the membrane. Device development efforts have focused on at least two goals: the ability to improve the likelihood of delivering compound directly to the round window niche and the capability for either continuous or multi-dose drug administration, in some cases self-administered. Concentration of drug delivered and residence time at the niche site are affected not only by the exact placement of the infusion line but also by residual fluid in the middle ear and the patency of the Eustachian tube. Numerous devices which can

be used for sustained release or multi-dose delivery have been developed in attempts to overcome the shortcomings of direct transtympanic injection. These include the Silverstein MicroWick (Micromedics, Eaton, MN), the Round Window Microcatheter or μ Cath™ (Durect Corp. Cupertino, CA) in conjunction with an electronically controlled pump, the Alzet osmotic pump (Durect Corp. Cupertino, CA) and other devices still in earlier stages of development. While these devices are sufficiently promising to warrant further study and development, the clinical results achieved by intratympanic delivery have to date been mixed. Despite demonstrations that higher concentrations of medication can be delivered to the cochlea, and that side effects are either completely alleviated or dramatically reduced as compared with systemic delivery methods [166], there are still major impediments to controlled, repeatable intratympanic drug delivery. As described earlier, anatomical variations can significantly alter the pathway from the delivery site to the round window. These include extraneous or false membranes, fibrous tissue and fatty plugs, and may be present in as high as one third of all patients [167]. In addition, there is a need for better characterization of pharmacokinetics in both the inner and middle ear. While substantial progress has been made on this front, particularly by Salt and Plontke [168-170], the inability to define consistent and accurate methods (or the lack of broad acceptance of such methods) for withdrawal and analysis of fluid samples taken from the inner ear during preclinical animal studies substantially impedes progress [43]. Certainly most reported clinical results do not include measurements of drug concentration at the round window or other quantities like middle ear fluid clearance rate that might be used to infer an approximate concentration. Even in preclinical animal experiments, measurement of cochlear concentrations is difficult. The need for continued development of improved methods for quantifying drug concentration in both the middle and inner ear is clear. Combined approaches, for example Hashimoto's combination of hearing test and subsequent morphologic examination of hair cell death [171] appear promising. Ultimately it appears as though wide acceptance of a particular device or method may require the development of measurement techniques that provide data which permits evaluation of drug delivery and treatment outcome against a pharmacokinetic model.

2.5.1.2.1 Round Window Microcatheter

The Round Window Microcatheters (μ -Cath™ and e-Cath™) were developed by IntraEAR and later acquired by Durect in 1999. While they have been used for a wide variety of applications in both human and animal studies, Durect discontinued sales of these devices in September 2003 due to a change in business focus (2003 Form 10-K SEC filing) and subsequently entered into a licensing

agreement with Neurosystem in the area of local drug delivery to the middle or inner ear for tinnitus (2004 Form 10-Q Ex.-10.39 SEC filing). The μ -Cath™ has two lumens, one for infusion and one for fluid withdrawal, and the e-Cath™ has a third lumen with electrode for monitoring ear signals. The microcatheter has a bulbous tip of 1.5, 2.0 or 2.5 mm diameter. General anesthesia is typically required to produce a tympanomeatal flap through which the round window niche is exposed. The tip of the catheter system is compressible and is designed specifically to lock in place in the round window bony niche. In theory, a variety of pumping methods can be used to infuse the catheter, but frequently pumps developed for wearable insulin dispensing (e.g. Disetronics pumps from Roche) are used because their size provides the portability required for extended treatment protocols [85]. As described earlier, anatomical variation can produce variability in the quantity of drug actually delivered to the cochlea. At least one effort has been made to formalize the surgical procedure for Microcatheter implantation, advise the use of a transtympanic endoscope, and identify likely complications [146, 172].

Human treatment studies are numerous and with varied results. As an example, Seidman reported preliminary data from a nine patient study using gentamicin for vertigo, methylprednisolone for SSNHL, papaverine and methylprednisolone for mild labyrinthitis and the glutamate antagonist magnesium sulfate for tinnitus [163, 173]. Improvements in vertigo, hearing and tinnitus were recorded for a majority of the patients. Methylprednisolone steroid infusion for 8-10 days was used to treat six patients with SSNHL, with measurable hearing improvement achieved in all patients [174].

Numerous animal studies have also been performed in an effort to understand pharmacokinetics using this delivery method. Two radioactively labeled antioxidants (D-methionine and thiourea) were administered for 1 hr in rat ears and elimination half-lives in the cochlea were found to be less than 1 hr for both compounds [175]. Ototoxic kanamycin was used in guinea pigs with differing concentration and delivery time intervals [171]. Outer hair cell disappearance rates were quantified as a function of position through the basal and second turn of the cochlea. As expected, large outer hair cell disappearance rates correlated with high delivery concentrations and longer delivery intervals, and much lower total quantities of compound were required to achieve a specific level of outer hair cell disappearance as compared to systemic delivery.

2.5.1.2.2 Silverstein MicroWick™

The primary use for the MicroWick in humans since its first description [176] has been the treatment of Meniere's related vertigo by perfusion of gentamicin. The polyvinyl acetate wick (1 mm

diameter by 9 mm length) absorbs medication administered external to the ear and transports it directly to the RWM. The wick is inserted through a ventilation tube which passes through the ear drum via myringotomy or laser tympanostomy. The insertion procedure requires only local anesthesia and a noncertified office surgery room. Patients are able to self-administer medication, and hearing and vestibular functional tests are used for appropriate medication titration and therapy discontinuation. A typical administration protocol requires three fifteen minute sessions per day using from 5 to 10 mg/ml gentamicin for one to three weeks. The MicroWick has also been used to administer dexamethasone for the treatment of SSNHL and AIED [176, 177]. While quantitative studies of drug concentration in the cochlea have not been published to our knowledge, therapeutic effect has been shown [82]. Complications include the removal of middle ear plugs or extraneous membranes prior to wick insertion, extrusion of the vent tube, and the administration of topical antibiotics (in the case of steroid infusion). Finally, the MicroWick has also been implemented as a delivery tool in numerous animal studies aimed at understanding pharmacokinetics. Chinchilla ears were perfused with gentamicin (10 mg/ml) to characterize hearing loss over time [178]. However, we know of no reported quantification of the MicroWick's effective delivery rate of drug as a function of time.

2.5.1.2.3 Preclinical Alzet osmotic pump

The implantable Alzet osmotic pump provides the means for continuous sustained delivery in a very small volume with simple form factor. This preclinical device was developed by ALZA Corporation and is now commercially available through Durect Corporation. The pump has reservoir volumes of 100 μ L, 200 μ L or 2 mL and flow rates ranging from 0.11 to 10 μ L/hr. The device can be configured with a microcatheter or other infusion cannula and implanted in small animals such as guinea pigs and other rodents. Typically, access to the RWM occurs through a drilled hole in the bulla, and the pump is implanted subcutaneously [16]. Depending on the model, these pumps provide continuous infusion ranging from 1 day to 6 weeks; however, they provide no capability to change delivery rates in situ. The pump operates with a semi-permeable outer membrane surrounding an osmotic driving agent. Within the agent compartment, an impermeable reservoir holds the drug. As water flows into the compartment holding the osmotic agent, pressure is exerted on the flexible drug reservoir, and the drug is forced out through the delivery port [179]. These systems have been widely used for middle and inner ear drug delivery as described in Section 4.

2.5.1.2.4 Other systems

A miniaturized fully-implanted device for discontinuous drug delivery has been evaluated for animals. The Totally Implantable Drug Delivery System (TI-DDS[®]) is implanted subcutaneously and dispenses 5 to 10 μ L of fluid via push button and can be refilled transcutaneously [180, 181]. We have not found publicized descriptions dated later than 2001 and are thus unclear on the status of development of this promising device.

2.5.2 Intracochlear drug delivery

A second local delivery approach for the inner ear is intracochlear delivery. A variety of tools including syringes, osmotic pumps, and other newer devices have been employed. Access is created via a cochleostomy through the RWM or directly through the otic capsule.

2.5.2.1 Syringe delivery

A simple method of delivering therapeutics directly into the inner ear is with a syringe. Direct injections and perfusions have been used in the clinical setting as well as in research. They allow for study of pharmaceutical effects without the added complications of more advanced delivery systems. However, direct injections do not allow for prolonged delivery.

Currently the only clinical use of direct intracochlear injection is in conjunction with cochlear prosthesis implantation. Cochlear prosthesis implantation has been shown to elicit an inflammatory response. As reported by De Ceulaer et al., at the time of prosthesis insertion, a single dose of steroid was placed in the cochlea with a syringe. The treatment resulted in reduced reactive fibrosis that is usually caused by tissue insult. In general, fibrosis leads to increased impedance of the electrode which decreases electrode performance. The steroid injection was done to maintain optimal performance of the implant through reduced tissue growth [182]. Similarly, a direct injection of triamcinolone immediately prior to insertion of the electrode array reduced electrode impedance for 5-10 days post-surgery. The improvement was more pronounced at basal contacts than apical contacts showing an uneven distribution of steroid along the scala tympani [183].

2.5.2.2 Direct injection

Direct injection is a useful tool for researchers to study the effects of novel therapies for the inner ear [184, 185]. Stover et al. tested the use of adenovirus for gene transfer of reporter gene

though both the round window and cochleostomy. The round window was injected with a 5 μ L bolus using a 30 gauge needle, and a cannula was sealed in the cochleostomy to facilitate delivery. The cochleostomy delivery route resulted in better distribution throughout the cochlea and a higher degree of transfection [186]. Similarly, liposomes with plasmid DNA were injected via the RWM to test them as alternatives to viral vectors. Gene expression persisted for 14 days without evidence of inflammation [159]. Other work has been done to deliver agents to reduce damage in the inner ear, such as D-JNKI-1 to block the apoptotic cascade or glutamate antagonists to block firing of inner hair cell afferents [185, 187].

2.5.2.3 Syringe pump delivery

A variation on the direct injection method involves sealing a cannula into the cochlea and employing a syringe pump for drug infusion, usually with an outlet hole placed in the apex [188]. While the pump allows for continued delivery and can be easily programmed for constant infusion, it can only be used for acute animal experiments while the subject remains under anesthesia. In developing a surgical technique for delivery to the mouse cochlea, a syringe pump was used to deliver agents to confirm maintenance of hearing during surgery [189]. Also useful in pharmacokinetic studies, ions and microspheres can be delivered for tissue labeling and concentration studies [190, 191].

2.5.2.4 Osmotic pump delivery

Initial tests were used to show the effectiveness and safety of delivery by osmotic pump. The device delivered the toxin, TTX, for three days [16], and later experiments improved on cannula materials and sealing [192]. Carvalho et al. used the pump to deliver artificial perilymph to show the effect of cochleostomy and infusion on hearing. ABR was tested at 3 and 7 days after implantation, and results showed some threshold shifts at high frequency while low frequency hearing was preserved [193].

The osmotic pump has proven useful in testing a variety of compounds for many applications including otoprotection and neural preservation, as it offers a controlled delivery profile and proven surgical technique. Steroids have been administered at the time of cochlear prosthesis implantation to protect the cochlea from electrode insertion trauma [194] and at the time of ototoxic antibiotic exposure to prevent hair cell death [75].

Osmotic pumps were employed to test the effectiveness of steroid treatment to prevent hearing loss from noise trauma. The devices allowed for a dosage study of pre- and post-treatment with dexamethasone for noise exposure, and histology showed less hair cell loss than in untreated cochleae [49]. A similar study showed that 7 day infusion of steroid following impulse noise trauma resulted in no significant threshold difference after 14 days [50].

In order to study the ototoxicity of cisplatin chemotherapy treatment, researchers have utilized osmotic pumps to infuse various doses of cisplatin and record the increase in hearing thresholds [63]. To counter the damage to hair cells inflicted by cisplatin, STS was infused using the Alzet pump with a glass cannula [72]. STS protects the hair cells from death when given in combination with cisplatin. However, the local delivery afforded by the osmotic pump is essential, as the STS would inactivate the cisplatin throughout the body if dosed systemically. Other compounds have been investigated to block signaling events in the apoptotic pathway started by cisplatin ototoxicity [195].

Osmotic pumps allow testing of novel therapies such as growth factors for various applications. Neurotrophins, such as BDNF, have been studied as treatments to preserve neurons in deafened ears. This has implication in the degree of success a patient would achieve using a cochlear implant. Several studies continued to deliver neurotrophic factors for two to four weeks after deafening, and these therapies show increased survival of SGN in the inner ear [102, 104, 196-198].

The pump is being used to test other compounds such as D-JNKI-1, a peptide inhibitor of the apoptotic pathway, and BN82270, a peroxidation inhibitor to reduce free radical production, for their protective effects on the cochlea. BN82270, delivered into the cochlea via osmotic pump prior to trauma, was used to prevent damage from NIHL [199]. The application of D-JNKI-1 to rescue hair cells from aminoglycoside antibiotic ototoxicity or NIHL resulted in protection from both types of damage. In this study, the cochlea was perfused for seven days beginning two days after exposure [60].

2.5.2.5 Cochlear prosthesis-based delivery

Since the introduction of cochlear prostheses, researchers have worked to continuously improve their effectiveness in providing enhanced auditory function to patients. Cochlear implants stimulate the auditory neurons in the cochlea through an electrode inserted into the scala tympani. Hearing loss that causes patients to receive implants causes the continued degradation of neurons which can reduce the effectiveness of the electrodes. Evidence suggests the application of drugs in combination with the electrode can lead to better outcomes (reviewed in [200, 201]). By combining a drug delivery platform

with the implant electrode, drugs such as neurotrophic factors may prevent further auditory degradation and maintain the number of surviving nerve fibers, thus improving the effectiveness of cochlear implants for long-term use [202]. In addition, steroids and other compounds could be used to prevent tissue growth on the electrode to keep impedance and, thus, power requirements low [203].

Med-El is a cochlear implant company investigating the combination of drug delivery with a prosthesis. Their development effort includes an electrode with a fluid channel connected to an infusion pump with outlets that allow delivery of drug into the basal turn. Cross-turn diffusion would supply the apical regions of the cochlea [203]. Cochlear, Ltd. is another cochlear implant company investigating drug delivery combined with the prosthesis [204].

Significant work has gone into testing these devices on the bench top prior to study in a guinea pig. Dyes were used to visualize the flow and delivery through the electrode platform and ensure patency, and various numbers and locations of openings in the fluid channel were tested to optimize the delivery profile [203-205]. Multiple openings led to the fastest distribution in a plastic cochlea model [206].

Testing in guinea pigs began with a standard electrode having polyimide tubing running through its center to an osmotic pump. The electrode was inserted through the round window and delivered 200 μ L of drug over 28 days. Using neomycin, an ototoxic antibiotic, as a model compound, the assembly remained operational for the full delivery duration and showed minimal tissue response [18]. In a study using therapeutic agent BDNF designed to protect neurons for 28 days, results showed reduced hearing thresholds when compared to control [106].

2.5.2.6 Other delivery devices

Multiple pumping devices are in development, including a micro-injector and a reciprocating drug delivery device. Kingma et al. created a micro-injector from a syringe fitted with a screw to regulate the infused volume of drug for a chronic animal study. The cannula remained implanted allowing for daily injections of a toxin for 8 to 14 days [17].

Chen et al. have reported on a reciprocating drug delivery system [19]. The microfluidic device is being developed for use as an implantable long-term infusion system for a variety of drug types. The device uses a reciprocating fluidic system with one cannula directly implanted in the scala tympani that acts as both the inlet and outlet. The drug concentrated in this fluid diffuses and mixes with the

perilymph in the scala tympani. During withdrawal, the same volume of less concentrated fluid is returned to the device. This pulsatile method may protect the sensitive hair cells from damaging changes in cochlear volume and pressure while also creating a net increase in drug concentration. The electronically-controlled device provides for precise control of delivery volumes, delivery of multiple therapeutics, and timed, sequenced delivery that can be altered as indicated [19, 207].

2.6 CONCLUDING REMARKS

As treatment options improve for many inner ear diseases and injuries, methods for delivering precise and controlled doses become vital. Researchers in the field of inner ear drug delivery will continue to advance new and existing techniques that will support the arrival of better and better therapeutic compounds. Those suffering from hearing related disorders can look forward to improved quality of life as the field progresses.

Rights were reserved to reprint portions of this chapter from: Swan, E., et al., *Inner ear drug delivery for auditory applications*. Adv Drug Del Rev, 2008. **60**: p. 1583-1599.

2.7 REFERENCES

1. Juhn, S., *Barrier systems in the inner ear*. Acta Otolaryngol Suppl, 1988. **458**: p. 79-83.
2. Juhn, S. and L. Rybak, *Labyrinthine barriers and cochlear homeostasis*. Acta Otolaryngol, 1981. **91**: p. 529-534.
3. McCabe, B.F., *Autoimmune inner ear disease: therapy*. Am J Otol, 1989. **10**: p. 196-197.
4. Moskowitz, D., K.J. Lee, and H.W. Smith, *Steroid use in idiopathic sudden sensorineural hearing loss*. Laryngoscope, 1984. **94**: p. 664-666.
5. Wilson, W.R., F.M. Byl, and N. Laird, *The efficacy of steroids in the treatment of idiopathic sudden hearing loss. A double-blind clinical study*. Arch Otolaryngol, 1980. **106**: p. 772-776.
6. Parnes, L.S., A.-H. Sun, and D.J. Freeman, *Corticosteroid pharmacokinetics in the inner ear fluids: an animal study followed by clinical application*. The Laryngoscope, 1999. **109**(7 Pt 2): p. 1-17.
7. Holley, M.C., *Application of new biological approaches to stimulate sensory repair and protection*. Br Med Bull, 2002. **63**: p. 157-169.
8. Ryan, A.F., et al., *Immunological damage to the inner ear: current and future therapeutic strategies*. Adv Otorhinolaryngol, 2002. **59**: p. 66-74.

9. Shinohara, T., et al., *Neurotrophic factor intervention restores auditory function in deafened animals*. PNAS, 2002. **99**(3): p. 1657-1660.
10. Kanazaki, S., et al., *Glial cell line-derived neurotrophic factor and chronicelectrical stimulation prevent VIII cranial nerve degeneration following denervation*. J Comp Neurol, 2002. **454**: p. 350-360.
11. Lalwani, A., et al., *In vitro and in vivo assessment of the ability of adeno-associated virus-brain-derived neurotrophic factor to enhance spiral ganglion cell survival following ototoxic insult*. Laryngoscope, 2002. **112**: p. 1325-1334.
12. Schuknecht, H.F., *Ablation therapy for the relief of Meniere's disease*. Laryngoscope, 1956. **66**: p. 859-870.
13. Salt, A.N. and P.E. Stopp, *The effect of cerebrospinal fluid pressure on perilymphatic flow in the opened cochlea*. Acta Otolaryngol, 1979. **88**: p. 198-202.
14. Nuttall, A.L., M.J. LaRouere, and M. Lawrence, *Acute perilymphatic perfusion of the guinea pig cochlea*. Hear Res, 1982. **6**: p. 207-221.
15. Tonndorf, J., A.J. Duvall, and J.P. Reneau, *Permeability of intracochlear membranes to various vital stains*. Ann Otol Rhinol Laryngol, 1962. **71**: p. 801-841.
16. Brown, J.N., et al., *Osmotic pump implant for chronic infusion of drugs into the inner ear*. Hear Res, 1993. **70**: p. 167-172.
17. Kingma, G.G., J.M. Miller, and M.W. Myers, *Chronic drug infusion into the scala tympani of the guinea pig cochlea*. J Neurosci Methods, 1992. **45**: p. 127-134.
18. Shepherd, R.K. and J. Xu, *A multichannel scala tympani electrode array incorporating a drug delivery system for chronic intracochlear infusion*. Hear Res, 2002. **172**: p. 92-98.
19. Chen, Z., et al., *Inner Ear drug delivery via a reciprocating perfusion system in the guinea pig*. J Control Release, 2005. **110**: p. 1-19.
20. Schuknecht, H., *Pathology of the Ear*. 1993, Malvern, PA: Lea and Febiger.
21. Medina, J. and D. Drescher, *The amino-acid content of perilymph and cerebrospinal fluid from guinea-pigs and the effect of noise on the amino-acid composition of perilymph*. Neuroscience, 1981. **6**: p. 505-509.
22. Scheibe, F. and H. Haupt, *Biochemical differences between perilymph, cerebrospinal fluid and blood plasma in the guinea pig*. Hear Res, 1985. **17**: p. 61-66.
23. Thalmann, I., et al., *Protein profile of human perilymph: in search of markers for the diagnosis of perilymph fistula and other inner ear disease*. Otolaryngol Head Neck Surg, 1994. **111**(3): p. 273-280.

24. Thalmann, I., et al., *High resolution two-dimensional electrophoresis: technique and potential applicability to the study of inner ear disease*. Am J Otol, 1995. **16**(2): p. 153-157.
25. Thalmann, R., T. Comegys, and I. Thalmann, *Amino acid profiles in inner ear fluids and cerebrospinal fluid*. Laryngoscope, 1982. **92**: p. 321-328.
26. Igarashi, M., K. Ohashi, and M. Ishii, *Morphometric comparison of endolymphatic and perilymphatic spaces in human temporal bones*. Acta Otolaryngol, 1986. **101**: p. 161-164.
27. Jahnke, K., *The fine structure of freeze-fractured intercellular junctions in the guinea pig inner ear*. Acta Otolaryngol Suppl, 1975. **336**: p. 1-40.
28. Axelsson, A. and A.F. Ryan, *Circulation of the inner ear: I. Comparative study of the vascular anatomy in the mammalian cochlea*, in *Physiology of the Ear*, Santos-Sacchi, Editor. 1988, Raven Press: New York. p. 295-316.
29. Kimura, R. and C. Ota, *Ultrastructure of the cochlear blood vessels*. Acta Otolaryngol, 1974. **77**: p. 231-250.
30. Hara, A., A.N. Salt, and R. Thalmann, *Perilymph composition in scala tympani of the cochlea: influence of cerebrospinal fluid*. Hear Res, 1989. **42**: p. 265-272.
31. Gopen, Q., J. Rosowski, and S. Merchant, *Anatomy of the normal human cochlear aqueduct with functional implications*. Hear Res, 1997. **107**: p. 9-22.
32. Rask-Andersen, H., et al., *Perilymph/modiolar communication routes in the human cochlea*. Ear Hear, 2006. **27**: p. 457-465.
33. Sterkers, O., E. Ferrary, and C. Amiel, *Production of inner ear fluids*. Physiol Rev, 1988. **68**: p. 1083-1128.
34. Wangemann, P. and J. Schacht, *Homeostatic mechanisms in the cochlea*, in *The Cochlea*, P. Dallos, A. Popper, and R. Fay, Editors. 1996, Springer-Verlag: New York. p. 130-185.
35. Zou, J., et al., *In vivo observation of dynamic perilymph formation using 4.7 T MRI with gadolinium as a tracer*. Acta Otolaryngol, 2003. **123**: p. 910-915.
36. Shepherd, R. and M. Colreavy, *Surface microstructure of the perilymphatic space: implications for cochlear implants and cell- or drug-based therapies*. Arch Otolaryngol Head Neck Surg, 2004. **130**(5): p. 518-523.
37. Schuknecht, H. and A. Seifi, *Experimental Observations on the Fluid Physiology of the Inner Ear*. Ann Otol Rhinol Laryngol, 1963. **72**: p. 687-712.
38. Thalmann, I., et al., *Protein profiles of perilymph and endolymph of the guinea pig*. Hear Res, 1992. **63**: p. 37-42.

39. Salt, A.N., *Pharmacokinetics of drug entry into cochlear fluids*. *Volta Rev*, 2005. **105**(3): p. 277-298.
40. Salt, A.N., *Simulation of methods for drug delivery to the cochlear fluids*. *Adv Otorhinolaryngol*, 2002. **59**: p. 140-148.
41. Salt, A.N., K. Ohyama, and R. Thalmann, *Radial communication between the perilymphatic scalae of the cochlea. I Estimation by tracer perfusion*. *Hear Res*, 1991. **56**: p. 29-36.
42. Salt, A.N., K. Ohyama, and R. Thalmann, *Radial communication between the perilymphatic scalae of the cochlea. II Estimation by bolus injection of tracer into the sealed cochlea*. *Hear Res*, 1991. **56**: p. 37-43.
43. Salt, A.N. and S.K.R. Plontke, *Local inner-ear drug delivery and pharmacokinetics*. *Drug Discov Today*, 2005. **10**(19): p. 1299-1306.
44. Juhn, S., Y. Hamaguchi, and M. Goycoolea, *Review of round window membrane permeability*. *Acta Otolaryngol Suppl*, 1989. **457**: p. 43-48.
45. Goycoolea, M. and L. Lundman, *Round window membrane, structure function and permeability: a review*. *Microsc Res Tech*, 1997. **36**: p. 201-211.
46. Ohyama, K., A.N. Salt, and R. Thalmann, *Volume flow rate of perilymph in the guinea pig cochlea*. *Hear Res*, 1988. **35**: p. 119-130.
47. Lynch, E.D. and J. Kil, *Compounds for the prevention and treatment of noise-induced hearing loss*. *Drug Discov Today*, 2005. **10**(19): p. 1291-1298.
48. Henderson, D., et al., *The role of antioxidants in protection from impulse noise*. *Ann N Y Acad Sci*, 1999. **28**: p. 368-380.
49. Takemura, K., et al., *Direct inner ear infusion of dexamethasone attenuates noise-induced trauma in guinea pig*. *Hear Res*, 2004. **196**: p. 58-68.
50. Sendowski, I., et al., *Therapeutic efficacy of intra-cochlear administration of methylprednisolone after acoustic trauma caused by gunshot noise in guinea pigs*. *Hear Res*, 2006. **221**: p. 119-127.
51. Uemaetomari, I., et al., *Protective effect of calcineurin inhibitors on acoustic injury of the cochlea*. *Hear Res*, 2005. **209**: p. 86-90.
52. Coleman, J.K.M., et al., *Pharmacological rescue of noise induced hearing loss using N-acetylcysteine and acetyl-L-carnitine*. *Hear Res*, 2007. **226**: p. 104-113.
53. Campbell, K.C.M., et al., *Prevention of noise- and drug-induced hearing loss with D-methionine*. *Hear Res*, 2007. **226**: p. 92-103.

54. Darrat, I., et al., *Auditory research involving antioxidants*. *Curr Opin Otolaryngol Head Neck Surg*, 2007. **15**(358-363).
55. Duan, M., et al., *Low-dose, long-term caroverine administration attenuates impulse noise-induced hearing loss in the rat*. *Acta Otolaryngol*, 2006. **126**: p. 1140-1147.
56. Iwai, K., et al., *Cochlear protection by local insulin-like growth factor-1 application using biodegradable hydrogel*. *Laryngoscope*, 2006. **116**: p. 529-533.
57. Shoji, F., et al., *Differential protective effects of neurotrophins in the attenuation of noise-induced hair cell loss*. *Hear Res*, 2000. **146**: p. 134-142.
58. Coleman, J.K.M., et al., *AM-111 protects against permanent hearing loss from impulse noise trauma*. *Hear Res*, 2007. **226**: p. 70-78.
59. Harris, K.C., et al., *Prevention of noise-induced hearing loss with Src-PTK inhibitors*. *Hear Res*, 2005. **208**: p. 14-25.
60. Wang, J., et al., *A peptide inhibitor of c-Jun n-terminal kinase protects against both aminoglycoside and acoustic trauma-induced auditory hair cell death and hearing loss*. *J Neurosci*, 2003. **23**(24): p. 8596-8607.
61. Rybak, L.P. and C.A. Whitworth, *Ototoxicity: therapeutic opportunities*. *Drug Discov Today*, 2005. **10**(19): p. 1313-1321.
62. Wanamaker, H., *Perfusion of the inner ear: basic science considerations*. *Curr Opin Otolaryngol Head Neck Surg*, 2001. **9**: p. 329-332.
63. O'Leary, S.J., et al., *Perilymphatic application of cisplatin over several days in albino guinea pigs: dose-dependency of electrophysiological and morphological effects*. *Hear Res*, 2001. **154**: p. 135-145.
64. Rybak, L., *Mechanisms of cisplatin ototoxicity and progress in ototprotection*. *Curr Opin Otolaryngol Head Neck Surg*, 2007. **15**: p. 364-369.
65. Rybak, L.P. and V. Ramkumar, *Ototoxicity*. *Kidney Int*, 2007. **72**: p. 931-935.
66. Lefebvre, P.P., et al., *Pharmacologic treatment of inner ear: from basic science to the patient*. *Acta Otorhinolaryngol Belg*, 2002. **56**: p. 45-49.
67. Sergi, B., et al., *The role of antioxidants in protection from ototoxic drugs*. *Acta Otolaryngolog Suppl*, 2004. **552**: p. 42-45.
68. Li, G., et al., *Round window membrane delivery of L-methionine provides protection from cisplatin ototoxicity without compromising chemotherapeutic efficacy*. *Neurotox*, 2001. **22**: p. 163-176.

69. Wimmer, C., et al., *Round window application of D-methionine, sodium thiosulfate, brain-derived neurotrophic factor, and fibroblast growth factor-2 in cisplatin-induced ototoxicity*. *Otol Neurotol*, 2004. **25**: p. 33-40.
70. Ekborn, A., et al., *Intracochlear administration of thiourea protects against cisplatin-induced outer hair cell loss in the guinea pig*. *Hear Res*, 2003. **181**: p. 109-115.
71. Rybak, L.P., et al., *Mechanisms of cisplatin-induced ototoxicity and prevention*. *Hear Res*, 2007. **226**: p. 157-167.
72. Wang, J., et al., *Local application of sodium thiosulfate prevents cisplatin-induced hearing loss in the guinea pig*. *Neuropharmacology*, 2003. **45**: p. 380-393.
73. Stocks, R.M.S., et al., *Ototoxic protection of sodium thiosulfate: daily vs constant infusion*. *Otolaryngol Head Neck Surg*, 2004. **131**(1): p. 115-119.
74. Hochman, J., et al., *Prevention of aminoglycoside-induced sensorineural hearing loss*. *J Otolaryngol*, 2006. **35**(3): p. 153-156.
75. Himeno, C., et al., *Intra-cochlear administration of dexamethasone attenuates aminoglycoside ototoxicity in the guinea pig*. *Hear Res*, 2002. **167**: p. 61-70.
76. Bhandare, N., et al., *Ototoxicity after radiotherapy for head and neck tumors*. *Int J Radiat Oncol Biol Phys*, 2007. **67**(2): p. 469-479.
77. Jereczek-Fossa, B.A., et al., *Radiotherapy-induced ear toxicity*. *Cancer Treat Rev*, 2003. **29**: p. 417-430.
78. Ye, Q., et al., *Application of a corticosteroid (Triamcinolon) protects inner ear function after surgical intervention*. *Ear Hear*, 2007. **28**(3): p. 361-369.
79. Light, J. and H. Silverstein, *Transtympanic perfusion: indications and limitations*. *Curr Opin Otolaryngol Head Neck Surg*, 2004. **12**: p. 378-383.
80. Mosnier, I., D. Bouccara, and O. Sterkers, *Management of idiopathic sudden sensorineural hearing loss*. *Otorhinolaryngol Nova*, 1999. **9**: p. 217-223.
81. Hoffmann, K.K. and H. Silverstein, *Inner ear perfusion: indications and applications*. *Curr Opin Otolaryngol Head Neck Surg*, 2003. **11**: p. 334-339.
82. Jackson, L.E. and H. Silverstein, *Chemical perfusion of the inner ear*. *Otolaryngol Clin North Am*, 2002. **35**: p. 639-653.
83. Chandrasekhar, S.S., *Intratympanic dexamethasone for sudden sensorineural hearing loss: clinical and laboratory evaluation*. *Otol Neurotol*, 2001. **22**: p. 18-23.

84. Plontke, S.K., et al., *Outcomes research analysis of continuous intratympanic glucocorticoid delivery in patients with acute severe to profound hearing loss: basis for planning randomized controlled trials*. *Acta Otolaryngol*, 2005. **125**(8): p. 830-839.
85. Kopke, R.D., et al., *Targeted topical steroid therapy in sudden sensorineural hearing loss*. *Otol Neurotol*, 2001. **22**: p. 475-479.
86. Plaza, G. and C. Herraiz, *Intratympanic steroids for treatment of sudden hearing loss after failure of intravenous therapy*. *Otolaryngol Head Neck Surg*, 2007. **137**: p. 74-78.
87. Gianoli, G.J. and J.C. Li, *Transtympanic steroids for treatment of sudden hearing loss*. *Otolaryngol Head Neck Surg*, 2001. **125**(3): p. 142-146.
88. Dallan, I., et al., *Transtympanic steroids as a salvage therapy in sudden hearing loss: preliminary results*. *ORL J Otorhinolaryngol Relat Spec*, 2005. **68**: p. 247-252.
89. Rauch, S., *Intratympanic steroids for sensorineural hearing loss*. *Otolaryngol Clin North Am*, 2004. **37**: p. 1061-1074.
90. Haynes, D.S., et al., *Intratympanic dexamethasone for sudden sensorineural hearing loss after failure of systemic therapy*. *Laryngoscope*, 2007. **117**: p. 3-15.
91. Battista, R., *Intratympanic dexamethasone for profound idiopathic sudden sensorineural hearing loss*. *Otolaryngol Head Neck Surg*, 2005. **132**(6): p. 902-905.
92. Ryan, A.F., J.P. Harris, and E.M. Keithley, *Immune-mediated hearing loss: basic mechanisms and options for therapy*. *Acta Otolaryngol Suppl*, 2002. **548**: p. 38-43.
93. Yang, G.S.Y., et al., *Intratympanic immunosuppressives for prevention of immune-mediated sensorineural hearing loss*. *Am J Otol*, 2000. **21**: p. 499-504.
94. Matteson, E.L., et al., *Autoimmune inner ear disease: diagnostic and therapeutic approaches in a multidisciplinary setting*. *J Am Acad Audiol*, 2003. **14**(4): p. 225-230.
95. Richardson, R.T., F. Noushi, and S. O'Leary, *Inner ear therapy for neural preservation*. *Audiol Neurootol*, 2006. **11**: p. 343-356.
96. Beck, D.L., *Hair cells: review, regeneration and protection*. *Oticon Clinical Update*, 2007. **1**: p. 14.
97. Kuang, R., et al., *Glial cell line-derived neurotrophic factor. Potential for otoprotection*. *Ann N Y Acad Sci*, 1999. **28**(884): p. 128-137.
98. Lopez, I., et al., *The protective effect of brain-derived neurotrophic factor after gentamicin ototoxicity*. *Am J Otol*, 1999. **20**(3): p. 317-324.
99. Oestreicher, E., et al., *Neurotrophin 3 potentiates glutamatergic responses of IHC afferents in the cochlea in vivo*. *Eur J Neurosci*, 2000. **12**(5): p. 1584-90.

100. Gillespie, L.N., G.M. Clark, and M. Phillip, *Delayed neurotrophin treatment supports auditory neuron survival in deaf guinea pigs*. Neuroreport, 2004. **15**(7): p. 1121-1125.
101. Gluekert, R., et al., *Deafferentation-associated changes in afferent and efferent processes in the guinea pig cochlea and afferent regeneration with chronic intrascalar brain-derived neurotrophic factor and acidic fibroblast growth factor*. J Comp Neurol, 2008. **507**(4): p. 1602-21.
102. Miller, J.M., et al., *Delayed neurotrophin treatment following deafness rescues spiral ganglion cells from death and promotes regrowth of auditory nerve peripheral processes: effects of brain-derived neurotrophic factor and fibroblast growth factor*. J Neurosci Res, 2007. **85**: p. 1959-1969.
103. Maruyama, J., J.M. Miller, and M. Ulfendahl, *Glial cell-line derived neurotrophic factor and antioxidants preserve electrical responsiveness of the spiral ganglion neurons after experimentally induced deafness*. Neurobiol Dis, 2008. **29**: p. 14-21.
104. Gillespie, L.N., et al., *BDNF-induced survival of auditory neurons in vivo: cessation of treatment leads to accelerated loss of survival effects*. J Neurosci Res, 2003. **71**: p. 785-790.
105. Shepherd, C., and Epp, *Neurotrophins and electrical stimulation for protection and repair of spiral ganglion neurons following sensorineural hearing loss*. Hear Res, 2008. **242**(1-2): p. 100-109.
106. Shepherd, R.K., et al., *Chronic depolarization enhances the trophic effects of brain-derived neurotrophic factor in rescuing auditory neurons following a sensorineural hearing loss*. J Comp Neurol, 2005. **486**: p. 145-158.
107. Pau, H. and R.W. Clarke, *Advances in genetic manipulations in the treatment of hearing disorders*. Clin Otolaryngol, 2004. **29**: p. 574-576.
108. Scully, J.L., C. Rippberger, and C. Rehmann-Sutter, *Non-professionals' evaluations of gene therapy ethics*. Soc Sci Med, 2004. **58**: p. 1415-1425.
109. Staeker, H., et al., *Brain-derived neurotrophic factor gene therapy prevents spiral ganglion degeneration after hair cell loss*. Otolaryngol Head Neck Surg, 1998. **119**(1): p. 7-13.
110. Hakuba, N., et al., *Adenovirus-mediated overexpression of a gene prevents hearing loss and progressive inner hair cell loss after transient cochlear ischemia in gerbils*. Gene Ther, 2003. **10**: p. 426-433.
111. Kawamoto, K., et al., *Hearing and hair cells are protected by adenoviral gene therapy with TGF- β 1 and GDNF*. Mol Ther, 2003. **7**(4): p. 484-492.
112. Bowers, W.J., et al., *Neurotrophin-3 Transduction attenuates cisplatin spiral ganglion neuron ototoxicity in the cochlea*. Mol Ther, 2002. **6**(1): p. 12-18.

113. Kawamoto, K., et al., *Antioxidant gene therapy can protect hearing and hair cells from ototoxicity*. *Molecular Therapy*, 2004. **9**(2): p. 173-181.
114. Izumikawa, M., et al., *Auditory hair cell replacement and hearing improvement by Atoh1 gene therapy in deaf mammals*. *Nat Med*, 2005. **11**(3): p. 271-276.
115. Kawamoto, K., et al., *Math1 gene transfer generates new cochlear hair cells in mature guinea pigs in vivo*. *J Neurosci*, 2003. **23**(11): p. 4395-4400.
116. Brown, S.D., R.E. Hardisty-Hughes, and P. Mburu, *Quiet as a mouse: dissecting the molecular and genetic basis of hearing*. *Genetics*, 2008. **9**: p. 277-290.
117. Kesser, B.W., G.T. Hashisaki, and J.R. Holt, *Gene transfer in human vestibular epithelia and the prospects for inner ear gene therapy*. *Laryngoscope*, 2008. **118**(5): p. 821-831.
118. Kudo, T., et al., *Transgenic expression of a dominant-negative connexin26 causes degeneration of the organ of Corti and non-syndromic deafness*. *Hum Mol Genet*, 2003. **12**(9): p. 995-1004.
119. Van Eyken, E., et al., *The contribution of GJB2 (Connexin 26) 35delG to age-related hearing impairment and noise-induced hearing loss*. *Otol Neurotol*, 2007. **28**: p. 970-975.
120. Cohen-Salmon, M., et al., *Targeted ablation of connexin26 in the inner ear epithelial gap junction network causes hearing impairment and cell death*. *Curr Biol*, 2002. **12**(13): p. 1106-11.
121. Maeda, Y., et al., *Cochlear expression of a dominant negative GJB2R75W construct delivered through the round window membrane in mice*. *Neurosci Res*, 2007. **58**: p. 250-254.
122. Hildebrand, M.S., et al., *Advances in molecular and cellular therapies for hearing loss*. *Mol Ther*, 2008. **16**(2): p. 224-236.
123. Staecker, H., et al., *Drug delivery to the inner ear using gene therapy*. *Otolaryngol Clin North Am*, 2004. **37**: p. 1091-1108.
124. Lowenheim, H., et al., *Gene disruption of p27Kip1 allows cell proliferation in the postnatal and adult organ of Corti*. *Proc Nat Acad Sci*, 1999. **96**: p. 4084-4088.
125. Chen, Z.-y., *Cell cycle, differentiation and regeneration*. *Cell Cycle*, 2006. **5**(22): p. 2609-2612.
126. Cheng, A.G., L.L. Cunningham, and E. Rubel, *Mechanisms of hair cell death and protection*. *Curr Opin Otolaryngol Head Neck Surg*, 2005. **13**: p. 343-348.
127. Oliveira, S., G. Storm, and R.M. Schiffelers, *Targeted Delivery of siRNA*. *J Biomed Biotechnol*, 2006. **2006**: p. 1-9.
128. Xie, F.Y., M.C. Woodle, and P.Y. Lu, *Harnessing in vivo siRNA delivery for drug discovery and therapeutic development*. *Drug Discov Today*, 2006. **11**(1/2): p. 67-73.

129. Gary, D.J., N. Puri, and T.-T. Won, *Polymer-based siRNA delivery: perspectives on the fundamental and phenomenological distinctions from polymer-based DNA delivery*. J Control Release, 2007. **121**: p. 64-73.
130. Maeda, Y., et al., *In vitro and in vivo suppression of GJB2 expression by RNA interference*. Hum Mol Genet, 2005. **14**(12): p. 1641-1650.
131. Sellick, P., et al., *A method for introducing non-silencing siRNA into the guinea pig cochlea in vivo*. J Neurosci Methods, 2008. **167**: p. 237-245.
132. Li, H., et al., *Stem cells as therapy for hearing loss*. Trends Mol Med, 2004. **10**(7): p. 309-315.
133. Nakagawa, T. and J. Ito, *Application of cell therapy to inner ear diseases*. Acta Otolaryngol, 2004. **124**(Suppl. 551): p. 6-9.
134. Rejali, D., et al., *Cochlear implants and ex vivo BDNF gene therapy protect spiral ganglion neurons*. Hear Res, 2007. **228**: p. 180-187.
135. Iguchi, F., et al., *Trophic support of mouse inner ear by neural stem cell transplantation*. Neuroreport, 2003. **14**(1): p. 77-80.
136. Parker, M.A., et al., *Neural stem cells injected into the sound-damaged cochlea migrate throughout the cochlea and express markers of hair cells, supporting cells, and spiral ganglion cells*. Hear Res, 2007. **232**: p. 29-43.
137. Coleman, B., et al., *Fate of embryonic stem cells transplanted into the deafened mammalian cochlea*. Cell Transplant, 2006. **15**(5): p. 369-380.
138. Hildebrand, M.S., et al., *Survival of partially differentiated mouse embryonic stem cells in the scala media of the guinea pig cochlea*. J Assoc Res Otolaryngol, 2005. **6**: p. 341-354.
139. Hu, Z., M. Ulfendaho, and N.P. Olivius, *Central migration of neuronal tissue and embryonic stem cells following transplantation along the adult auditory nerve*. Brain Res, 2004. **1026**: p. 68-73.
140. Sakamoto, T., et al., *Fates of mouse embryonic stem cells transplanted into the inner ears of adult mice and embryonic chickens*. Acta Otolaryngol, 2004. **124**(Suppl. 55): p. 48-52.
141. Li, H., et al., *Generation of hair cells by stepwise differentiation of embryonic stem cells*. Proc Nat Acad Sci, 2003. **100**(23): p. 13495-13500.
142. Martinez-Monedero, R., et al., *The potential role of endogenous stem cells in regeneration of the inner ear*. Hear Res, 2007. **22**: p. 48-52.
143. Oshima, K., et al., *Differential distribution of stem cells in the auditory and vestibular organs of the inner ear*. J Assoc Res Otolaryngol, 2007. **8**: p. 18-31.

144. Matsuoka, A., et al., *Enhanced survival of bone-marrow derived pluripotent stem cells in an animal model of auditory neuropathy*. *Laryngoscope*, 2007. **117**: p. 1629-1635.
145. Naito, Y., et al., *Transplantation of bone marrow stromal cells into the cochlea of chinchillas*. *Neuroreport*, 2004. **15**(1): p. 1-4.
146. Plontke, S.K., et al., *Transtympanic endoscopy for drug delivery to the inner ear using a new microendoscope*. *Adv Otorhinolaryngol*, 2002. **59**: p. 149-155.
147. Banerjee, A. and L.S. Parnes, *The biology of intratympanic drug administration and pharmacodynamics of round window drug absorption*. *Otolaryngol Clin North Am*, 2004. **37**: p. 1035-1051.
148. Alzamil, K.S. and F.H.J. Linthicum, *Extraneous round window membranes and plugs: possible effect on intratympanic therapy*. *Ann Otol Rhinol Laryngol*, 2000. **109**(1): p. 30-32.
149. Goycoolea, M., *The round window membrane under normal and pathological conditions*. *Acta Otolaryngol Suppl*, 1992. **493**: p. 43-55.
150. Arnold, W., et al., *Novel slow- and fast-type drug release round-window microimplants for local drug application to the cochlea: an experimental study in guinea pigs*. *Audiol Neurootol*, 2005. **10**: p. 53-63.
151. Pasic, T. and R. EW, *Rapid changes in cochlear nucleus cell size following blockage of auditory nerve electrical activity in gerbils*. *J Comp Neurol*, 1989. **283**: p. 474-480.
152. Noushi, F., et al., *Delivery of neurotrophin-3 to the cochlea using alginate beads*. *Otology & Neurotology*, 2005. **26**: p. 528-533.
153. Albrecht, J., S. Gaudet, and K.F. Jensen. *Rapid free flow isoelectric focusing via novel electrode structures*. in *9th International Conference on Miniaturized Systems for Chemistry and Life Sciences (MicroTAS)*. 2005. Boston.
154. Ito, J., et al., *A new method for drug application to the inner ear*. *ORL J Otorhinolaryngol Relat Spec*, 2005. **67**: p. 272-275.
155. Endo, T., et al., *Novel strategy for treatment of inner ears using a biodegradable gel*. *Laryngoscope*, 2005. **115**: p. 2016-2020.
156. Tamura, T., et al., *Drug delivery to the cochlea using PLGA nanoparticles*. *Laryngoscope*, 2005. **115**: p. 2000-2005.
157. Praetorius, M., et al., *Transsynaptic delivery of nanoparticles to the central auditory nervous system*. *Acta Otolaryngol*, 2007. **127**(5): p. 486-490.
158. Ge, X., et al., *Distribution of PLGA nanoparticles in chinchilla cochleae*. *Otolaryngol Head Neck Surg*, 2007. **137**: p. 619-623.

159. Wareing, M., et al., *Cationic liposome mediated transgene expression in the guinea pig cochlea*. *Hear Res*, 1999. **128**: p. 61-69.
160. Schuknecht, H.F., *Ablation therapy in the management of Meniere's disease*. *Acta Otolaryngol Suppl*, 1957. **132**: p. 3-42.
161. Sakata, Ito, and Itoh, *Clinical experiences of steroid targeting therapy to inner ear for control of tinnitus*. *International Tinnitus J*, 1997. **3**(2): p. 117-121.
162. Blakley, B.W., *Update on Intratympanic Gentamicin for Meniere's Disease*. *Laryngoscope*, 2000. **110**(2): p. 236-240.
163. Seidman, M.D. and T.R. Van de Water, *Pharmacologic manipulation of the labyrinth with novel and traditional agents delivered to the inner ear*. *Ear Nose Throat J*, 2003. **82**(4): p. 276-300.
164. Lange, G., *Transtympanic gentamycin in the treatment of Ménière's disease*. *Rev Laryngol Otol Rhinol (Bord)*, 1995. **116**(2): p. 151-2.
165. Hoffer, M., et al., *Use of sustained release vehicles in the treatment of Meniere's disease*. *Otolaryngol Clin North Am*, 1997. **30**(6): p. 1159-66.
166. Parnes, L.S., A.-H. Sun, and D.J. Freeman, *Corticosteroid pharmacokinetics in the inner ear fluids: an animal study followed by clinical application*. *Laryngoscope*, 1999. **109**(7 Pt 2): p. 1-17.
167. Alzamil, K.S. and F.H. Linthicum Jr., *Extraneous round window membranes and plugs: possible effect on intratympanic therapy*. *Ann Otol Rhinol Laryngol*, 2000. **109**(1): p. 30-32.
168. Salt, A.N. and S.A. Hale. *Longitudinal distribution of drugs in perilymph assessed by cochlear action potentials*. in *28th Mid Winter Research Meeting of the ARO*. 2005.
169. Salt, A.N., S.A. Hale, and S.K. Plontke, *Perilymph sampling from the cochlear apex: a reliable method to obtain higher purity perilymph samples from the scala tympani*. *J Neurosci Methods*, 2005.
170. Salt, A.N. and Y. Ma, *Quantification of solute entry into cochlear perilymph through the round window membrane*. *Hear Res*, 2001. **154**: p. 88-97.
171. Hashimoto, Y., et al., *Pattern of cochlear damage caused by short-term kanamycin application using the round window microcatheter method*. *Acta Otolaryngol*, 2007. **127**: p. 116-121.
172. Plontke, S.K.R., A.W. Wood, and A.N. Salt, *Analysis of gentamicin kinetics in fluids of the inner ear with round window administration*. *Otol Neurotol*, 2002. **23**: p. 967-974.
173. Seidman, M.D., *Glutamate antagonists, steroids, and antioxidants as therapeutic options for hearing loss and tinnitus and the use of an inner ear drug delivery system*. *Int Tinnitus J*, 1998. **4**(2): p. 148-154.

174. Lefebvre, P.P. and H. Staecker, *Steroid Perfusion of the Inner Ear for Sudden Sensorineural Hearing Loss after Failure of Conventional Therapy: A Pilot Study*. *Acta Otolaryngol*, 2002. **122**(7): p. 698-702.
175. Laurell, G., et al., *Local administration of antioxidants to the inner ear: Kinetics and distribution*. *Hear Res*, 2002. **173**: p. 198-209.
176. Silverstein, H., *Use of a new device, the MicroWick, to deliver medication to the inner ear*. *Ear Nose Throat J*, 1999. **78**(8): p. 595-600.
177. Hillman, T.M., M.A. Arriaga, and D.A. Chen, *Intratympanic Steroids: Do They Acutely Improve Hearing in Cases of Cochlear Hydrops?* *Laryngoscope*, 2003. **113**(11): p. 1903-1907.
178. Killian, P. and M. Hoffer, *MicroWick-delivered transtympanic gentamicin: Hearing effects*. *Otolaryngol Head Neck Surg*, 2004. **131**(2): p. 153-4.
179. Theeuwes, F. and S.I. Yum, *Principles of the design and operation of generic osmotic pumps for the delivery of semisolid or liquid drug formulations*. *Ann Biomed Eng*, 1976. **4**(4): p. 343-353.
180. Lehner, R., et al., *A totally implantable drug delivery system for local therapy of the middle and inner ear*. *Ear Nose Throat J*, 1997. **76**(8): p. 567-570.
181. Praetorius, M., et al., *A novel microperfusion system for the long term local supply of drugs to the inner ear: implantation and function in the rat model*. *Audiol Neurotol*, 2001. **6**: p. 250-258.
182. De Ceulaer, G., et al., *Long-term evaluation of the effect of intracochlear steroid deposition on electrode impedance in cochlear implant patients*. *Otol Neurotol*, 2003. **24**: p. 769-774.
183. Paasche, G., et al., *Changes of postoperative impedances in cochlear implant patients: the short-term effects of modified electrode surfaces and intracochlear corticosteroids*. *Otol Neurotol*, 2006. **27**: p. 639-647.
184. Praetorius, M., et al., *Pharmacodynamics of adenovector distribution within the inner ear tissues of the mouse*. *Hear Res*, 2007. **227**: p. 53-58.
185. Oestreicher, E., et al., *New approaches for inner ear therapy with glutamate receptors*. *Acta Otolaryngol*, 1999. **119**: p. 174-178.
186. Stover, T., M. Yagi, and Y. Raphael, *Cochlear gene transfer: round window versus cochleostomy inoculation*. *Hear Res*, 1999. **136**: p. 124-130.
187. Eshraghi, A.A. and T.R. Van de Water, *Cochlear implantation trauma and noise-induced hearing loss: apoptosis and therapeutic strategies*. *Anat Rec*, 2006. **228A**: p. 473-481.
188. Konishi, T. and E. Kelsey, *Effect of sodium deficiency on cochlear potentials*. *J Acoust Soc Am*, 1968. **43**(3): p. 462-470.

189. Chen, Z., et al., *A method for intracochlear drug delivery in the mouse*. J Neurosci Methods, 2006. **150**: p. 67-73.
190. Salt, A.N., et al., *Marker retention in the cochlea following injections through the round window membrane*. Hear Res, 2007. **232**: p. 78-86.
191. Richardson, R.T., et al., *Tracing neurotrophin-3 diffusion and uptake in the guinea pig cochlea*. Hear Res, 2004. **198**: p. 25-35.
192. Prieskorn, D.M. and J.M. Miller, *Technical report: chronic and acute intracochlear infusion in rodents*. Hear Res, 2000. **140**: p. 212-215.
193. Carvalho, G.J. and A.K. Lalwani, *The effect of cochleostomy and intracochlear infusion on auditory brain stem response threshold in the guinea pig*. Am J Otol, 1999. **20**(1): p. 87-90.
194. Eshraghi, A.A., et al., *Local dexamethasone therapy conserves hearing in an animal model of electrode insertion trauma-induced hearing loss*. Otol Neurotol, 2007. **28**: p. 842-849.
195. Wang, J., et al., *Caspase inhibitors, but not c-Jun NH2-terminal kinase inhibitor treatment, prevent cisplatin-induced hearing loss*. Cancer Res, 2004. **64**: p. 9217-9224.
196. Wise, A.K., et al., *Resprouting and survival of guinea pig cochlear neurons in response to the administration of the neurotrophins brain-derived neurotrophic factor and neurotrophin-3*. J Comp Neurol, 2005. **487**: p. 147-165.
197. Shinomori, Y., et al., *Volumetric and dimensional analysis of the guinea pig inner ear*. Ann Otol Rhinol Laryngol, 2001. **110**: p. 91-98.
198. Schindler, R.A., et al., *Enhanced preservation of the auditory nerve following cochlear perfusion with nerve growth factor*. Am J Otol, 1995. **16**(3): p. 304-309.
199. Wang, J., et al., *A novel dual inhibitor of calpains and lipid peroxidation (BN82270) rescues the cochlea from sound trauma*. Neuropharmacology, 2007. **52**: p. 1426-1437.
200. Pettingill, L.N., et al., *Neurotrophic factors and neural prostheses: potential clinical applications based upon findings in the auditory system*. IEEE Trans Biomed Eng, 2007. **54**(6): p. 1-5.
201. Garnham, C., et al., *Drug delivery to the cochlea after implantation: consideration of the risk factors*. Cochlear Implants Int, 2006. **6**(S1): p. 12-14.
202. Duan, M.L., et al., *Protection and treatment of sensorineural hearing disorders caused by exogenous factors: experimental findings and potential clinical application*. Hear Res, 2002. **169**: p. 169-178.
203. Hochmair, I., et al., *MED-EL cochlear implants: state of the art and a glimpse into the future*. Trends Amplif, 2006. **10**(4): p. 201-220.

204. Paasche, G., et al., *Technical report: Modification of a cochlear implant electrode for drug delivery to the inner ear*. Otol Neurotol, 2003. **24**: p. 222-227.
205. Stover, T., et al., *Development of a drug delivery device: using the femtosecond laser to modify cochlear implant electrodes*. Cochlear Implants Int, 2007. **8**(1): p. 38-52.
206. Paasche, G., et al., *Substance distribution in a cochlea model using different pump rates for cochlear implant drug delivery electrode prototypes*. Hear Res, 2006. **212**: p. 74-82.
207. Leary Swan, E.E., et al. *Microfabricated components for fully implantable microfluidic drug delivery to the inner ear*. in *34th Annual Meeting and Exhibition of the Controlled Release Society*. 2007. Long Beach, CA.

3.0 DRUG DELIVERY MODELING AND EXPERIMENTATION

A lumped-element model of the delivery system and cochlea was constructed. Mechanical parameters were converted to their electrical analogues, and two modules were created. The flow module incorporated the flow parameters in the delivery system and the physical aspects of the cochlea influencing the flow profile. The transport module coupled the convective and diffusive elements of transport to predict the concentration profile of the drug along the length of the cochlea. The model was validated using a bench-top glass capillary tube as a reservoir to allow for flow visualization. The concentration was measured by fluorescence intensity and compared to modeled results. Animal experimental data was also compared to modeled concentration predictions.

3.1 DESCRIPTION OF THE DEVICE

The basis of the delivery device is a reciprocating flow system for perfusion of drugs into the cochlear perilymph through a single hole in the basal turn of the scala tympani (ST). The single cannula was directly implanted in the scala tympani and acted as both inlet and outlet. The system has been constructed and tested with acute perfusion in the guinea pig. The guinea pig is an excellent animal model to develop the microfluidic interface, because the inner ear is large and accessible and because a large body of knowledge exists about its physiology, biochemistry, and pharmacology. Using the endogenous perilymph as the fluid, the system repeatedly injects a small volume (0.2 to a few μl) of liquid into the cochlea over a short (few sec) time, and then withdraws the liquid over a period of several minutes. A diagram of the microfluidic loop is shown in Figure 3.1. The critical elements of this device consist of an overall size consistent with surgical placement within a small cavity behind the ear, a pumping element capable of infusing the drug into recirculating perilymph, a valve-controlled drug reservoir, and integration with sensors for control of flow rate. Ultimately, an integrated drug delivery device with sensors for flow, concentration and bioactivity would provide customized therapy based on individual responses to treatment.

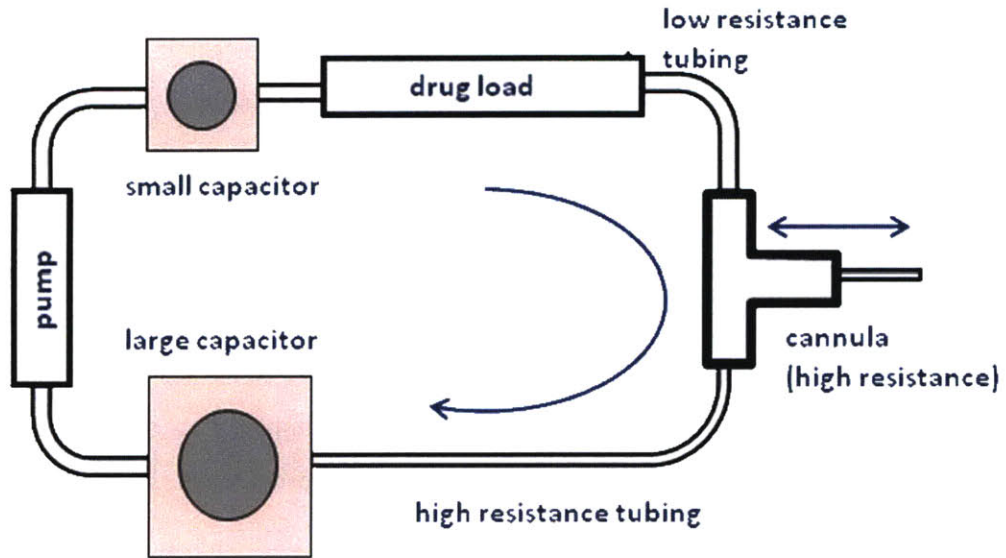


Figure 3.1: Recirculating microfluidic delivery system with resistive and capacitive elements to tune the delivery profile through the cannula

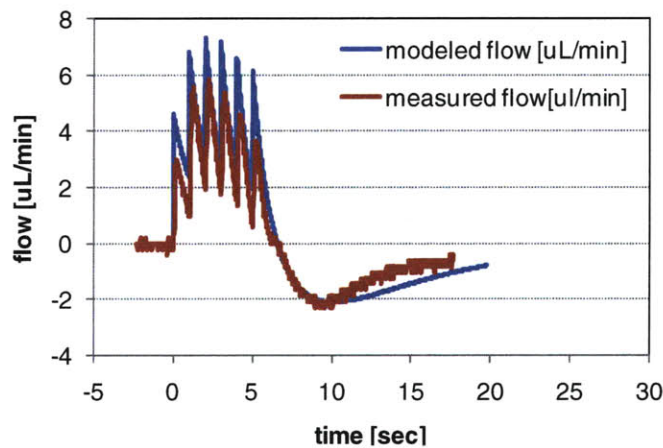


Figure 3.2: Example flow profile exiting the microfluidic system

By balancing resistances and capacitances in the fluidic network of the device, a series of fixed volume pump pulses results in approximately 0.5 to 2 μL of fluid exiting the cannula over a few seconds as shown in Figure 3.2. A combination of compliant diaphragm membranes and high resistance tubing is incorporated into the system to reduce the peak flow rate and volume exiting the cannula. Tubing compliance and resistance in the fluid network can be used to scale and filter the output pulse entering the cochlea as desired. This is done to reduce damage to sensitive structures in the inner ear that are susceptible to large volume or pressure changes. The volumes and pressures of the exiting fluid are tunable through the circuit parameters, minimizing the possibility of cochlear trauma.

The basic principle of the recirculating system is that a fluid pulse is ejected through the discharge capillary, a cannula placed in the ear, and slowly drawn back into the recirculating loop. The system has the following characteristics: 1) the pump generates discrete volume displacements over short periods of time when in the on state (0.5 μL over 30 msec) and blocks flow in the reverse direction when in the off state, 2) the tubing and components of the pump-outlet portion of the loop and the outlet cannula have a combined fluidic compliance and flow resistance that result in a charging time constant on the order of seconds, 3) the tubing and components on the pump inlet side of the pump have a combined compliance and resistance resulting in a charging time constant on the order of minutes. The system operates in the following way: during excitation the pump displaces a net volume, approximately 1 μL , from its inlet to outlet, and thus charges the outlet to a high positive pressure, and the inlet to a negative (gauge) pressure. Because of the designed difference in charging time constants of the loop, the pressured pump outlet is forced to quickly discharge out the cannula, rather than back into the pump-inlet side of the loop. The pump-inlet side of the loop slowly recharges, pulling fluid primarily from the cannula. Consequently fluid is ejected over a few seconds and then returns to the loop slowly over a period of minutes. The cycle may be repeated at whatever interval is required to achieve the desired fluid delivery rate and circulation rate of the drug in perilymph. Multiple pulses may be applied in rapid succession to increase the volume ejected per cycle. The result is a system capable of safely accommodating the pulse volumes from the pump, restricting the flow into and out of the ear, and producing no net average flow into the cochlea. Actual drug delivery occurs through diffusion and mixing of the high concentration fluid injected into the inner ear. Lower concentration fluid is returned to the recirculating loop. Over time, no net volume change in the cochlea occurs while the drug concentration in the cochlea increases. The intent of this method is to protect the sensitive hair cells from changes in perilymph volume and pressure while also creating a net increase in drug concentration.

The apparatus incorporates a miniature biocompatible solenoid pump manufactured by Wilson Greatbatch (Clarence, NY) with a stroke volume of 500 nL at pressures up to 100 MPa. The pump is controlled with a lab-designed electronic controller which delivers a low voltage pulse to the solenoid at frequencies selectable from 0.1 to 10 Hz. Supply, return, and discharge tubing join at a 3-port manifold, machined in the lab. To achieve the desired compliance mismatch, a large compliant diaphragm is located on the return side of the pump, while lines to and from the pump are rigid. A smaller capacitor on the pump outlet side reduces the maximum flow rate upon infusion. By selecting the resistance of the return line in relation to the resistance of the discharge cannula, the discharged volume at each

outlet cycle is controlled. To introduce drugs or other compounds to the circulating liquid, a micromachined valve manifold (see Chapter 5) was designed and fabricated for insertion into the supply line.

Design of circuit parameters allows for precise control of delivery volumes and times, and can allow for dosing of multiple therapeutics [1].

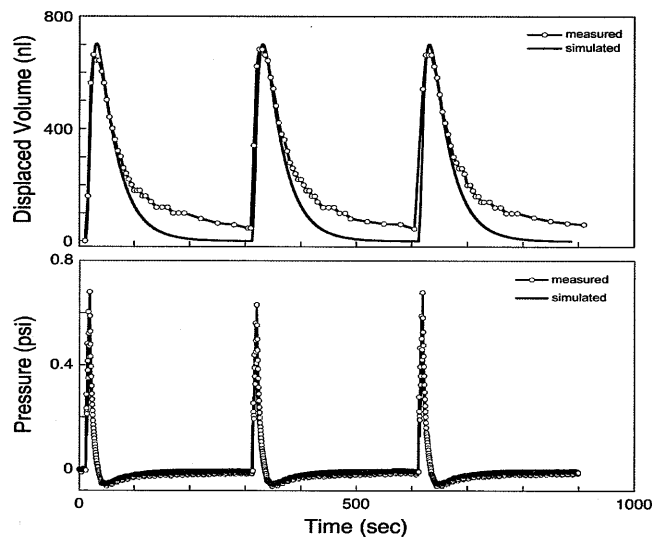


Figure 3.3: Sample output volume and pressure from fluidic circuit

A second fluidic system is also used. The concept is an actuator pushing on a membrane-covered reservoir for delivery into the cochlea, coupled with relaxation of the actuator and capacitance of the membrane for return of the fluid to the system. In normal operation, the solenoid actuator impinges on the pumping chamber's membrane to decrease its chamber volume and dispenses fluid from the reservoir into the cochlea. Releasing the membrane refills the system with cochlear fluid. Similar to the circulating system, the infusion and withdrawal cycles are timed such that substantial mixing of drug and perilymph occurs in the cochlea. The refill step draws diluted fluid back into the reservoir. This system results in similar output volumes and flow rates. The oscillating device was designed to reproduce the flow rate and dispense volume characteristics of the recirculating system, but with sufficient flexibility to alter these parameters either by component modification or by electrical input. While it is being developed, a syringe pump is utilized in initial bench-top and in vivo experiments to achieve identical flow characteristics. The pump substitutes for the membrane and actuator. A commercial flow sensor (Sensirion 1430, Staefa, Switzerland) is added to the system just prior to the cannula outlet for improved flow monitoring.

3.2 DESCRIPTION OF A PREVIOUS COCHLEAR DELIVERY SIMULATOR

A large body of work in computer simulation of drug transport within the cochlea has been published by Alec Salt and Stefan Plontke and coworkers [2-5]. The analyses have shown that the drug distribution is highly dependent on delivery protocol and application location along with drug choice and biological aspects of the inner ear.

Salt developed a one-dimensional finite-element model entitled “Washington University Cochlear Fluids Simulator” that is available for download free of charge at <http://oto2.wustl.edu/cochlea/>. The simulator [4] utilized cross-sectional area measurements of the scalae as functions of distance from [6] and area and location measurements of the round window membrane from [7]. Salt outlined the algorithm for his model in 1991 [2, 3]. Each scala had two arrays: A for cross-sectional area of each segment, and M for amount of agent in each segment. The concentration for any element (c_i) was defined as

$$c_i = \frac{M_i}{A_i x} \quad \text{Equation 3.1}$$

where x was the segment length. The transport was predominated by passive diffusion, so the rate of solute movement (dn/dt) was defined by Fick’s 2nd Law

$$\frac{dn}{dt} = -DA \frac{dc}{dx} \quad \text{Equation 3.2}$$

where A was the cross-sectional area, and dc/dx was the concentration gradient as a function of distance. For short segments, the concentration gradient was assumed to be linear. Therefore, the amount of agent (N) was found by

$$N = \frac{-DA_i t (c_i - c_{i+1})}{x} \quad \text{Equation 3.3}$$

and iterative calculations were done for each scala. For processes in addition to diffusion, such as bolus injections or perfusion, the amount of agent was added to each array element. For example, the bolus injection was addressed as

$$N = c_b V_b \quad \text{Equation 3.4}$$

where c_b and V_b were concentration and volume of the bolus [2]. Salt published an overview of the model as it appears on the website and described a summary of the features including the available drug applications of round window diffusion, bolus injection, and steady perfusion [5].

A number of publications compared the simulation to experimental results for middle ear delivery, direct injection, and others [8-11]. Additionally, Plontke and Salt developed a three-dimensional model and then compared a simplified geometry with the one-dimensional model for diffusion through the round window membrane. No flow was incorporated [12].

These models are useful due to a general lack of knowledge of the pharmacokinetics within the inner ear. In addition, samples cannot be withdrawn during experimentation due to the possibility of damage to sensory elements and contamination from cerebrospinal fluid (CSF). However, the Salt model lacks the ability to use the reciprocating fluidic delivery and does not account for protein interactions with the drugs.

3.3 GOVERNING EQUATIONS

Prior to constructing the model, an analytical understanding of the governing equations is necessary. Drug transport in the cochlea is governed by the law of mass conservation as

$$\frac{\partial c}{\partial t} = -\nabla \cdot \underline{N} + R - (\underline{v} \cdot \nabla) c \quad \text{Equation 3.5}$$

where c is drug concentration, t is time, \underline{N} is flux, R is reaction, and \underline{v} is velocity. The flux is defined by passive diffusion. The constitutive equation is Fick's 1st Law,

$$\underline{N} = -D\nabla c \quad \text{Equation 3.6}$$

where D is diffusivity, assumed to be constant in this case. These equations define the phenomena contributing to drug transport. The passive diffusion proceeds through Brownian motion of the particles. The reaction depends on multiple biological processes including drug binding, tissue uptake, and clearance to the vascular system, among others. Finally, the velocity is defined by the flow exiting the delivery system. The perilymph flow rate within the scala tympani is negligible, based on the measurement by Ohyama of 1.6 nL/min directed basally [13].

In defining the fluid velocity from the delivery system, the fluid is assumed to be incompressible and Newtonian. The mass conservation equation is

$$\nabla \cdot \underline{v} = 0 \quad \text{Equation 3.7}$$

and the momentum conservation is defined as

$$\rho \frac{D\underline{v}}{Dt} = \underline{F} \quad \text{Equation 3.8}$$

where ρ is density and \underline{F} is the sum of forces. The Reynolds number (Re) of the fluid flowing into the cochlea,

$$\text{Re} = \frac{\rho UL}{\mu} \quad \text{Equation 3.9}$$

where U is average velocity, L is characteristic length, and μ is viscosity, was computed using the average velocity generated by the root mean square of the pressure input. The result, Re on the order of 1, suggests laminar flow. Re calculated with maximum pressure yields a Re of the same order. The catheter dimensions were used in the calculation. The mass and momentum conservation equations result in the Navier-Stokes equation

$$\rho \frac{D\underline{v}}{Dt} = -\nabla P + \mu \nabla^2 \underline{v} \quad \text{Equation 3.10}$$

where P is the pressure driving the flow.

The Peclet number (Pe)

$$\text{Pe} = \frac{UL}{D} \quad \text{Equation 3.11}$$

is also based on the average velocity of fluid leaving the device. The Pe on the order of 10^3 displays the relative dominance of convective transport over diffusive transport. In this case, diffusion is enhanced due to the parabolic shape of the flow since both radial and axial diffusion can occur. The Re and Pe were calculated, as noted, using the cannula flow. Once the flow enters the cochlea, it splits, which may produce different values for this numbers.

For radially symmetric, unsteady flow in a circular tube, the Navier-Stokes equation reduces to

$$\frac{\partial v}{\partial t} = -\frac{1}{\rho} \frac{\partial P}{\partial z} + \frac{\mu}{\rho} \frac{1}{r} \frac{\partial}{\partial r} \left(r \frac{\partial v}{\partial r} \right) \quad \text{Equation 3.12}$$

where r is radius. For a pressure gradient periodic in time and independent of r or z , the solution was published by Aris [14].

For this tube, the mass transport equation simplifies to

$$\frac{\partial c}{\partial t} = D \left[\frac{\partial^2 c}{\partial z^2} + \frac{1}{r} \frac{\partial}{\partial r} \left(r \frac{\partial c}{\partial r} \right) \right] - v_z \frac{\partial c}{\partial z} \quad \text{Equation 3.13}$$

for no reaction.

Equation 3.13 cannot be solved analytically for this system. In this thesis, a lumped-element model was constructed to develop an approximate solution to the concentration distribution. This method was chosen to provide intuitive insight into the interactions of the device and cochlea. Alternatively, one may choose a standard numerical algorithm to solve the equation. For example, the equation is rewritten below for solution using the finite difference method. Concentration, $c(r_i, z_j, t_k)$, is equal to the value of c at $r=i$, $z=j$, and $t=k$. The centered difference approximation for the first order partial derivative is as follows:

$$\frac{\partial c}{\partial t} = \frac{c_{i,j,k+1} - c_{i,j,k-1}}{2\Delta t} + O(\Delta t^2) \quad \text{Equation 3.14}$$

where the order of accuracy is given by $O(\Delta t^2)$. The z -spatial derivation can be discretized in the same fashion. The second order derivative can be approximated as

$$\frac{1}{r} \frac{\partial}{\partial r} \left(r \frac{\partial c}{\partial r} \right) = \frac{c_{i+1,j,k} - 2c_{i,j,k} + c_{i-1,j,k}}{(\Delta r)^2} + \frac{c_{i+1,j,k} - c_{i-1,j,k}}{2r(\Delta r)} + O(\Delta r^2) \quad \text{Equation 3.15}$$

using the centered difference method. From equations 3.14 and 3.15, the concentration at any point (r,z,t) can be approximated by

$$\frac{c_{i,j,k+1} - c_{i,j,k-1}}{2\Delta t} = D \left[\frac{c_{i,j+1,k} - 2c_{i,j,k} + c_{i,j-1,k}}{(\Delta z)^2} + \frac{c_{i+1,j,k} - 2c_{i,j,k} + c_{i-1,j,k}}{(\Delta r)^2} + \frac{c_{i+1,j,k} - c_{i-1,j,k}}{2r(\Delta r)} \right] - v_z(r,t) \left[\frac{c_{i,j+1,k} - c_{i,j-1,k}}{2\Delta z} \right]$$

Equation 3.16

This finite difference equation may be solved using commonly available numerical solvers. The finite difference method provides a continuum approach to solution for r , z , and t . On the other hand, this approach uses lumped elements. It may not provide the level of precision the finite difference method offers without adding significantly more components; however the lumped-element approach allows for a more intuitive understanding of the relative contributions of various components.

3.4 LUMPED PARAMETER MODELING

The model was constructed with two coupled modules using lumped-element electrical circuit analogues and analyzed with circuit simulation software. The first module predicted pressure-driven flow in the cochlea generated by the delivery system and influenced by the various fluid loss mechanisms and compliances of the system and cochlea. The second module used input from the flow module to simulate transport of drug through the cochlea by combined flow and drug (solute) diffusion. The flow module used a pulsatile flow source, compliant elements and resistive elements to describe the delivery system. The drug transport module implemented lossy transmission line elements to simulate diffusion through the cochlea and current sources dependent on the first module's flow data to distribute the drug through the cochlea via bulk flow. In the lumped-element model, the cochlea was segmented, and the attributes of each segment, or lump, were assumed to be uniform over the volume of the segment [15]. As the model system's complexity evolves, additional components may be added to represent various other biological mechanisms such as drug binding, clearance to the vascular system, etc. The model was validated using simplified sets of input conditions, which permitted direct comparison with simpler bench-top experiments and an existing simulation tool.

Electrical analogues were used to describe the physical phenomena in the system. All of these electrical components were equivalent to their hydraulic and diffusive-transport counterparts with appropriate transformations. Equations of the same form are considered analogous equations and can be solved with substituted variables and constants. In all the systems, a potential difference applied to


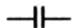
an element causes flow. For example, in an electrical system, voltage applied to a resistor causes current just as pressure difference applied to resistive tubing causes fluid flow in a hydraulic system [16].

All of the model components had electrical component analogues available in the Micro-Cap electrical circuit simulator (Spectrum Software, Sunnyvale, CA), and their specific values were transformed to maintain consistency throughout the model. This tool had a wide range of simple-to-use components, including the nonlinear elements necessary to simulate both the delivery system and the biological system. The lumped parameter model allowed for intuitive interpretation of various aspects of the two systems and provided versatility for examining the drug transport effects due to changes in the system (fluid flow, cannula placement, etc.).

3.4.1 Flow module

Lumped-element modeling of the flow module entailed describing the flow created by the device and incorporating elements of the reservoir, or cochlea, which influenced the fluid flow within the cochlea. The pump was modeled as a current source, and capacitive and resistive elements were utilized. The transformed mechanical to electrical analogues are shown in Table 3.1, as well as the associated symbols used in the electrical circuit simulator.

Table 3.1 Mechanical to electrical analogues and associated symbols.

Fluidic element	Electrical element	Element symbol
Pressure (P)	Voltage (V)	
Volume (v)	Charge (q)	
Volume flow (Q)	Current (I)	
Fluidic resistance (R_{fl})	Electrical resistance (R)	
Fluidic capacitance, compliance (C_{fl})	Electrical capacitance (C)	

3.4.1.1 Recirculating system

The first fluidic delivery system that was modeled was the recirculating system detailed above. Figure 3.4 shows the electrical circuit layout drawn in the simulator.

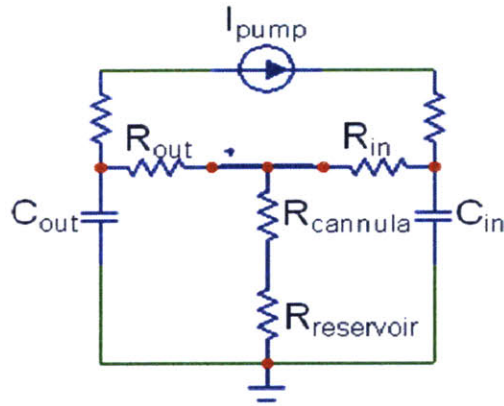


Figure 3.4: Micro-cap circuit representing the recirculating flow system.

In this drawing, I_{pump} represented the driving force applied to the system by the mechanical pump. The pump was modeled with a pulse defined by the 25 msec-stroke time and 1200 $\mu\text{L}/\text{min}$ -constant flow during that time. These values were the inherent values of the commercial pump. The four resistors labeled R_{in} and R_{out} described the resistance to flow due to the diameters and lengths of various tubing in the recirculating loop. The $R_{cannula}$ described the resistance of the cannula at the flow outlet. These resistances were calculated from the Hagen-Poiseuille flow equation for laminar, incompressible, cylindrical pipe flow.

$$R_{fl} = \frac{128\mu L}{\pi d^4} \quad \text{Equation 3.17}$$

where L was tube length and d was tube diameter. The value of viscosity, μ , was $7.2\text{e-}4$ Pa*sec for perilymph. The resistor labeled $R_{reservoir}$ described any generic reservoir where the fluid exited and was changed for various tests to describe the cochlea or test capillary tubes, as necessary. The two fluidic capacitors labeled C_{in} and C_{out} were diaphragm components designed and built specifically for this application. The capacitance of these elements was based on their diameter, membrane material, and membrane thickness. The elements and capacitance calculations are discussed below in Chapter 5.

Just as Ohm's Law describes electrical circuits, the mechanical analogues are related. Ohm's Law states that

$$V = IR \quad \text{Equation 3.18}$$

and the mechanical system is described by

$$P = QR_{fl} \quad \text{Equation 3.19}$$

Likewise, the current and volume flow are described as

$$I = \frac{dq}{dt}, Q = \frac{dv}{dt} \quad \text{Equations 3.20, 3.21}$$

respectively. Finally, electrical capacitance and fluidic capacitance are described as

$$C = \frac{dq}{dV}, C_{fl} = \frac{dv}{dP} \quad \text{Equations 3.22, 3.23}$$

respectively. The volume flow output of the system at the node immediately after $R_{cannula}$ was coupled to the transport module, described below.

The modeled flow is shown in comparison to measured flow out of the recirculating system in Figure 3.2. In this example, the pump was turned on for six pulses, and the flow was measured using a Sensirion 1430 flow sensor. Many configurations of pump pulses, different compliance values, and resistance values may be combined to yield various flow profiles as required for optimal delivery.

3.4.1.2 Biological considerations

Additions to this flow module allowed for representation of biological aspects of the cochlea affecting fluid flow as shown in Figure 3.5. First, the general $R_{reservoir}$ was replaced with resistance values of the scala tympani and scala vestibuli. These were calculated using Equation 3.17 above. The diameter and length values were obtained from [6] using MRI images. Because the cannula was inserted at 1.8 mm from the base of the cochlea (the 28 kHz region) as shown in Figure 3.6, the total fluid resistance was lumped into two values representing the sections on each side of the insertion site ($R_{ST\ basal}$, $R_{ST\ apical}$). The $R_{ST\ basal}$ was calculated to be 6.67×10^{-8} psi/ μ L/min and the $R_{ST\ apical}$ was 9.77×10^{-5} psi/ μ L/min. $R_{ST\ apical}$ was much larger because the length of the segment was 30 mm including the apical region of the scala tympani as well as the entire scala vestibuli.

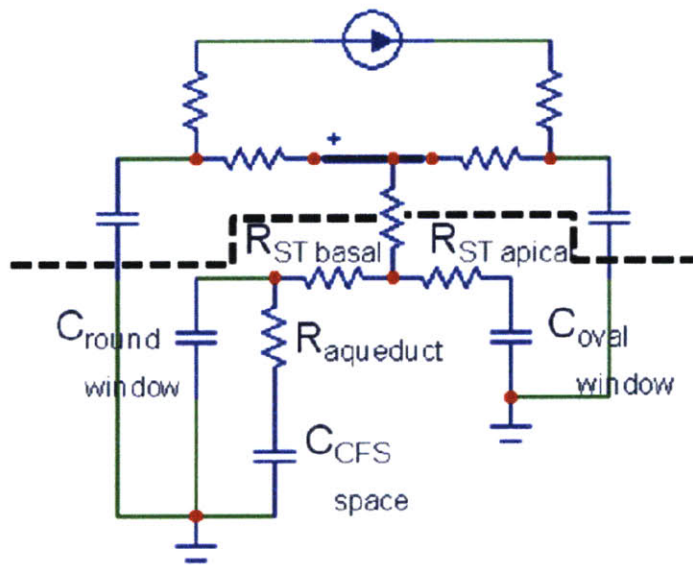


Figure 3.5: Fluidic module for reciprocating flow with cochlear elements (Elements below the dotted line are external to the device.)

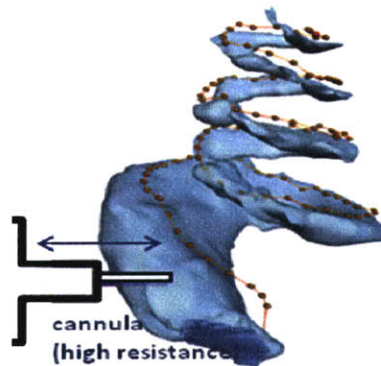


Figure 3.6: Three-dimensional reconstruction of a guinea pig scala tympani (from histological sections) showing the insertion point of the cannula. The round window membrane is shown at the base in dark blue.

As described in Chapter 2, the guinea pig cochlea has a patent aqueduct connecting the scala tympani to the CSF space. This tube is located at the base of the scala tympani near the round window and provides a path for the fluid to flow out of the cochlea. As the aqueduct is a tube ending in a relatively larger fluid space, a resistor and a capacitor are required to represent the anatomy. The cochlear aqueduct resistance ($R_{aqueduct}$) values were published by Wit [17]. The resistance is nonlinear as shown in Figure 3.7; however at pressures over 0.08 psi, $R_{aqueduct}$ is approximately linear with a value of

0.025 psi/ μ L/min. The capacitance of the CSF space ($C_{CSF\ space}$) was assumed to be large compared to the other capacitance values and set at 10 μ L/psi.

The round window, at the base of the scala tympani, is a compliant membrane and modeled as a capacitor ($C_{round\ window}$). As shown in Figure 3.7, $C_{round\ window}$ is slightly nonlinear [17], but output of the model showed no change whether a nonlinear or linear capacitive element was used. Therefore, $C_{round\ window}$ was set to 0.8 μ L/psi. The compliance of the oval window ($C_{oval\ window}$), at the end of the scala vestibuli is estimated to be approximately one order of magnitude less compliant than the round window [18]. Thus, $C_{oval\ window}$ was set to 0.08 μ L/psi.

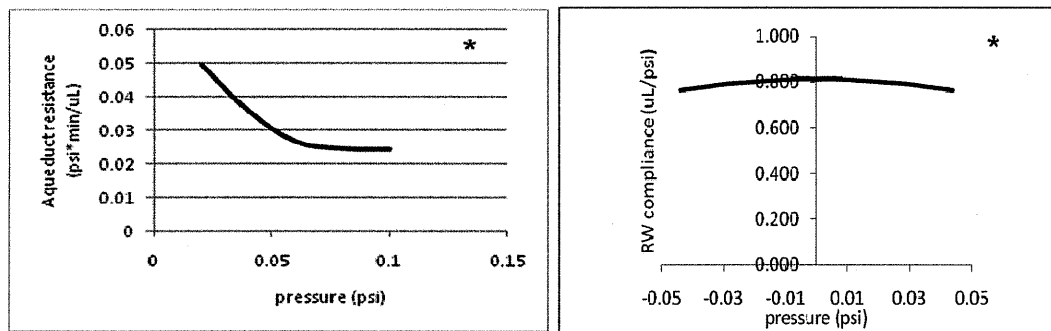


Figure 3.7: (left) Cochlear aqueduct resistance and (right) round window compliance as a function of pressure. *Plots were reproduced from data in [17].

3.4.1.3 Syringe pump system

The second flow system that was used was a syringe pump system that approximated the next-generation microfluidic flow system. This simplified set-up was used in both bench-top and animal studies, as discussed below. The system, as described by lumped elements, is shown in Figure 3.8. Again, the pump was represented by the current generator, and $R_{cannula}$ represented the small-bore tubing used for the cannula. Parasitic compliance in the syringe and syringe pump and intentionally introduced compliance in the pump's outlet tubing were lumped into a single element, C_{pump} . This value was dependent on the amount of air trapped in the system during filling, the types of syringe and tubing, and the security of the syringe placement in the pump holder. This value was fit to the experimental data.

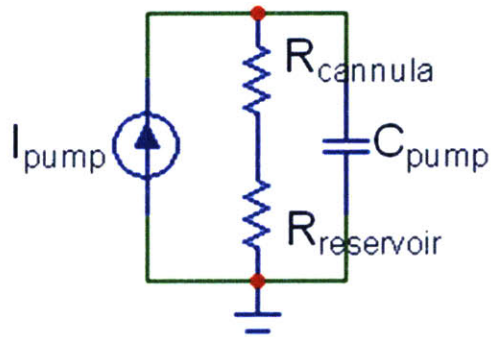


Figure 3.8: Circuit diagram of simplified syringe pump delivery system

A bench-top experiment to visualize and model flow from the syringe pump system into a glass capillary tube is described below. This experiment was used to validate the model. In order to accurately represent the flow exiting the device, the flow module shown in Figure 3.8 was modified and is shown in Figure 3.9.

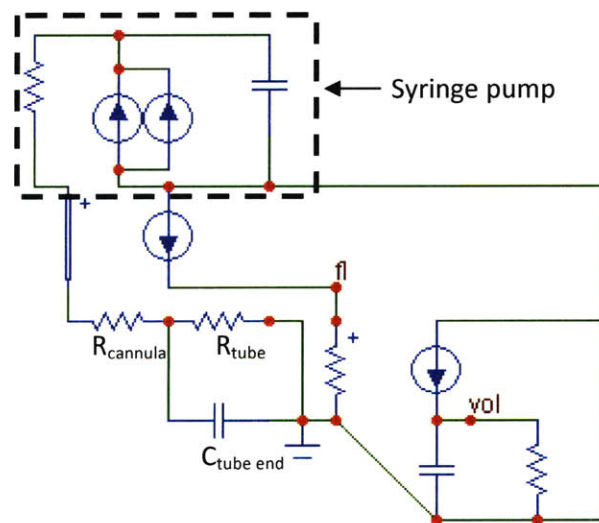


Figure 3.9: Circuit diagram of syringe pump system used in experiments

The syringe pump itself required two pulse current sources, one representing flow into the cochlea (positive) and the other representing flow exiting the cochlea (negative). The resistor and capacitor modeled measured parasitics. The other change was the addition of a volume integrator so that the flow rate at node (fl) could be integrated to determine the volume discharged from the system.

$R_{cannula}$ and R_{tube} (glass capillary) were calculated from Equation 3.17 using the dimensions of these tubes. $C_{tube\ end}$ represented the open end of the capillary opposite the in-flow end and was set to a high value since capacitance was infinite there. Figure 3.10 shows an example flow rate graph comparing model output to measured flow for this module. The flow was measured using the Sensirion Model 1430 flow sensor.

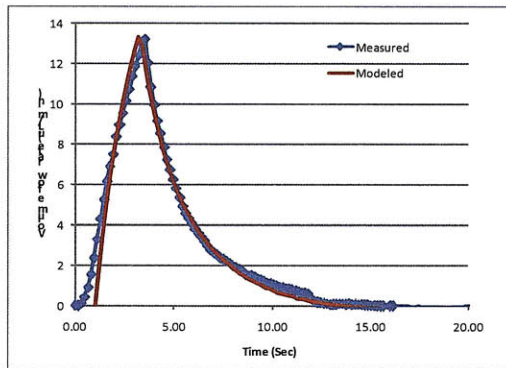


Figure 3.10: Example comparison of flow rate experimental results to modeled results

Figure 3.11 shows how the flow module in Figure 3.9 was modified to represent flow into the guinea pig cochlea. R_{tube} and $C_{tube\ end}$ were replaced by resistances of the scala tympani and scala vestibuli, compliances of the round and oval windows, and resistance and compliance of the aqueduct and associated CSF space, as described above.

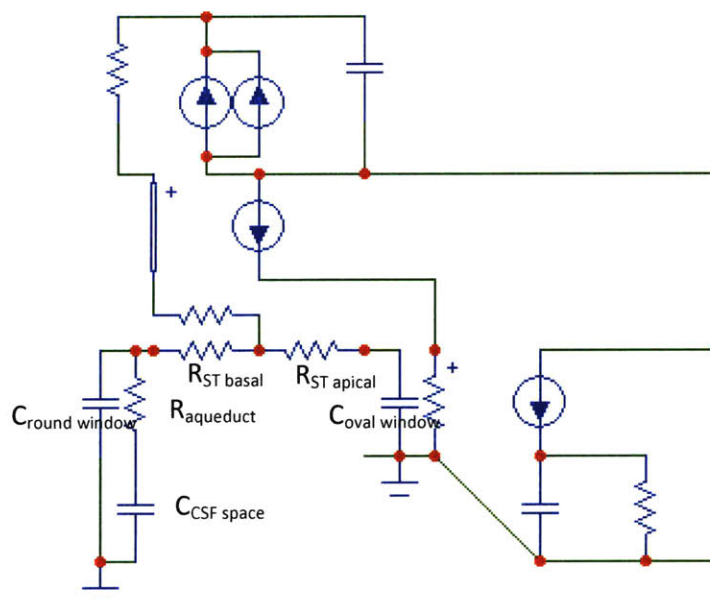





Figure 3.11: Circuit diagram of syringe pump system for delivery into guinea pig cochlea.

The flow module of the lumped parameter model is highly versatile and easily changed to represent different flow systems and different reservoirs. By describing the flow in this way, intuitive understanding of the role of each element can be gained, and the effects of changes of values of each element can be shown.

3.4.2 Drug transport module

Lumped parameter modeling of transport and dispersion of the drug or solute within the cochlea was accomplished using the transport module. Both diffusive and convective forces were represented. Additional elements may be added to represent clearance mechanisms and drug binding encountered in the cochlea. As in the fluidic module, electrical analogues were used in place of transport parameters. These transformations are summarized in Table 3.2.

Table 3.2: Transport to electrical analogues and associated symbols.

Transport element	Electrical element	Element symbol
Concentration (c)	Voltage (V)	
Number of particles ($\#$)	Charge (q)	
Bulk solute flow (f)	Current (I)	
Diffusive resistance (R_d)	Electrical resistance (R)	
Segment volume (v_s)	Electrical capacitance (C)	

Concentration was represented by voltage at any point along the cochlea or tube, and the initial concentration of the drug was defined by the experimental parameters. Electrical charge was analogous to the number of particles of the drug (concentration multiplied by volume). Current was defined in Equation 3.20. Similarly, concentration in a given segment was described by

$$c = \frac{\#}{v_s} \quad \text{Equation 3.24}$$

Segment volume was represented by electrical capacitance. The segment value is calculated by the average cross-sectional area of the segment multiplied by the length of the segment. In the glass tube experiment, the tube was constant in diameter; however in the case of the guinea pig cochlea, the diameter was not constant. Values from literature [6] were used to calculate the segment volumes.

The diffusive resistance was defined as

$$R_d = \frac{L_s}{DA_s} \quad \text{Equation 3.25}$$

where L_s is segment length, D is solute diffusivity, and A_s is segment area. R_d was represented by electrical resistance.

Current represented bulk solute flow. The bulk solute flow (f) was generated by the delivery device and defined as concentration multiplied by the volume flow from the device. The flow module was coupled to the transport module through the current source.

An example circuit representation of the transport module is shown in Figure 3.12.

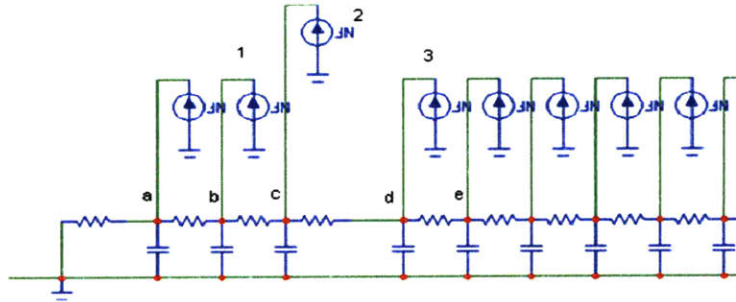


Figure 3.12: Circuit diagram of transport module.

In order to more clearly explain the nonlinear current values, the current sources at points 1, 2, and 3 in Figure 3.12 are defined below in Table 3.3.

Table 3.3: Current source definition in circuit

1	If $V_{fi} > 0$, $.9V_{fi}(V_c - V_b)$, else $-.9V_{fi}(V_a - V_b)$
2	If $V_{fi} > 0$, $V_{fi}(V_{initial} - V_c)$, else $-V_{fi} [.9V_b + .1(V_d - V_c)]$
3	If $V_{fi} > 0$, $.1V_{fi}(V_c - V_d)$, else $-.1V_{fi}(V_e - V_d)$

where V_{fi} is the fluid volume flow from the flow module, V_{a-e} are the segment concentrations, and $V_{initial}$ is the solute concentration of the drug in the device. Note that the current source at point 2 was a special case as this was the entry point of the cannula into the cochlea. Also, the 0.9 and 0.1 factors represent the fact that the oval window was one-tenth less compliant than the round window, and as a result approximately 90% of the fluid flow is toward the round window and only 10% towards the oval window. For the glass tube case, these definitions were simplified by removing the multiplied factors. The cannula was placed at the end of the tube rather than some distance in, as was the case for the cochlea.

The R-C pair in each segment can be replaced by a lossy transmission line as shown below. The R-C pair describes diffusion of the solute. Figure 3.13 shows a transmission line schematically and as an element in the circuit solver.

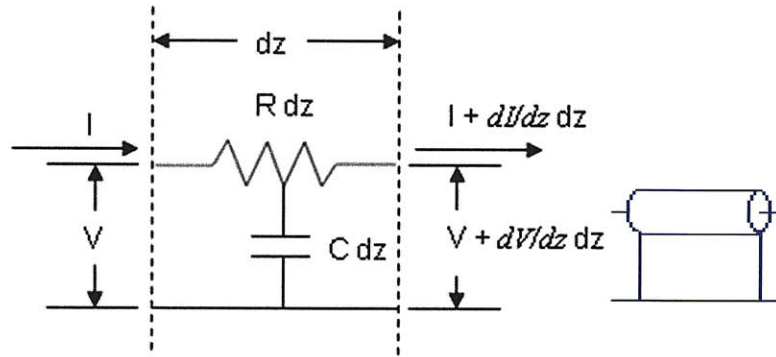


Figure 3.13: (left) Schematic interpretation of a transmission line and (right) Micro-cap transmission line element

From the schematic representation,

$$\frac{dV}{dz} dz = -R I dz \quad \text{Equation 3.26}$$

Differentiating both sides with respect to z results in

$$\frac{d^2V}{dz^2} = -R \frac{dI}{dz} \quad \text{Equation 3.27}$$

Also, from the schematic,

$$\frac{dI}{dz} dz = -C dz \frac{dV}{dt} \quad \text{Equation 3.28}$$

Cancelling dz yields

$$\frac{dI}{dz} = -C \frac{dV}{dt} \quad \text{Equation 3.29}$$

Combining Equations 3.27 and 3.29 yields

$$\frac{d^2V}{dz^2} = RC \frac{dV}{dt} \quad \text{Equation 3.30}$$

which is Fick's 2nd Law of diffusion in one dimension. RC is equivalent to the inverse of diffusivity, and voltage is equivalent to concentration.

Calculations of lumped volume and diffusive resistance were based on diameter values of the cochlea along the length of the scala tympani and scala vestibuli. An example calculation of one segment of the cochlea is shown in Table 3.4. This segment extended apically from 1 mm from the base up to 1.7 mm from the base.

Table 3.4: Sample calculation of lumped parameters

Length (mm)	Diameter (mm)	volume (μL)	R_d (sec/cm ³)	Lumped v_s (μL)	Lumped R_d (sec/cm ³)
1	1.281	0.128	1.66E+05	0.974	7.31E+05
1.1	1.279	0.129	1.65E+05		
1.2	1.266	0.127	1.67E+05		
1.3	1.244	0.124	1.72E+05		
1.4	1.235	0.121	1.76E+05		
1.5	1.229	0.119	1.79E+05		
1.6	1.197	0.116	1.84E+05		
1.7	1.182	0.111	1.92E+05		

In R_d , diffusivity was $4.70\text{e-}6$ cm²/sec for the example solute. The lumped volume was the sum of the individual values for the given segment. The lumped diffusive resistance was the sum of the individual resistances from the center of one segment to the center of the next segment.

Two transmission lines in parallel can be assigned to each segment with the lumped volume and diffusive resistance split between them. With a resistor between them, the model can better represent laminar flow. The shape of the laminar flow in a pipe is parabolic with higher velocity flow in the inner core and slower flow in the outer ring. A fast core may be defined as some portion of the tube diameter and the R and C values calculated from the new diameter. Likewise, the outer ring represents the remainder of the diameter. The resistor connecting the two transmission lines represented the radial diffusion due to the difference in velocity. This lumped element was calculated by dividing the segment length by the diffusivity and the cross-sectional area of the midpoint of the inner core to the midpoint of the outer ring. Additionally, a second current source is added so both average flow rates are represented at the same proportion as the diameters. The fast and slow cores will model the larger concentration gradient due to varied convective transport across the tube cross-section. More transmission lines could be added for improved accuracy and better defined flow. An example of the circuit is shown in Figure 3.14.

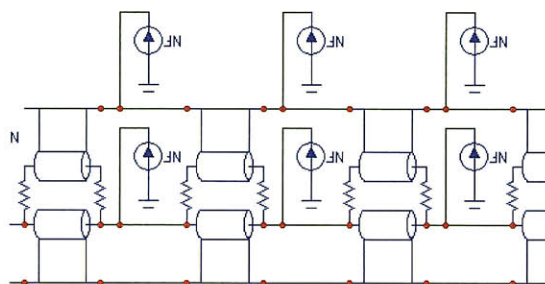


Figure 3.14: Circuit showing additional transmission lines to better translate laminar flow

3.5 COMPARISON OF THE MODEL TO THE DIFFUSION-ONLY ANALYTIC SOLUTION

The first validation of the transport module compared the model configured for diffusion only to the analytical solution of diffusive transport. For one-dimensional diffusion in a pipe, the solution for concentration at any point along the pipe (x) is

$$c = c_0 \left[1 - \operatorname{erf} \left(\frac{x}{2(Dt)^{1/2}} \right) \right] \quad \text{Equation 3.31}$$

where c_0 is the initial concentration of the solute entering the tube. The diffusivity of fluorescein, $7.83 \times 10^{-6} \text{ cm}^2/\text{sec}$, was used in the analysis and model. Figure 3.15 shows the circuit that was used to solve the diffusion-only case. It represented a simplified version of the general transport module. The initial concentration, $100 \text{ } \mu\text{M}$, was modeled as a battery with voltage equal to c_0 since there was a constant source of fresh solution at the entrance to the tube. The current sources were removed because there was no volume flow. The 100 mm-long glass tube was divided into eight segments. The first seven segments were each 1 mm long, and the last one was 93 mm long. The lumped resistance was $2.2 \times 10^6 \text{ sec/cm}^3$ and the lumped capacitance was $5.8 \times 10^{-4} \text{ cm}^3$ based on the tubing diameter of 0.86 mm.

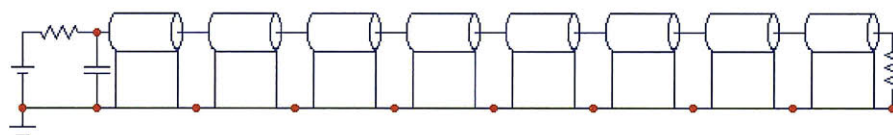


Figure 3.15: Circuit diagram of diffusion-only transport module.

The results of the analytical solution and the model solution are compared in Figure 3.16 for the first 6 mm of tubing. Very precise overlay of the two solutions is apparent. Even for a shorter time interval,

the solutions match very closely, as shown in Figure 3.17. This demonstrates that the transmission lines accurately represent diffusion.

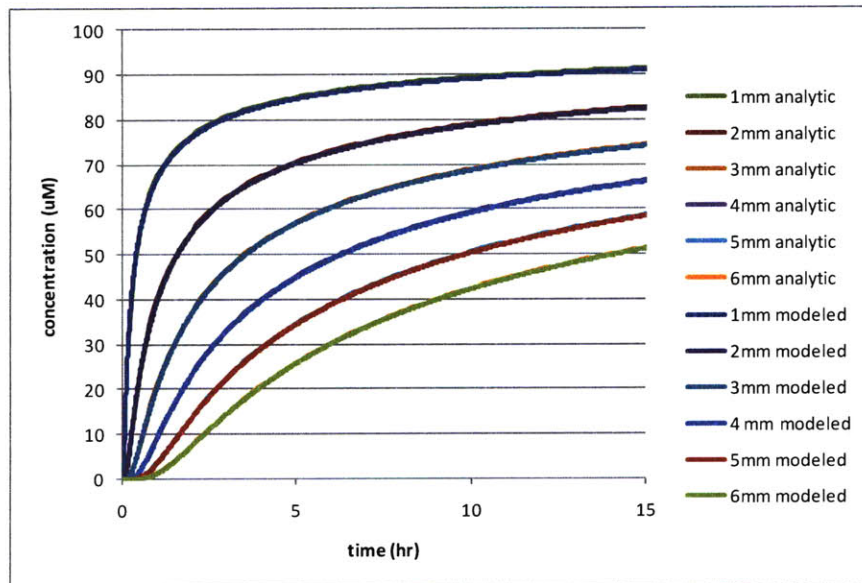


Figure 3.16: Comparison of analytical solution of diffusion to modeled solution for several hours

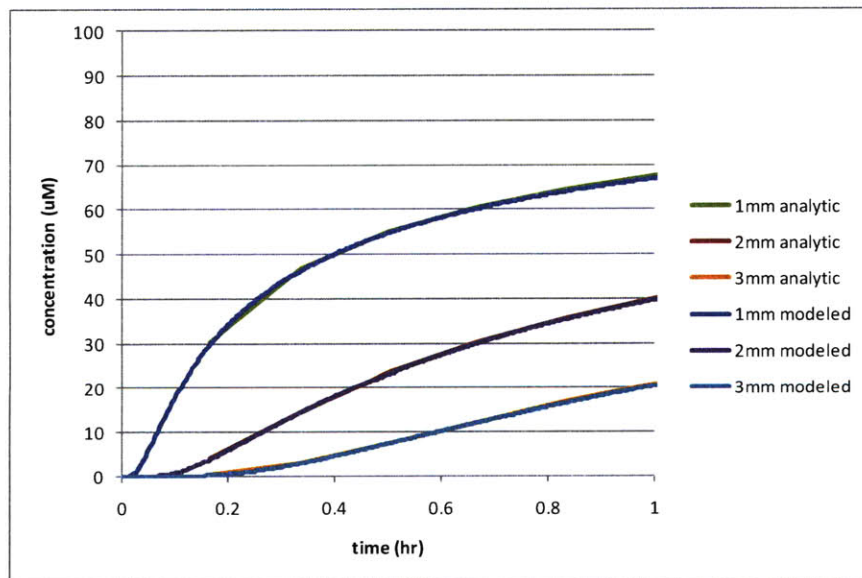


Figure 3.17: Comparison of analytical solution of diffusion to modeled solution for one hour

3.6 DRUG TRANSPORT MODELING IN GLASS CAPILLARY TUBE

Another validation of the model involved flow visualization in a glass capillary. Bench-top experiments were conducted using the syringe pump system to deliver fluorescein into glass tubes.

Fluorescence intensity was continuously imaged under a microscope and converted to a relative concentration. The model was used to predict the fluorescein concentration over time due to pulsatile flow and diffusion and was compared to experimental results. Figure 3.18 shows a montage of false-color images of fluorescein transport into the tube. Each image shows a 2-sec time-step, and the series of images shows one delivery system infusion cycle followed by withdrawal of the fluid back into the system.

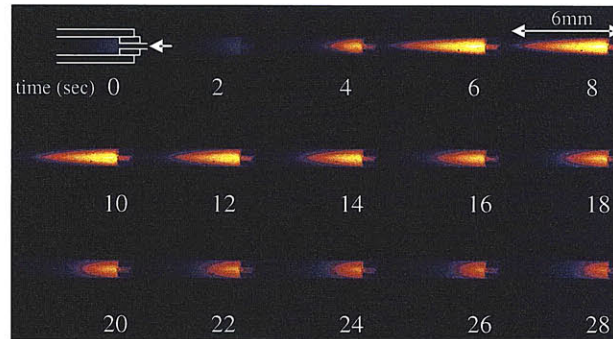


Figure 3.18: Time-step images of fluorescein output into tube

3.6.1 Method

The syringe pump (Harvard Apparatus PHD 2000) was connected to the computer to allow for Labview control using a customized program that set the flow parameters and controlled pump infusion and withdrawal at intervals set by the user. A length of large bore, rigid Teflon tubing was connected to a flow sensor (Sensirion 1430). The sensor provided input to the Labview program so volume and flow could be continuously monitored throughout the experiment. The outlet of the flow sensor was then connected to the manifold housing the cannula for cochlear implantation. As shown in Figure 3.19, a second manifold connected the solute reservoir to the infusion line. A pump attached to a timer-controlled power source ensured that the solute was completely refreshed in the slug of fluid about to enter the cochlea between each cycle. The solute loop was filled with 100 μ M fluorescein (Sigma, St. Louis, MO) in deionized water. All other components were carefully filled with deionized water as the system was built to eliminate bubbles in the system. After filling, the other end of the Teflon tubing was connected to a 100 μ L glass Hamilton syringe that was placed on the syringe pump.

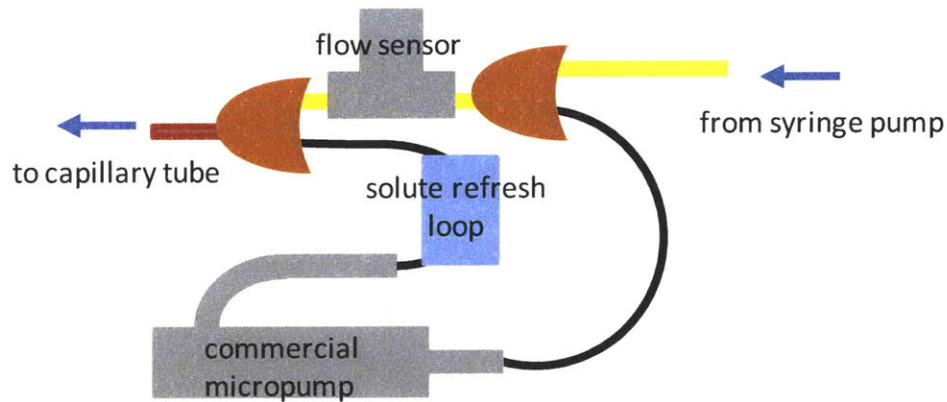


Figure 3.19: Diagram of syringe pump flow system

The cannula was placed in a water reservoir for system testing. The Labview program was set to the required infuse and withdraw rates and durations to achieve the following desired flow characteristics: 12 $\mu\text{L}/\text{min}$ infusion rate, 1 μL infused volume, complete withdrawal over 1 min, repeated every 150 sec. The sensor output was monitored to ensure agreement between the settings and actual flow from the cannula. The solute loop pump was also tested. It was cycled enough times to push 1 μL of fresh drug solution into the infuse loop, usually 2-3 pump pulses. The timer box was set to repeat every 150 sec to match the period of syringe pump cycling. After demonstration of proper performance of the pump on the bench, the cannula was inserted into a water-filled glass capillary (0.86mm ID, Chase Scientific Glass, Rockwood, TN). The microscope camera (Olympus SZX12, Center Valley, PA) was set to save an image every 1 sec for the duration of the test.

At the conclusion of the experiment, the images were loaded into ImageJ software (freeware from <http://rsbweb.nih.gov/ij/>) as a stack. The fluorescence intensity, at lengths of 1-6 mm from the cannula, was measured for all images in the stack.

A set of fluorescence standards was constructed of identical glass capillary tubes filled with concentrations of fluorescein varying from 300 μM down to 300 nM. The linear region on the log plot, as shown in Figure 3.20, was used to convert the fluorescence intensity measurements from the experiment to concentration values.

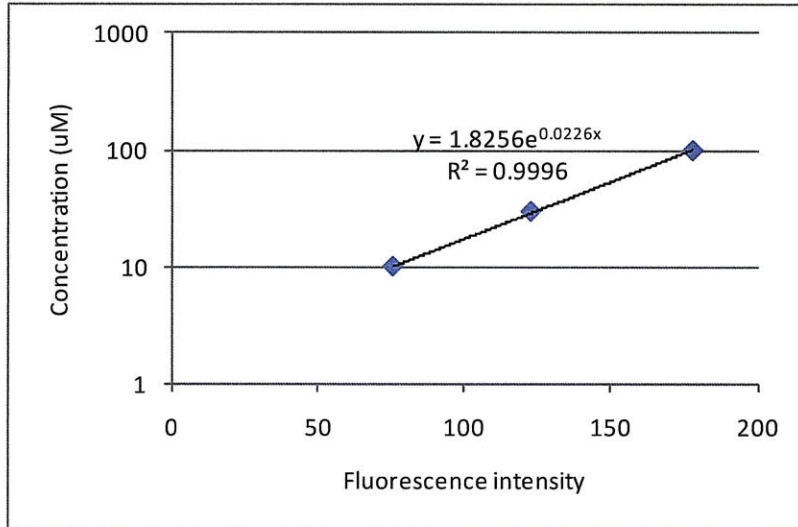


Figure 3.20: Relationship between fluorescence intensity and concentration

3.6.2 Results

Results of the experiment are shown in Figures 3.21 and 3.22. The figures show the change in concentration with time at 4 locations along the length of the glass tube. The results of the pulsatile flow were apparent in the periodic spikes in concentration followed quickly by reduction in concentration. The overall trend, however, shows increasing concentration over time. Figure 3.21 shows the maximum concentration values at the points of interest across the diameter of the tube, while Figure 3.22 shows the mean concentration across the diameter.

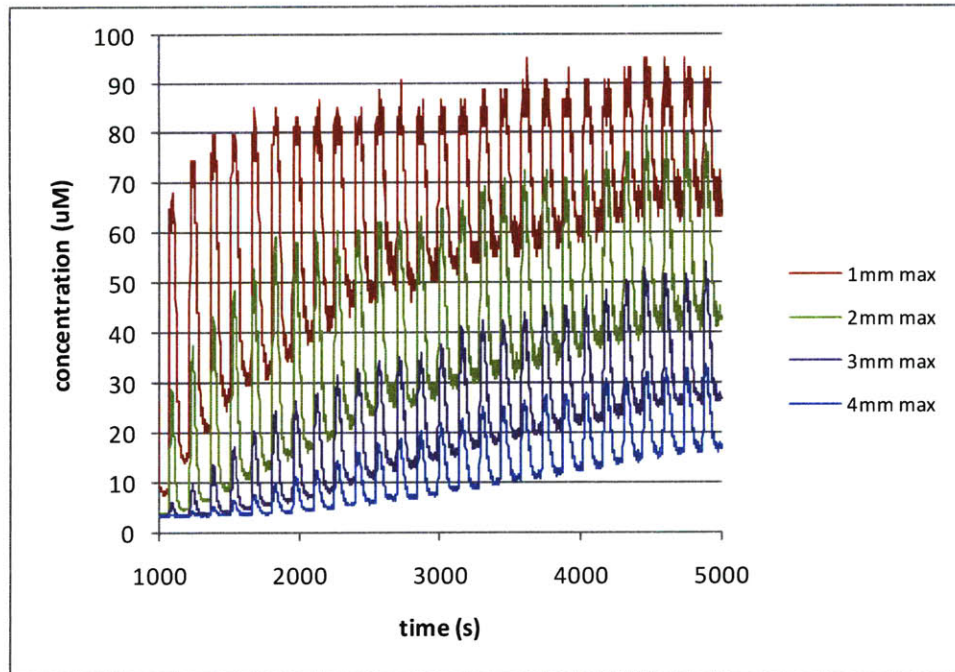


Figure 3.21: Maximum concentration as a function of time for 4 locations along tube length

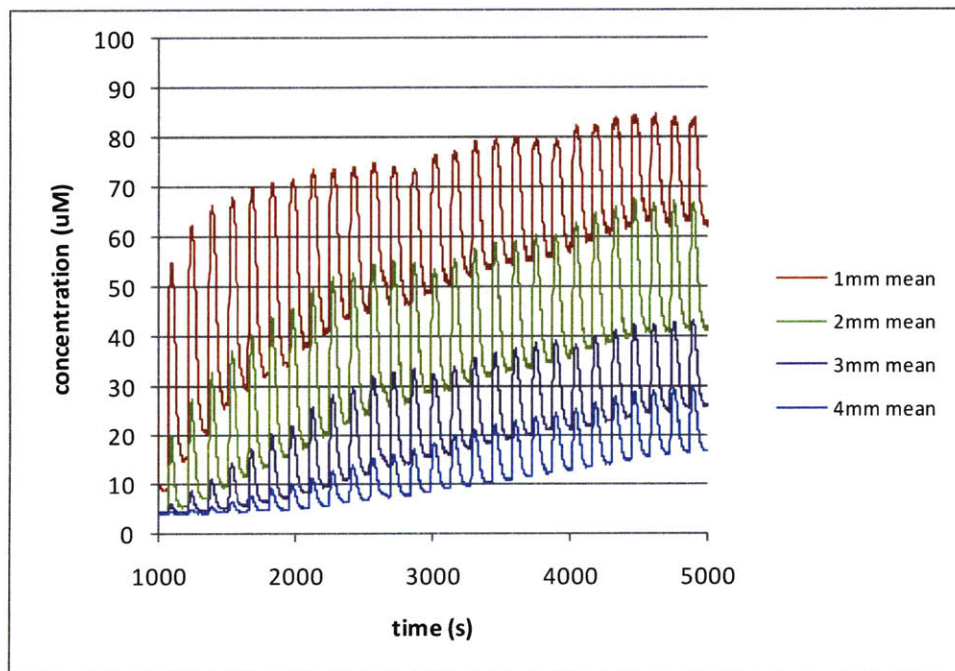


Figure 3.22: Mean concentration as a function of time for 4 locations along tube length

The model utilized the syringe pump flow module discussed above. The circuit is shown below in Figure 3.23 with key component values. Figure 3.9 above has these components labeled to show the physical system parts they represent.

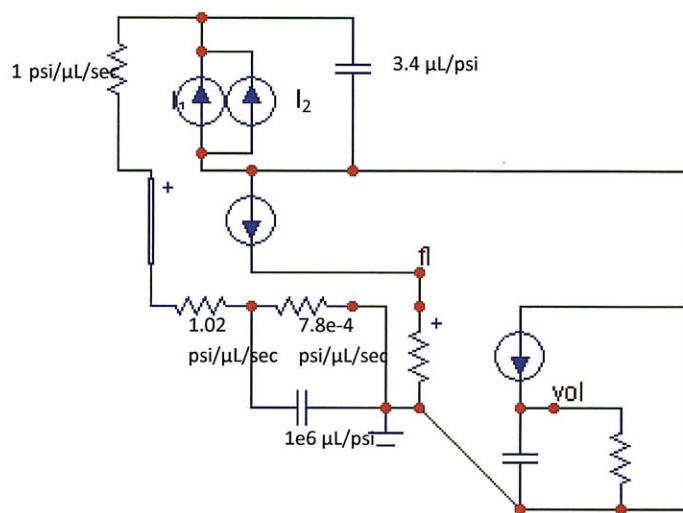


Figure 3.23: Syringe pump flow module where I_1 and I_2 have the following settings (initial current value[$\mu\text{L}/\text{sec}$], pulsed current value, time delay before pulse [sec], pulse rise time, pulse fall time, pulse width, pulse period): I_1 (0, 0.64, 1.2, 0, 2.8, 0.2, 150), I_2 (0, -0.016, 35, 0, 0, 59, 150)

The values for the syringe pump were fit to flow sensor output data as the Labview syringe pump settings did not exactly match flow sensor data due to resistance and compliance in the delivery system. The flow rate and displaced volume from the experiment and model are compared in Figure 3.24. Only one cycle is shown, but it was repeated every 150 sec for the duration of the experiment.

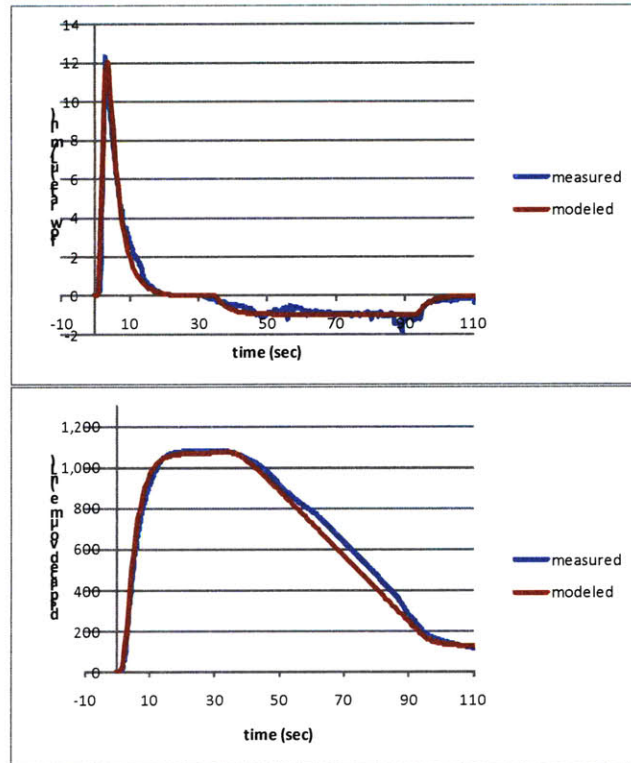


Figure 3.24: Comparison of measured versus modeled flow rate (top) and displaced volume (bottom) versus time in glass tube experiment.

The flow sensor was placed in the system upstream of the cannula, which has a high resistance, so the flow data does not accurately represent the flow entering the glass tube. Figure 3.25 shows the measured data from the flow sensor compared to the modeled flow at the cannula exit. This was done to illustrate the effects on flow characteristics due to the high resistance of the cannula, a lower maximum flow rate but an equal maximum displaced volume.

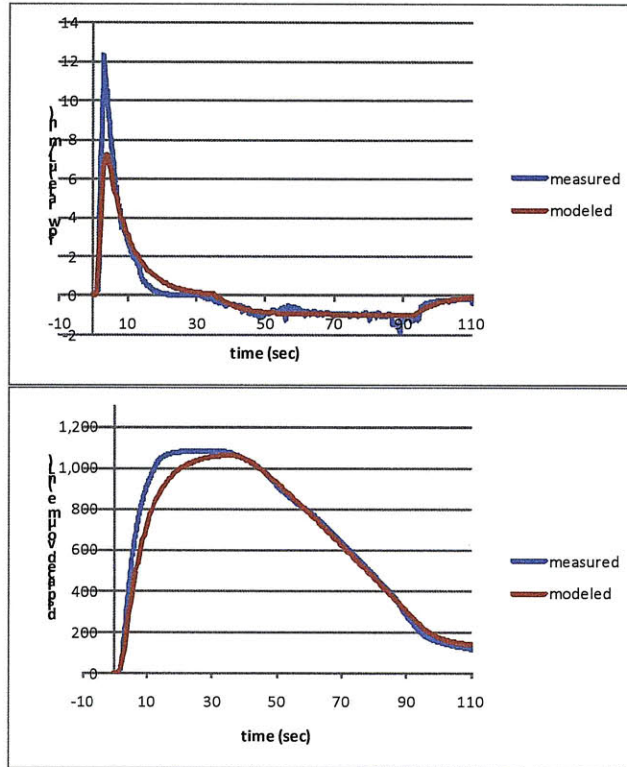


Figure 3.25: Modeled flow (top) and volume (bottom) going into tube versus measured flow upstream of cannula.

The transport module shown above in Figure 3.14 was used to model the convective diffusion of fluorescein along the length of the glass tube. Table 3.5 shows values used to calculate the electrical components used in the circuit.

Table 3.5: Component values of transport module in glass tube experiment

Segments tube divided into (#)	10
Glass capillary tube length (mm)	100
Glass capillary inner diameter (mm)	0.86
Fluorescein diffusivity (cm^2/sec)	$7.83\text{e-}6$
Fluorescein concentration (μM)	100
Lossy transmission line (fast core)	
Capacitance (μL)	0.209
Resistance (sec/mm^3)	$6.11\text{e}3$
Lossy transmission line (slower outer ring)	
Capacitance (μL)	0.372
Resistance (sec/mm^3)	$3.44\text{e}3$
Lossy transmission line length (mm)	9 segments: 1 mm, last segment: 91 mm
Radial diffusive resistance (sec/mm^3)	$8.8\text{e}3$

Results of the model are compared to experimental data in Figures 3.26 to 3.31 for points at 1, 2 and 3 mm from the cannula along the length of the glass tube. In Figures 3.26 to 3.28, the results are compared to maximum concentration, while Figures 3.29 to 3.31 compare mean concentration. The modeled data shows the long-term trend of concentration increase with time that was seen in the experimental data. The peaks in concentration correspond to the pulsatile flow profile, and the peaks in the modeled data match the mean experimental concentration better than the maximum concentrations. This agrees with the way the model was designed as the output voltage at each location represents the average concentration at that point. The diffusivity that was used was the published value, but it appears that a slightly lower value may provide better agreement to the experimental results.

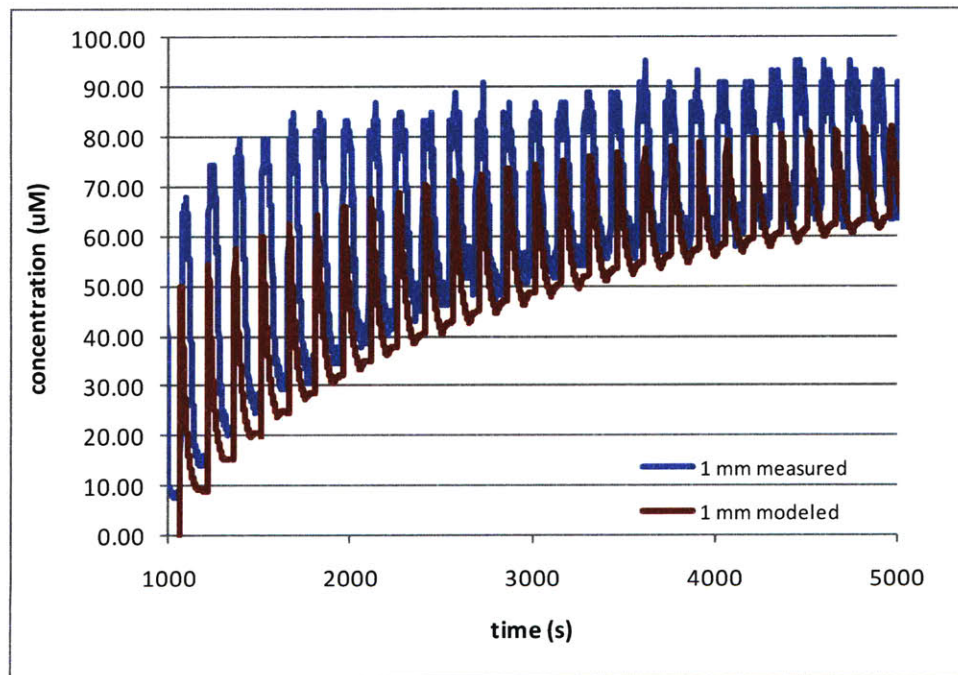


Figure 3.26: Maximum measured concentration at 1 mm compared to modeled concentration

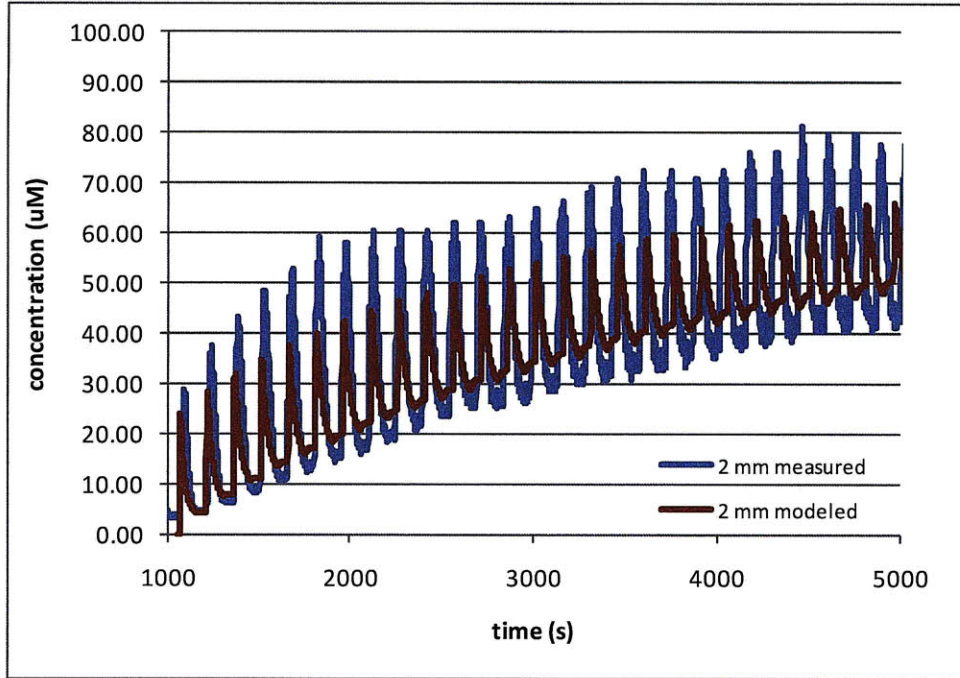


Figure 3.27: Maximum measured concentration at 2 mm compared to modeled concentration

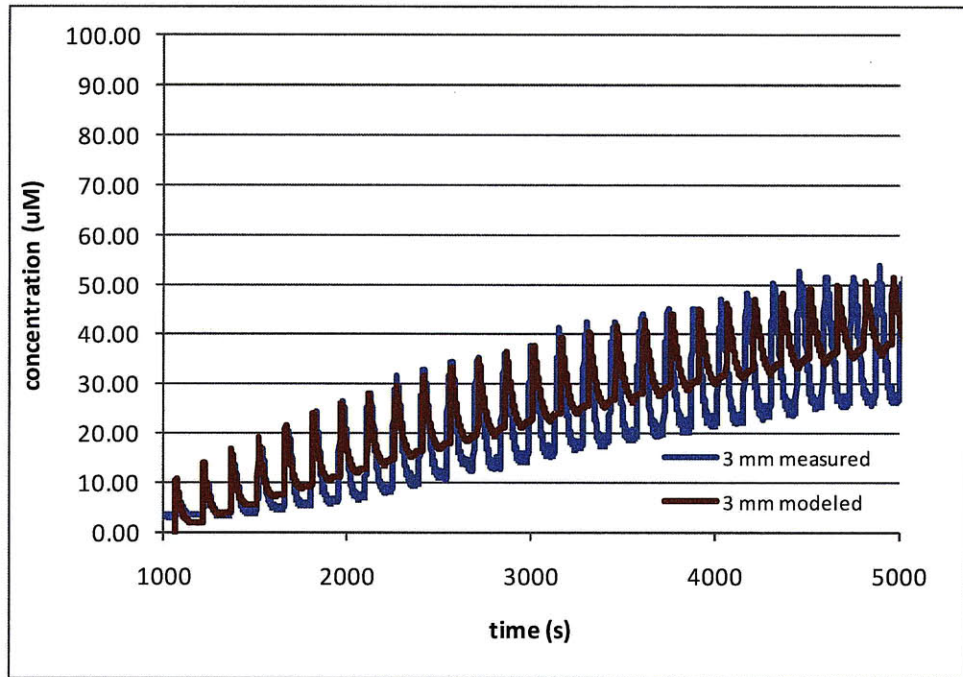


Figure 3.28: Maximum measured concentration at 3 mm compared to modeled concentration

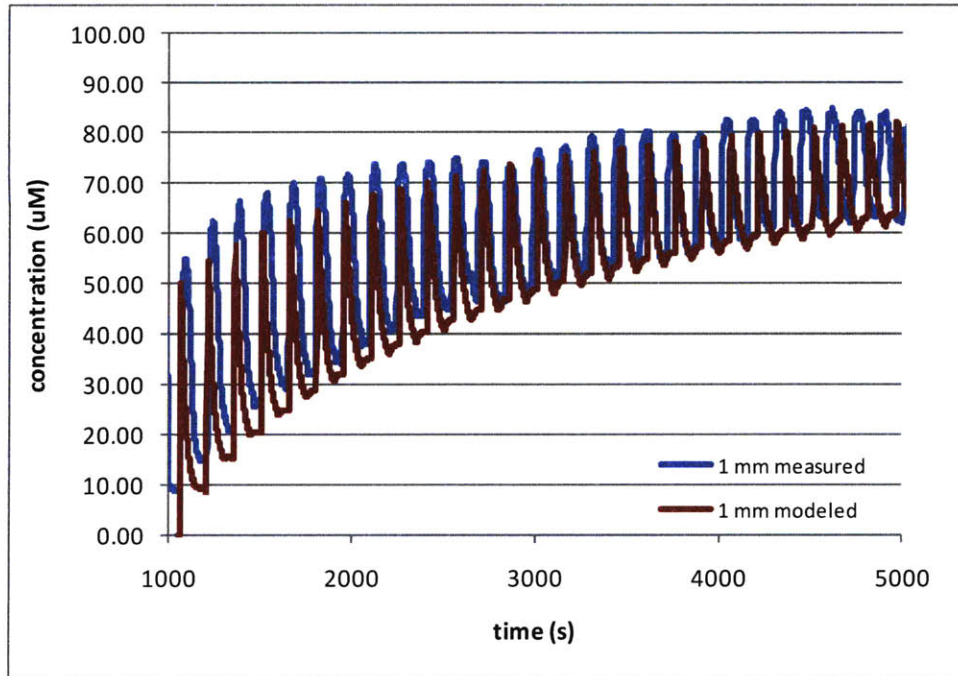


Figure 3.29: Mean measured concentration at 1 mm compared to modeled concentration

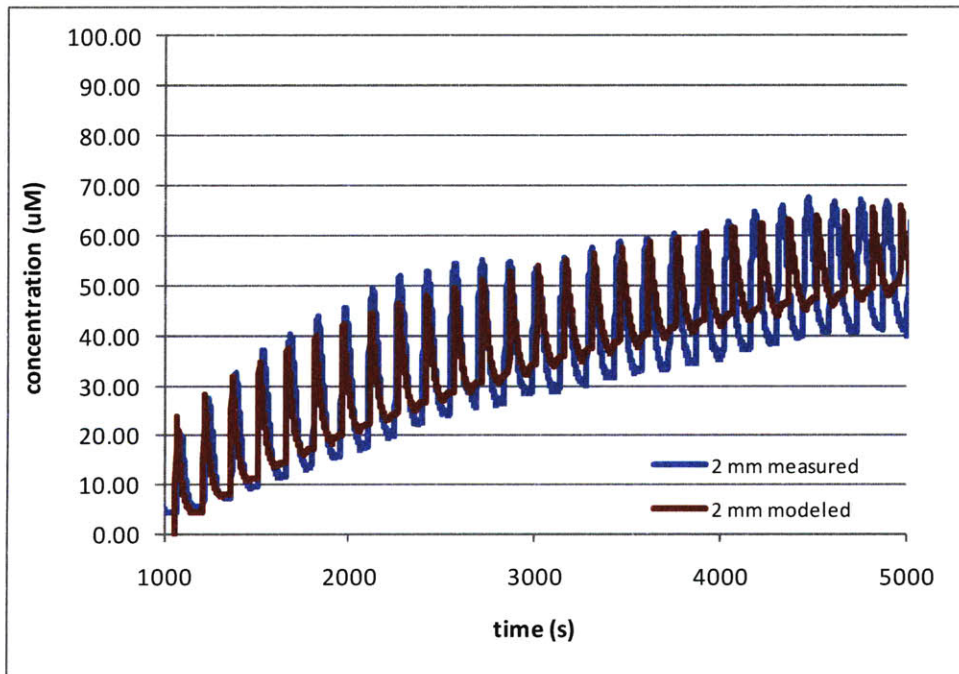


Figure 3.30: Mean measured concentration at 2 mm compared to modeled concentration

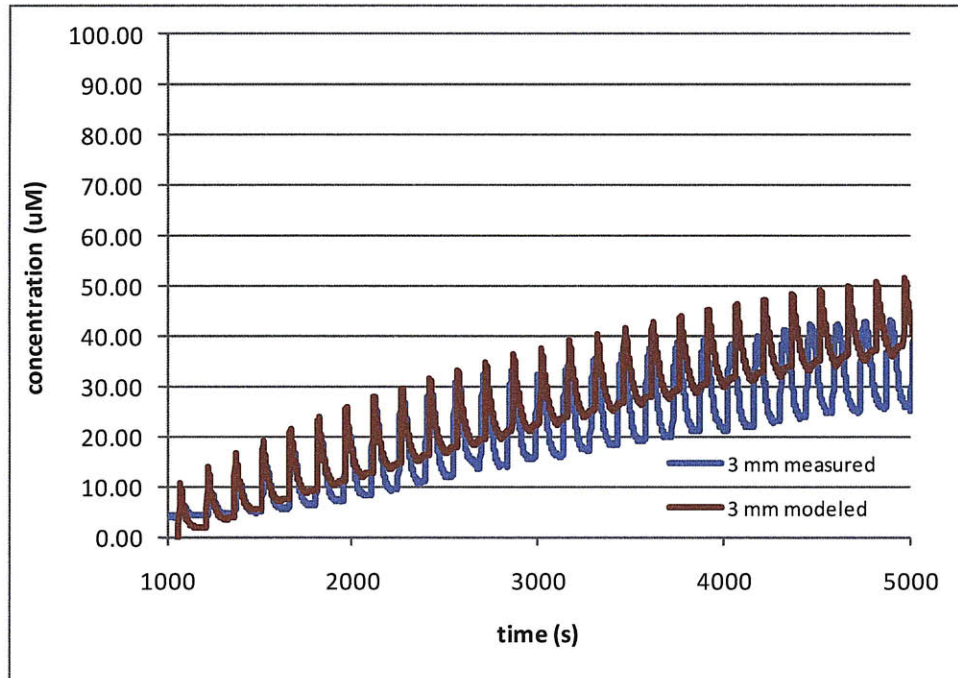


Figure 3.31: Mean measured concentration at 3 mm compared to modeled concentration

3.7 MODELING OF DRUG DELIVERY IN GUINEA PIG COCHLEA

The model was altered for use in understanding transport in the cochlea, and it was compared to experimental results from guinea pig tests. For the experiment, a bioassay was used for in vivo monitoring to follow the time course of drug activity in the ST. The cochlea is organized so that the range of frequencies that can be heard is tonotopically distributed along its length, as shown in Figure 3.32 [6, 19].

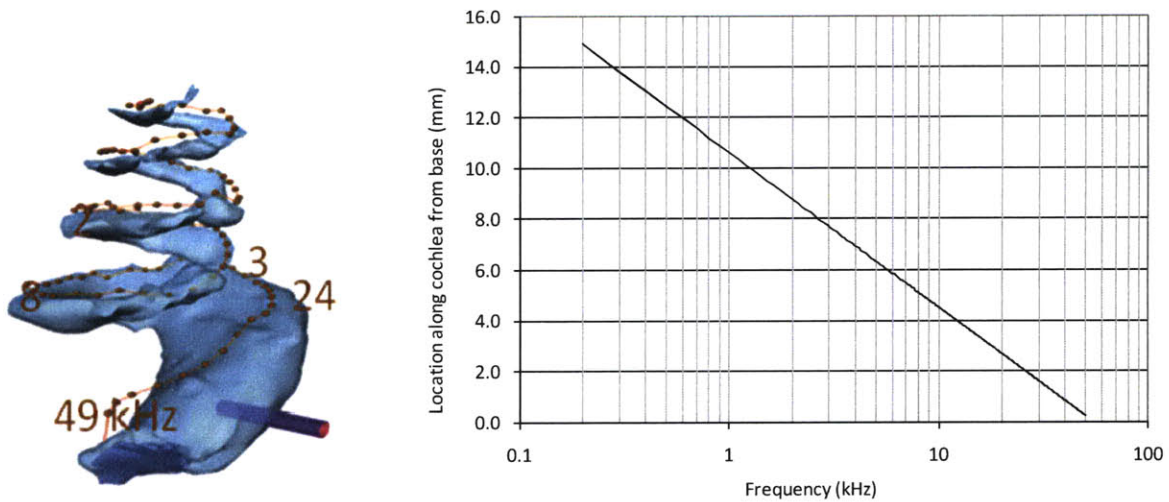


Figure 3.32: (left) Reconstruction of guinea pig cochlea showing tonotopic relationship of frequency, (right) characteristic frequency along length of guinea pig cochlea (reproduced from data in [19]).

Electrophysiological assessment of solute transport allowed real-time analysis of delivery over periods of hours [1]. A drug that increases hearing thresholds, 6-7-dinitroquinoxaline-2,3-dione (DNQX), was delivered to the guinea pig cochlea, and as thresholds at frequency locations were sequentially elevated, the progression of the drug along the length of the cochlea was tracked. Hearing tests to measure compound action potentials and distortion products, as described below, tracked the sound level thresholds for response. One drawback to this method was that the exact concentration of drug needed to eliminate hearing at a specific site was not known and has only been estimated through dose-response curves [1]. In addition, direct fluid sampling was not possible as hearing thresholds would be elevated or destroyed by the surgical technique and withdrawal of perilymph. Also, in the guinea pig, the ST is in direct fluidic communication with CSF through the cochlear aqueduct. Removal of perilymph would lead to the infiltration of CSF, dilution of perilymph and drug, and inaccurate measurements. For these reasons, only indirect measurements of drug levels through the bioassay were possible.

The necessary changes for the flow module to represent delivery into the guinea pig cochlea were addressed above. The reservoir resistance was replaced by the flow resistance of the scala tympani and scala vestibuli, and the components representing the round window, oval window, and cochlear aqueduct were added (Figure 3.11). Precise dimensions of the guinea pig cochlear fluid spaces are available from magnetic resonance imaging [6]. For each 0.1 mm-segment of the scala tympani and

scala vestibuli, the cross-sectional area was reported. The perilymph viscosity was 1.75×10^{-9} psi*min. The cannula was placed at 1.8 mm from the base. The flow resistance values were calculated using Equation 3.17. The other component values were provided in the literature.

The diffusive resistors and capacitors in the transport module for the guinea pig cochlea were calculated in a similar manner as for the glass tube. In animal experiments, as described below, the fluorescein was replaced by DNQX. Also, for comparison purposes, the scalae were divided into unequal segments to match locations of measured frequencies in the experiment. Table 3.6 summarizes the values.

Table 3.6: Circuit element values in the transport module for the guinea pig experiment

Segments cochlea divided into (#)	11
DNQX diffusivity (cm^2/sec) (estimated from molecular weight=232)	4.70×10^{-6}
DNQX concentration (μM)	300
Capacitance (μL) (45 kHz region)	0.932
Resistance (sec/cm^3)	1.57×10^6
Capacitance (μL) (32 kHz region)	0.974
Resistance (sec/cm^3)	1.37×10^6
Capacitance (μL) (28 kHz region)	0.108
Resistance (sec/cm^3)	1.97×10^5
Capacitance (μL) (24 kHz region)	0.655
Resistance (sec/cm^3)	3.04×10^6
Capacitance (μL) (16 kHz region)	0.927
Resistance (sec/cm^3)	4.99×10^6
Capacitance (μL) (12 kHz region)	0.232
Resistance (sec/cm^3)	6.15×10^6
Capacitance (μL) (8 kHz region)	0.227
Resistance (sec/cm^3)	7.97×10^6
Capacitance (μL) (5.6 kHz region)	0.191
Resistance (sec/cm^3)	2.65×10^7
Capacitance (μL) (4 kHz region)	0.515
Resistance (sec/cm^3)	1.21×10^8
Capacitance (μL) (2.78 kHz region)	0.432
Resistance (sec/cm^3)	2.27×10^8
Capacitance (μL) (more apical ST and SV)	3.652
Resistance (sec/cm^3)	6.17×10^7

It should be noted that the actual diffusivity of DNQX was not available. The value was estimated from its molecular weight.

Additional biological aspects of the cochlea are not as easily modeled. Little is known of the various clearance and binding mechanisms in the cochlea, and these are dependent on the specific drug or solute. Protein binding is hypothesized to play a major role in limiting access of drugs to the target tissues. As discussed in Chapter 4, a large amount of protein present in the perilymph is capable of binding various types of drugs. Also, many enzymes are found in perilymph that could modify the molecular structure of drugs. Other mechanisms include clearance through the vasculature, diffusion into tissue, and metabolism. Time courses for these are not known. More details will be discussed below.

3.7.1 Comparison of model to Salt simulator

As described above, a free cochlear delivery simulator is available online from A. Salt. Additional validation of the lumped parameter model was done using the simulation tool developed by Salt [4, 5]. The Salt tool simulates bolus or steady infusion modes of delivery, and, similar to the lumped model, captures drug transport via both diffusion and pressure-driven flow. The Salt model is not capable of capturing the pulsatile flow profile of this delivery system and does not incorporate drug binding mechanisms. Figures 3.33 to 3.35 show the user interface for the Salt simulator. Delivery parameters included: bolus volume of 0.655 μL , solute concentration of 300 μM , and solute diffusivity of $9.4\text{E-}6 \text{ cm}^2/\text{sec}$. The bolus was administered at a point 2.2 mm from the base of the scala tympani.

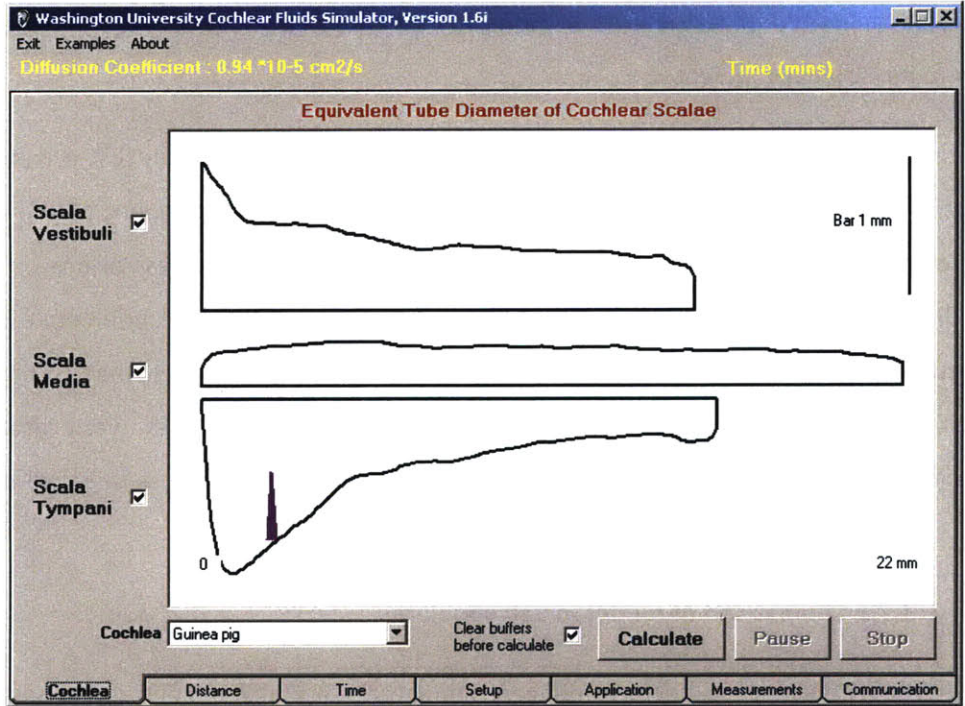


Figure 3.33: Salt simulator window showing position of bolus entry in scala tympani

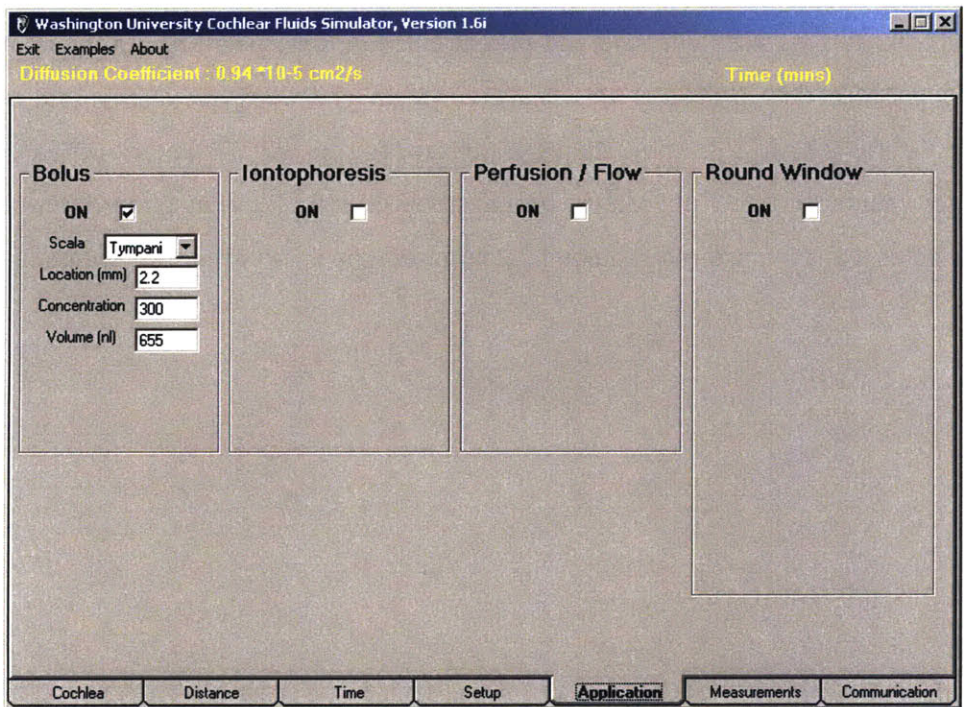


Figure 3.34: Salt simulator window showing bolus application inputs

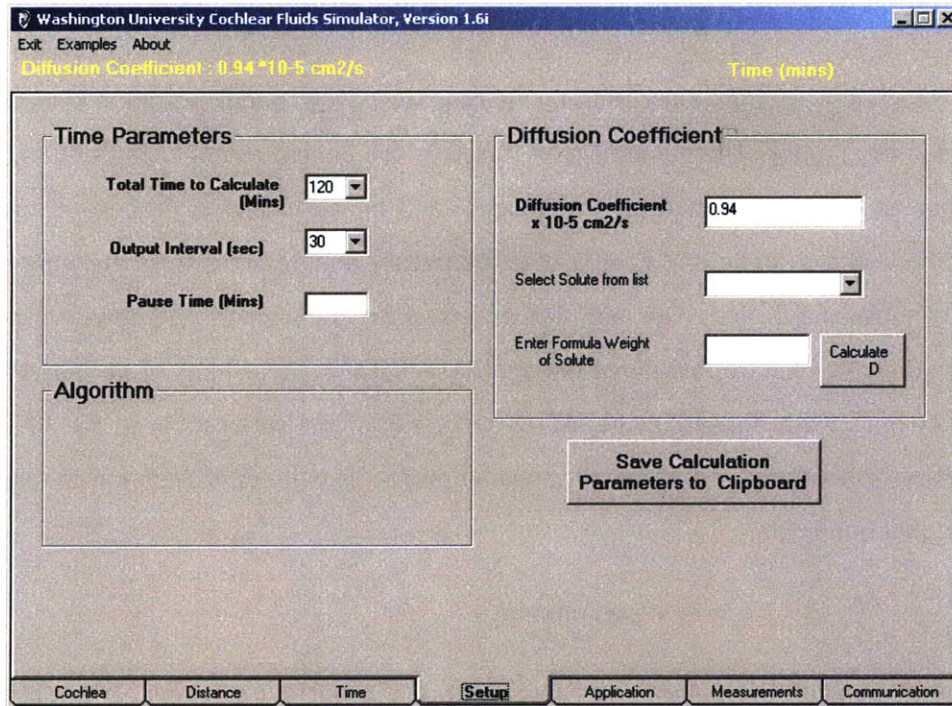


Figure 3.35: Salt simulator window showing time and diffusion parameters

Figure 3.36 shows comparative plots of the two simulators for a bolus delivery. Concentration profiles in the 32 kHz and 8 kHz regions show good agreement in concentration amounts and in long-term trends.

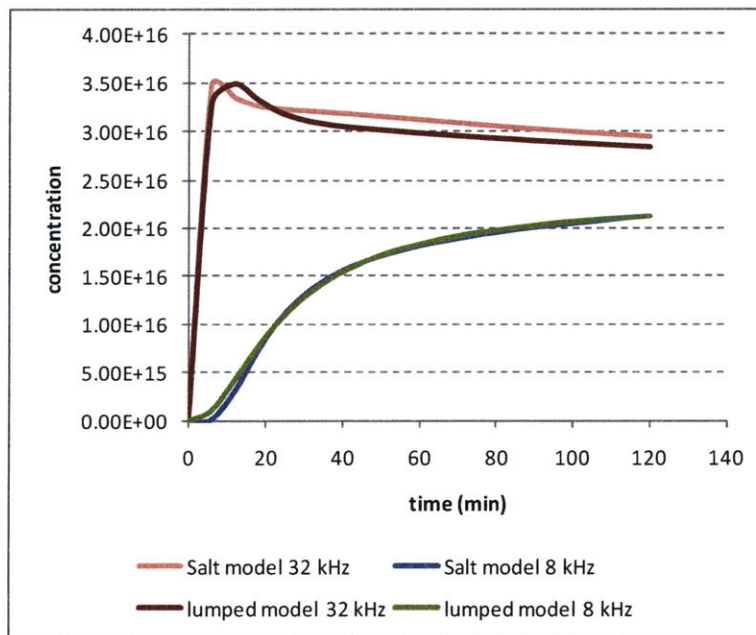


Figure 3.36: Comparison of Salt simulator to lumped element model for two frequency locations

3.7.2 Guinea pig cochlea drug delivery experimental method

In vivo guinea pig studies were undertaken using the syringe pump system to compare results to those of the delivery model. The guinea pig was used as the animal model because it has a large and accessible inner ear and its anatomical, physiological and pharmacological properties are thoroughly understood. The animals are easily kept in the laboratory and tolerate well the long surgery and implantation of tubes and devices. The team has extensive experience perfusing the inner ear of guinea pigs and in quantifying, electrophysiologically and histologically, the effects of various treatments in guinea pigs. Animals were housed in the IACUC-approved animal care facility at the MEEI. Surgical, perfusion, testing, euthanasia and tissue preparation protocols were approved and monitored by the MEEI Animal Care Committee.

3.7.2.1 System preparation

In preparation for the guinea pig experiment, the artificial perilymph (AP) was thawed and placed in the heated chamber to equilibrate to body temperature. The syringe pump (Harvard Apparatus PHD 2000) was connected to the computer to allow for Labview control using a customized program that set the flow parameters and controlled pump infusion and withdrawal at intervals set by the user. A 6-foot length of large-bore, rigid Teflon tubing was connected to an electronically shielded flow sensor (Sensirion 1430). The sensor provided input to the Labview program so volume and flow could be continuously monitored throughout the experiment. The length allowed the syringe pump to be maintained outside of the acoustically-shielded chamber while the remaining system components resided in close proximity to the animal. The outlet of the flow sensor was then connected to the manifold housing the cannula for cochlear implantation. As shown in the diagram (Figure 3.19), a second manifold connected the drug reservoir to the infusion line. A pump attached to a timer-controlled power source ensured that the drug was completely refreshed in the slug of fluid entering the cochlea between each cycle. The drug loop was filled with 300 μ M DNQX. All other components were carefully filled with AP as the system was constructed to eliminate bubbles in the system. After filling, the other end of the Teflon tubing was connected to a 100 μ L glass Hamilton syringe that was placed on the syringe pump.

The cannula was placed in an AP reservoir for system testing. The Labview program was set to the desired infuse and withdraw rates and durations to provide the desired flow characteristics, and the sensor output was monitored to ensure agreement between the settings and actual flow from the

cannula. The drug loop pump was also tested. It was cycled enough times to push 1 μL of fresh drug solution into the infuse loop, usually 2-3 pump pulses. The timer box was set to repeat every 3 minutes to match the period of syringe pump cycling. After demonstration of proper performance of the pump on the bench, the animal was prepared for surgery.

3.7.2.2 Surgical Preparation

All procedures were accomplished in an acoustically and electrically shielded, heated (34 °C) chamber. Adult albino guinea pigs (Charles River, 350-500 g) were anesthetized with a combination of pentobarbital sodium (25 mg/kg intraperitoneal), fentanyl (0.2 mg/kg intramuscular), and droperidol (10 mg/kg intramuscular). Anesthetic boosters of one-third the original dose were administered every 2 hr or as required to maintain an adequate depth of anesthesia. The head and neck/upper chest areas were shaved, the animal was placed supine, and the surgical area of the ventral neck was cleaned. The bulla was exposed via a retroauricular incision, and an opening in the bulla was created with a sharp blade to visualize the cochlear basal turn and the round window membrane. A cochleostomy, an approximately 150-200 μm opening into the scala tympani of the cochlear basal turn, was created using a modified pick shaved specifically for this purpose. During placement of the perfusion tubing (flexible fused silica; 150 μm O.D.; 75 μm I.D.) into the cochleostomy, dental cement (ESPE, 3M, St. Paul MN) was placed around the tubing to secure it and to seal the cochleostomy. The perfusion line, attached to the manifold, was then cemented to the bulla to prevent movement. Heart rate was monitored throughout the experiment as an indicant of depth of anesthesia.

The compound action potential (CAP) electrode was placed near the round window niche and acoustic apparatus was properly positioned in the ear canal. Baseline responses (CAP and distortion product otoacoustic emission [DPOAE]) were monitored, as described below. After demonstration of normal baseline sensitivity, the pump was started at 150 sec intervals with AP only. The round window membrane was visualized through the bulla opening. Bulging of the round window membrane was seen during the pulses, confirming proper functioning of the perfusion system. The AP alone was perfused for a half of an hour, and stable hearing was maintained. The drug was then incorporated into the AP. CAP responses were measured approximately half-hourly, and DPOAE responses were monitored hourly throughout the course of drug perfusion.

3.7.2.3 Control Solution and Drug

An AP solution served as a control solution and also as the vehicle for the test drug. It was mixed in-house and was composed of (in mM): NaCl, 120; KCl, 3.5; CaCl₂, 2; glucose, 5.5; HEPES, 20, and it was titrated with NaOH to pH 7.5 in a deionized and filtered water base for a total Na⁺ of 130 mM. The experimental drug, the glutamate receptor antagonist, DNQX (300 μM), was dissolved in the AP and pH-adjusted as needed. DNQX was first dissolved in a small amount of dimethyl sulfoxide (DMSO; final concentration, 0.05%) which did not, on its own, produce significant changes in cochlear responses. All drugs were from Sigma chemicals. DNQX acted to block transmission between inner hair cells and the auditory nerve and effected CAP thresholds, which are described below. It had no impact on DPOAE levels (described below) as these originated at the outer hair cells. DPOAE acted as an internal control during drug delivery.

3.7.2.4 Electrophysiologic and otoacoustic measures

Stimuli were created and responses monitored using 16-bit A/D, D/A boards (National Instruments, Austin TX) controlled in a Labview environment by a computer. Signals used to elicit CAP and DPOAE were delivered to the ear using a custom coupler that accommodates transducers (Tucker Davis EC1) and a Knowles EK3103 electret microphone to measure ear-canal sound pressure (for DPOAEs) via a probe tube concentric with the 2.54 mm (O.D.) sound delivery tube. Sensitivity versus frequency calibration curves were generated for the monitoring and probe microphones, respectively, enabling conversion from voltage to sound pressure level (SPL) (in dB re: 20 μPa). The probe assembly was then placed at the animal's ear canal where 'in-animal' calibration sweeps were accomplished and used to determine the actual SPLs generated at the entrance to the bony canal. After calibration, the probe assembly remained in place for the duration of the experiment.

CAP, a measure of activity of the auditory nerve, was elicited using tone pip stimuli (2.78 – 32.0 kHz, 0.5-ms duration, 0.5-ms rise-fall, cos² onset envelope, 16/sec). Levels were incremented in 5 dB steps from 0 to 80 dB SPL. Responses were detected via a silver-wire electrode at the round window niche, amplified (10,000 times), filtered (300 Hz to 3 kHz), and averaged across 32 samples. Response values (e.g., thresholds, peak-to-peak amplitudes) and waveforms were stored. CAP threshold was defined as the lowest stimulus level at which response peaks were clearly and reproducibly present.

When two primary tones (f₁, f₂) were played simultaneously to the ear, acoustic distortion products of their interaction in the cochlea were propagated back out through the middle ear and detected using a

sensitive microphone placed in the external ear canal. The distortion product corresponding to the frequency ($2f_1-f_2$) was used as a metric of cochlear and, in particular, outer hair cell function. These ($2f_1-f_2$) DPOAEs were recorded as response amplitude versus primary level functions ($L_1=10-75$ dB SPL, $L_2=L_1-10$, primaries incremented together in 5 dB steps) spanning the frequency range $f_2 = 2.78 - 32.0$ kHz (selected to equal CAP test frequencies, $f_2/f_1 = 1.2$). Ear-canal sound pressure was amplified, digitally sampled, and averaged (25 discrete spectra at each frequency-level combination), and Fast-Fourier transforms were computed from averaged pressures. DPOAE level at ($2f_1-f_2$) and surrounding noise floor values (± 50 Hz of $2f_1-f_2$) were extracted. Iso-response contours (L_2 levels required to generate a DPOAE amplitude criterion of 0 SPL) were constructed from amplitude versus sound level data to facilitate comparison with CAPs.

3.7.3 Results

DNQX, at a concentration of 300 μ M, was delivered to the cochlea using the syringe pump system. The system was configured to deliver a maximum volume of 750 nL at a maximum flow rate of 8.5 μ L/min and withdraw the same amount in 90 sec. The cycle was repeated every 150 sec. Consistent with a site of action at the inner hair cell-afferent fiber synapse, perfusion of DNQX elevated CAP thresholds. Drug effects on CAP were frequency sensitive; responses to high frequency stimuli were altered first and most, followed progressively by involvement of responses to mid- and then lower-frequency stimuli. This reflected the influence of location of drug administration through the cannula in the high frequency region (around 28 kHz). Threshold levels at 32 and 24 kHz immediately rose above the saturation level of the equipment and could not be measured. No change in threshold levels was seen in DPOAEs. This confirmed that the delivery mechanism itself did not cause damage to hearing. The threshold shifts resulted from the delivery of DNQX.

Drug-induced changes as a function of frequency are plotted in Figure 3.37. The data represents the averaged results of four guinea pig experiments. Threshold elevations in CAP were seen as far apically as 12 kHz, though they were smaller than those at basal frequencies. This suggested that longer perfusion times are needed for delivery to more apical regions of the cochlea. DPOAE thresholds are shown in Figure 3.38.

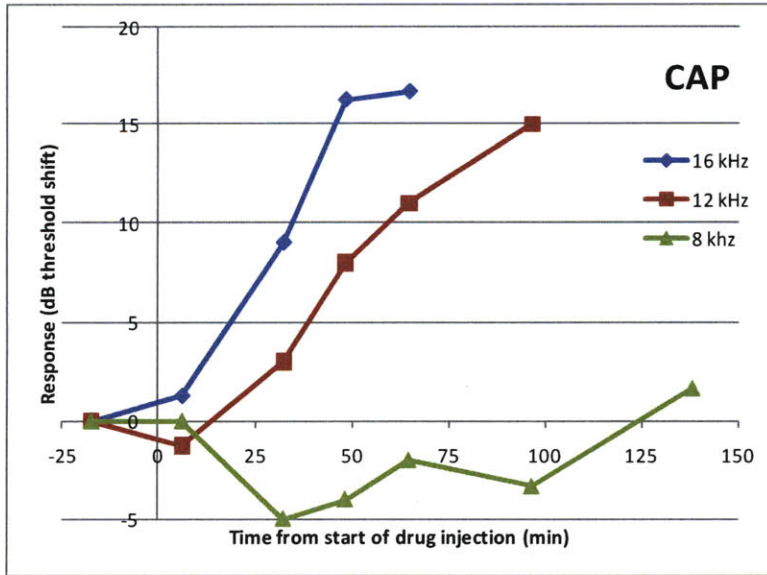


Figure 3.37: Average CAP response at several locations over time to DNQX delivery in guinea pigs

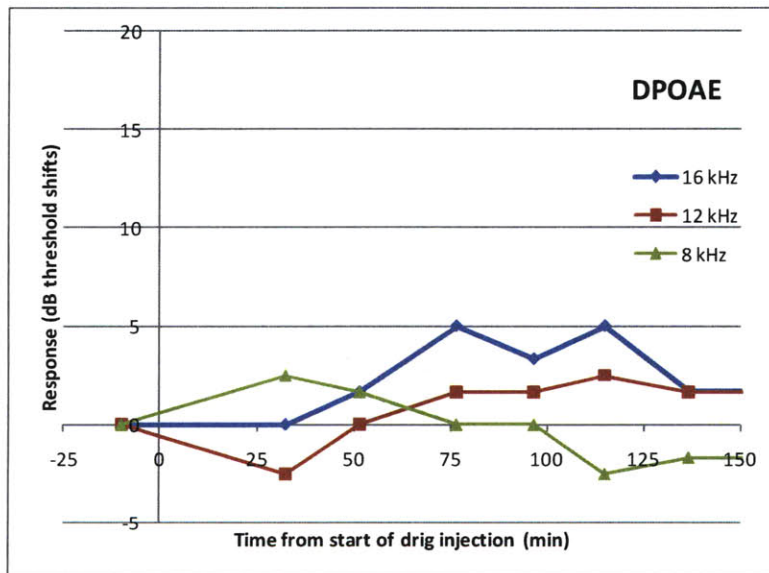


Figure 3.38: Average DPOAE response at several locations over time to DNQX delivery in guinea pigs

Identical experiments were conducted with maximum flow rates set at 13 $\mu\text{L}/\text{min}$ and 21 $\mu\text{L}/\text{min}$. In general, similar results were seen. The onset of drug action at lower frequencies occurred slightly more quickly with the higher flow rates, but DPOAE shifts were minimally higher suggesting damage to the cochlear structures due to the higher flow rate. Experiments to determine the optimal delivery profile with minimal damage continue.

3.7.4 Dose-response relationship

In order for experimental results to be compared to the model, the hearing response at the measurement points of the model must be inferred from the concentration based on a dose-response relationship. Unfortunately, this relationship has not been established for a range of DNQX concentrations. Equipment settings limit the recording of hearing threshold shifts above 30 dB. Any DNQX-induced changes above this value cannot be measured. It was found that the 300 μM concentration used in this series of experiments caused thresholds to increase beyond measurement limits at the higher frequencies. Therefore, the maximum response to these concentrations is not known. Based on these findings, the construction of an accurate dose-response curve was very difficult, and this proved to be one of the main limitations encountered in the attempt to compare experimental to modeled results. Additional limitations are outlined below. A dose response curve constructed with a linear fit for the small dB range (0-25dB) measurable in these experiments. The intercept was set to 0 and the slope to 0.5 dB/ μM as shown below in Figure 3.39. This relationship was used to convert model output concentration to hearing response for comparison to experimental results. Additional experiments need to be conducted to better understand the relationship.

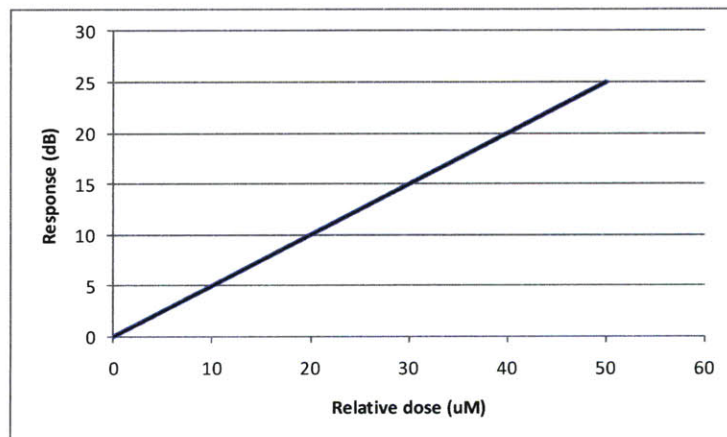


Figure 3.39: Constructed DNQX dose-response relationship

3.7.5 Mechanisms limiting drug availability

DNQX binding to protein in perilymph is hypothesized to play a major role in limiting the amount available to target tissue. As discussed later in Chapter 4, many proteins exist in perilymph that are capable of binding various drugs. In the case of DNQX, proteins that bind both acidic compounds and lipophilic

compounds may bind this drug. These proteins, including albumin and apolipoproteins, account for over 35% of all of the protein in perilymph.

Estimations of protein binding were undertaken to provide parameters to model the phenomenon. The experimental threshold shift at the 12 kHz region was compared to the estimated concentration expected due to diffusion alone. After approximately 200 min, the experimental concentration was only approximately 1% of what would be expected from diffusion alone. This estimate is in line with 2% estimated bioavailability of drugs with similar composition to DNQX.

In the short time period of acute experiments, the amount of protein present in the scala tympani is constant. Therefore, after all the available protein has bound to the DNQX, the rest of the drug will be available to cause a change in hearing response. On this short time course, the other loss mechanisms are assumed to be much slower than the protein binding.

In order to model the binding, the capacitors representing the cochlear segments were given initial conditions equal to $-1.75e17$, representing 99% of the DNQX concentration delivered. Only after the amount of DNQX in each segment rose above this value did the model predict an increase in hearing threshold levels, i.e. a positive charge on a capacitor indicated unbound DNQX. This crude method of accommodating protein binding delayed the onset of a response but did not slow the subsequent rise that was seen in the experimental data. Therefore, other methods of accommodating protein binding were employed.

After removing the initial condition on the capacitors, the diffusion coefficient was empirically altered to reflect a much larger molecule, DNQX bound to protein. The diffusivity was decreased 5-fold to slow the diffusive transport in the model and more accurately represent the experimental findings. While empirically chosen, the diffusion coefficient was estimated from an analysis of the diffusion-only case for mass transport, thus assuring a physical significance for the value.

In the future, additional work should be done to accurately represent this and other clearance and loss mechanisms limiting drug response. More loss elements (resistors) could be added to represent metabolism, clearance to vasculature, diffusion through surrounding tissue, etc. Storage elements (capacitors) could represent reversible binding to protein in tissue and refreshing of perilymph protein. However, elucidating the individual contributions of these mechanisms may prove very difficult and consuming. Figure 3.40 illustrates how additional elements could be incorporated into the model to represent other biological aspects.

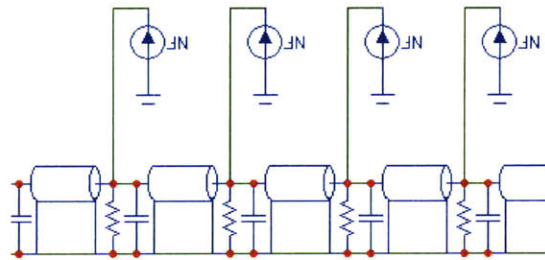


Figure 3.40: Circuit diagram showing the inclusion of additional elements to model biological phenomena

3.8 COMPARISON OF THE MODEL TO EXPERIMENTAL DATA

The experimental data from 32 and 24 kHz could not be compared to the model since the threshold almost immediately increased to and surpassed the maximum level the equipment could evaluate. The comparison of the modeled data to the experimental data at 16 and 12 kHz did not provide an adequate fit. It was hypothesized that mixing and other complicated flow characteristics were present in the region near the cannula insertion point that the model was not capturing. However, at some distance apical to the insertion point, these phenomena were no longer dominating, and diffusion was dominating. This position became the effective insertion point. In addition, a new initial concentration was established at this point due to dilution in the mixed area. Figure 3.41 shows a schematic of the cochlea with relevant distances marked. The location of the effective insertion point, 2.7 mm from the base, was determined from a curve fit to the experimental data. The effective initial concentration is dependent on this location due to the volume of perilymph diluting the drug. The volume was found to be four-fold greater than the volume of the actual drug injection. Therefore, the initial concentration at the new effective insertion point was four-fold smaller.

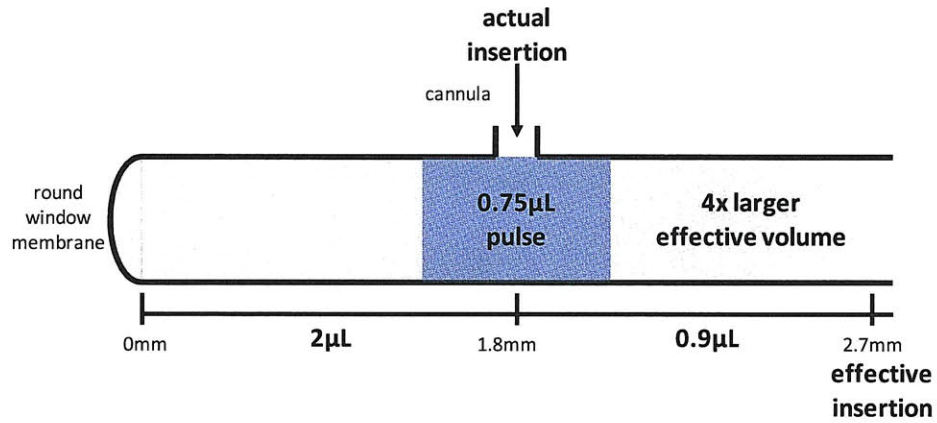


Figure 3.41: Schematic of effective insertion location in cochlea

These values were then used to guide optimization of the model. The model was manually fit by varying the insertion point and initial concentration. Figures 3.42 and 3.43 show the modeled data with an effective insertion location of 2.7 mm and an initial concentration of 50 μM compared to the individual data for the four experiments summarized above.

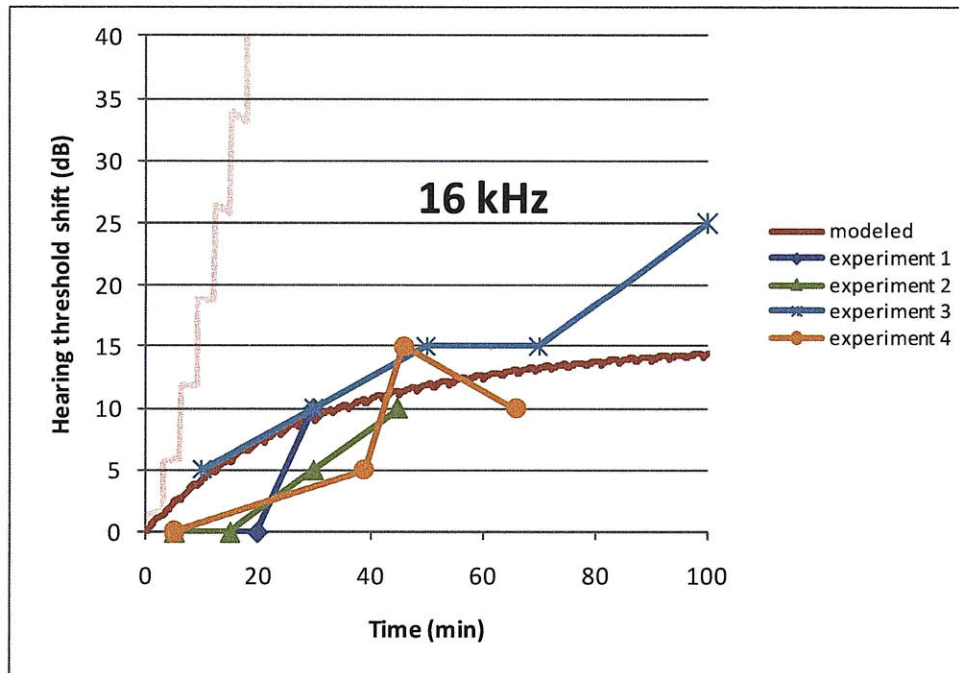


Figure 3.42: Comparison of experimental data to model at 16 kHz for guinea pig experiments. The light red line shows the modeled result using the actual experimental insertion point and concentration rather than the effective insertion point and concentration.

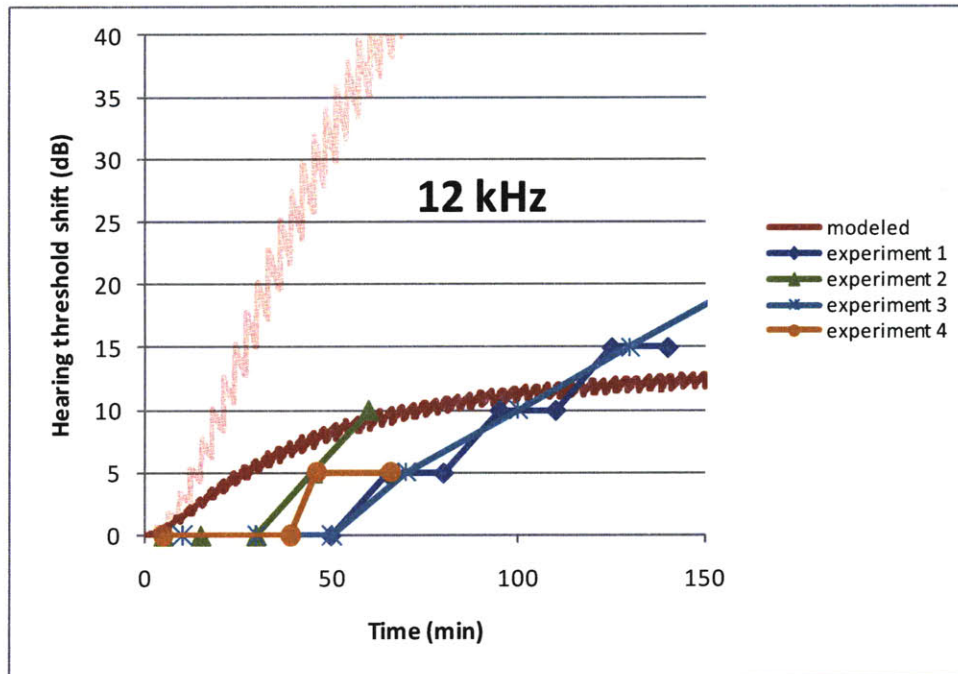


Figure 3.43: Comparison of experimental data to model at 12 kHz for guinea pig experiments. The light red line shows the modeled result using the actual experimental insertion point and concentration rather than the effective insertion point and concentration.

3.9 LIMITATIONS OF THE MODEL

Many limitations in modeling the in vivo experiments exist. No direct method for measurement of drug concentration in the cochlea exists, and direct fluid sampling from the cochlea is limited. Creating access for sampling causes damage to hearing, and CSF contamination of the sample occurs due to the guinea pigs' patent cochlea aqueduct. For these reasons, the concentration of drug must be inferred from the biological response. In the case of DNQX, no dose-response curve exists, and comparisons of this model were limited by the lack of knowledge of the relationship between concentration and hearing threshold elevation over multiple orders of magnitude. The DNQX dose-response curve had to be estimated. The potency of DNQX caused the thresholds to rise above hearing measurement limits when the concentration may still have been increasing.

Very little is known of the interactions between drugs and structures in the cochlea. The time courses of clearance and other loss and storage mechanisms are drug specific, and little research has been conducted. Because of its inaccessibility and sensitivity, pharmacokinetic studies are very difficult. Drug delivery up to this point has all been done by trial and error without methods to quantify concentrations and transport and clearance rates.

The impact of protein interactions with DNQX was believed to be significant, but only crude estimates were available for modeling purposes. The decreased diffusivity due to protein binding was empirically derived from the diffusion-only case. No long term experiments were conducted to learn the true time course and impact of these mechanisms.

The model did not capture the complex fluidic interactions near the point of cannula insertion. However, the model was useful for comparison to experimental results distant from this region. The effort to understand the physical implications and to estimate the region where diffusion again dominated proved very useful in gaining a broader understanding of drug delivery in the cochlea. This avenue of research and corresponding model refinement will be pursued next.

3.10 ADAPTATION OF THE MODEL FOR HUMANS

Adaptation of the model for use in modeling of delivery in humans is straightforward. The anatomical dimensions of the various cochlear structures must be adjusted, but these measurements are available from the literature or from cadaver temporal bones. One important difference between humans and guinea pigs is that most human cochlear aqueducts are not patent. The elements representing this structure should be removed from the model.

3.11 CONCLUSION

A lumped parameter model was created to characterize drug transport in the cochlea delivered by the pulsatile delivery system. This model was successfully validated using a bench-top flow visualization technique. More knowledge of biological interaction with the drug would enhance the usefulness of modeling in vivo studies. With additional refinement, a model such as this one would be extremely useful in development of drugs and drug delivery systems specifically for the cochlea. Human cochleae cannot be sampled in pharmacokinetic studies or clinical trials due to ethical concerns. Future device development can be driven by the knowledge gained from the model and the interactions of specific elements of the model.

3.12 REFERENCES

1. Chen, Z., et al., *Inner Ear drug delivery via a reciprocating perfusion system in the guinea pig*. J Control Release, 2005. **110**: p. 1-19.
2. Salt, A.N., K. Ohyama, and R. Thalmann, *Radial communication between the perilymphatic scalae of the cochlea. II Estimation by bolus injection of tracer into the sealed cochlea*. Hear Res, 1991. **56**: p. 37-43.

3. Salt, A.N., K. Ohyama, and R. Thalmann, *Radial communication between the perilymphatic scalae of the cochlea. I Estimation by tracer perfusion*. Hear Res, 1991. **56**: p. 29-36.
4. Plontke, S. and A. Salt, *Quantitative interpretation of corticosteroid pharmacokinetics in inner fluids using computer simulations*. Hearing Research, 2003. **182**: p. 34-42.
5. Salt, A.N., *Simulation of methods for drug delivery to the cochlear fluids*. Adv Otorhinolaryngol, 2002. **59**: p. 140-148.
6. Thorne, M., et al., *Cochlear fluid space dimensions for six species derived from reconstructions of three-dimensional magnetic resonance images*. The Laryngoscope, 1999. **109**: p. 1661-1668.
7. Ghiz, et al., *Quantitative anatomy of the round window and cochlear aqueduct in guinea pigs*. Hearing Research, 2001. **162**: p. 105-112.
8. Plontke, S.K.R., A.W. Wood, and A.N. Salt, *Analysis of gentamicin kinetics in fluids of the inner ear with round window administration*. Otol Neurotol, 2002. **23**: p. 967-974.
9. Plontke, S. and A. Salt, *Simulation of application strategies for local drug delivery to the inner ear*. ORL J Otorhinolaryngol Relat Spec, 2006. **68**(6): p. 386-392.
10. Salt, A.N. and Y. Ma, *Quantification of solute entry into cochlear perilymph through the round window membrane*. Hearing Research, 2001. **154**: p. 88-97.
11. Salt, A.N., et al., *Marker retention in the cochlea following injections through the round window membrane*. Hear Res, 2007. **232**: p. 78-86.
12. Plontke, S.K., et al., *Cochlear pharmacokinetics with local inner ear drug delivery using a three-dimensional finite-element computer model*. Audiology & Neurotology, 2007. **12**: p. 37-48.
13. Ohyama, K., A.N. Salt, and R. Thalmann, *Volume flow rate of perilymph in the guinea pig cochlea*. Hear Res, 1988. **35**: p. 119-130.
14. Aris, R., *On the dispersion of a solute in pulsating flow through a tube*. Proc of Royal Soc of London Series A Math and Physical Sciences, 1960. **259**(1298): p. 370-376.
15. Doebelin, E.O., *System Dynamics: Modeling and response*. 1972, Columbus, OH: Merrill Publishing Co.
16. Paskusz, G.F. and B. Bussell, *Linear Circuit Analysis*. 1963, Englewood Cliffs, NJ: Prentice-Hall Inc. 12-43.
17. Wit, H.P., R.A. Feijin, and F.W.J. Albers, *Cochlear aqueduct flow resistance is not constant during evoked inner ear pressure change in the guinea pig*. Hearing Research, 2003. **175**: p. 190-199.
18. Ivarsson and Pederson, *Volume-pressure properties of round and oval windows*. Acta Otolaryngol, 1977. **84**: p. 38-43.

19. Tsuji, J. and M.C. Liberman, *Intracellular labeling of auditory nerve fibers in guinea pig: central and peripheral projections*. The J of Comparative Neurology, 1997. **381**: p. 188-202.

4.0 PROTEIN COMPOSITION AND DEVICE INTERACTION

Protein interactions play a major role in the performance of implanted drug delivery systems. The presence of some proteins, albumin among others, has been associated with biofouling, the build-up of protein and cellular matter on the device materials. In the case of this device, any changes in the flow path such as narrowing of channels could alter the delivery profile. In addition, drug selection must be based on the knowledge of proteins present in the perilymph. Some drugs may be altered by enzymes or bound to lipoproteins making them unavailable to the target tissue.

Due to a limited knowledge of perilymph protein composition, a mass-spectrometry analysis was undertaken. Over 50 proteins were identified, many of which may impact drug delivery into the cochlea. In addition, a bench-top study of protein effects on materials typically used in the device was performed. Due to the small diameter channels in the recirculating system, there is a high potential for clogging and flow restrictions. Design parameters must accommodate these potentialities.

4.1 PROTEIN COMPOSITION ANALYSIS

4.1.1 Introduction

A major design consideration for implantable drug delivery systems is their ability to function properly while interacting with intrinsic biological factors. Proteins in perilymph can adsorb onto the surfaces of the implant which may lead to biofouling and changes in delivery profiles [1, 2]. Knowledge of protein composition of perilymph will help anticipate protein interactions with delivered agents and will allow implants and drug delivery regimens to be tailored for optimal performance through the device lifetime.

Previous analyses of proteins in perilymph were performed using electrophoretic techniques and candidate approaches to identification [3-6]. With the advent of mass-spectrometry-based proteomics, tools now exist to separate and identify in small sample quantities unprecedented numbers of proteins and to automate the identification of explicit protein isoforms. Salt et al.'s [7] perilymph collection procedures were adapted to the mouse to identify the most abundant proteins present in mouse perilymph and cerebrospinal fluid (CSF). The mouse was chosen because its proteome is relatively complete and because of its increasing importance as a genetic model for human disease.

4.1.2 Methods

4.1.2.1 Sample collection

CBA/CAJ male mice (Jackson Laboratories, Bar Harbor, ME) 3 months of age were anesthetized with a combination of 100 mg/kg of ketamine and 10 mg/kg of xylazine administered intraperitoneally. Anesthetic boosters (1/3rd the original dose) were administered every 20 min throughout the surgery. Procedures were performed in a heated (31°C) chamber. The surface of the tympanic bulla was exposed after making an incision extending from the mandibular symphysis to the clavicle. The digastric muscle was cut using a bipolar cautery. A wide opening in the bulla allowed access to the cochlear apex. An indelible pen was used to make a small mark on the apex of the cochlea where sampling would occur. Altering a method introduced by Salt et al. [7], the inner surface of the auditory bulla and the cochlea were coated with liquid cyanoacrylate glue and allowed to dry for 10-15 minutes. A thin layer of fingernail polish was applied on all surfaces within the bulla area to minimize contamination from surrounding tissues. An opening in the apical turn was created with a new 175 nm diameter carbide drill (Drill Bit City, Prospect Heights, IL). Samples were collected with a drawn glass capillary tube. After discarding the first tube with approximately 100 nL of perilymph, an additional 0.5 µL was collected and stored at -80° C for the proteomics analysis.

CSF was collected from one additional animal as described by Vogelweid et al. [8]. Skin and muscles layering the occipital bone and the atlas were removed, and the atlanto-occipital membrane was exposed, cleaned and dried. To minimize contamination during CSF collection, a layer of fingernail polish was placed over the membrane and allowed to dry for about 10-15 minutes. A 25 gauge needle was used to perforate the membrane, and 1 µL CSF was collected with a drawn glass capillary tube. The sample was stored at -80° C for analysis.

All procedures were approved by the Animal Care and Use Committee of the Massachusetts Eye and Ear Infirmary.

4.1.2.2 Sample preparation

Four samples were utilized for analysis: 3 perilymph samples of 0.5 µL, each collected from a different mouse, and CSF from an additional mouse. The 4 samples were reduced, alkylated, trypsin-digested and derivatized with the 114, 115, 116 and 117 iTRAQ reagents [9] using reagent solutions and following the standard protocol supplied with the iTRAQ™ kit (Applied Biosystems, Foster City, CA,

Chemistry Reference Guide). Once the samples were separately labeled with iTRAQ reagents, they were combined and cleaned by strong cation exchange (SCX) using a 4x15 mm POROSTM 50-HS SCX cartridge (Applied Biosystems). Samples were applied to the SCX cartridge in 2 mL of load buffer (Applied Biosystems, 10 mM potassium phosphate, 25% acetonitrile (ACN), pH 3.0). The column was washed with 1 mL of load buffer, and the pass through was collected. The sample was then eluted using 500 μ L elution buffer (Applied Biosystems, 10 mM potassium phosphate, 375 mM potassium chloride, 25% ACN, pH 3.0). The SCX elution solvent was removed by vacuum centrifugation. The peptides were re-suspended in 0.1% trifluoroacetic acid and cleaned on a C18 MicroSpinTM column (The Nest Group, Southborough, MA, Vydac C18 Silica). The eluant was dried in a speedvac.

4.1.2.3 Capillary liquid chromatography–mass spectrometry/mass spectrometry (LC-MS/MS) analysis

Data-dependent UPLC–MS/MS analyses were performed using a Waters nanoACQUITY UPLC[®] chromatography system and a Waters Q-TOF PremierTM MS system (Waters, Milford, MA). The combined sample (containing the 3 iTRAQ labeled perilymph samples and the CSF sample) was dissolved in 20 μ L of 2% ACN, 0.1% formic acid (FA) (solvent A), and quadruple analyses of the sample were performed (2 with 5 μ L of each and 2 with 2.5 μ L of each) using the nanoACQUITY auto sampler. The peptides were first trapped on a 180 μ m ID X 20 mm trapping column packed with 5 μ m Symmetry[®] C18 (Waters) with 3% ACN, 0.1% FA as the mobile phase, at a flow rate of 5 μ L/min for 3 minutes. The flow was then reduced to 350 nL/min and directed through the analytical 75 μ m (ID) X 10 cm C18 capillary UPLC[®] column (130 Å, 1.7 μ m BEH130 nanoACQUITY[®], Waters, Inc.) A solvent gradient was run from 3 to 40% ACN in 0.1% FA in 110 min at a rate of 350 nL/min. Nanoelectrospray ionization was performed at 3000 V with the heated capillary at 180° C. During the gradient elution, data dependant scans were performed with 4 scan events per cycle consisting of one full MS from mass/charge ratio (m/z) 300 – 1,800 followed by product ion scans on the 3 most intense ions in the full scan using charge state optimized collision energy programs. Precursor ions used to obtain product ion scans were dynamically excluded (m/z -0.1,+0.1) from reanalysis for 20 seconds. Lock-mass spectra (glucofibrogenen peptide, Sigma, St. Louis, MO) were acquired at 30 second intervals throughout the analyses.

4.1.2.4 Database searching and iTRAQ quantification

A Uniprot FASTA database containing all mouse protein sequences was downloaded from <http://www.informatics.jax.org/>, the mouse genome informatics website, on July 31, 2008, and

searched with Protein Lynx Global Server (PLGS) software (v2.2.5, Waters, Inc.). Variable modifications that were searched for included: iTRAQ derivatives on N-term and lysine, oxidation of methionine and alkylation of cysteine. The raw data was lock-mass corrected, de-isotoped, and charge state reduced by PLGS. Results were combined from four repeat LCMS analyses of the sample for data analysis. Determination of the iTRAQ reporter ion ratios was performed using the Expression Analysis routine in PLGS.

All proteins identified by the PLGS search engine were then individually evaluated by manual inspection. A concatenated target-decoy database analysis was also conducted to quantify the false positive rate [10]. Only one reversed sequence was found in the group of proteins identified by 2 or more peptides, resulting in an overall false positive rate of 1.75% for the reported protein identifications.

4.1.2.5 Protein quantification

For each protein, relative content in the samples was based on determination of the exponentially modified protein abundance index (emPAI) [11], which estimated relative protein concentration based on the ratio of observed to observable unique peptides. The number of observable peptides per protein was determined by (1) in-silico trypsin digestion of the identified proteins, (2) counting of the resulting peptides that conformed to the range of HPLC retention values (calculated by the procedure of Brown et al. [12]), and (3) molecular weight range observed from the list of all 443 peptides identified in all 4 analyses performed on the present set of samples. The iTRAQ reporter ion ratios provided relative ratios of each protein in the 4 samples analyzed. Assuming the protein content analyzed was the sum of the protein in each of the 4 contributing samples, an algebraic solution was used to determine the protein content in each of the 4 iTRAQ labeled samples. To quantify the relative amounts of each protein, a protein content index (P) was created for each of the 4 samples, where

$$P_{total} = P_{CSF} + P_{peri1} + P_{peri2} + P_{peri3} \quad \text{Equation 4.1}$$

iTRAQ reporter ion ratios provided the ratios of protein content in CSF to that in each of the perilymph samples, so

$$P_{CSF} = \frac{P_{total}}{\frac{P_{peri1}}{P_{CSF}} + \frac{P_{peri2}}{P_{CSF}} + \frac{P_{peri3}}{P_{CSF}} + 1} \quad \text{Equation 4.2}$$

Relative content of each protein in a sample was expressed on a molar basis as the mol%.

The samples were not centrifuged after collection, and consequently some hemoglobin was detected in the proteomics analysis. Still none of the samples appeared to have a reddish hue. The hemoglobin content was excluded from the analysis.

4.1.3 Results

Approximately 130 proteins were identified in the iTRAQ analysis of the sample that combined 3 perilymph and 1 CSF samples. From this data set, 50 proteins (Table 4.1, with additional detail in the supplementary table at the end of the chapter) were identified by at least 2 peptides and were judged to have a greater than 98% probability of correct identification by counting the number of segregate (reversed) proteins identified from the complete set of reversed sequences included in the database searched. The ratio of iTRAQ reporter ions allowed determination of relative amounts of each protein in each perilymph and CSF sample. The mass-spectrometry-based proteomics methods provided a quantitative estimate of the amounts of each protein in the sample based on the ratio of observed to observable tryptic peptides identified for each protein [11]. Using both the estimated total amounts of each protein and the iTRAQ ratios, the relative amounts of each protein between each perilymph and CSF sample were determined. The major proteins in perilymph and CSF were similar, though protein in perilymph was on average 2.8 times more concentrated than in CSF.

Albumin, the single protein found in highest concentrations in perilymph, accounted for around 14% of the protein in perilymph. Other proteins in relatively high concentrations (5% to 6%) included prostaglandin D synthase (a lipophilic ligand binding protein [13] thought to play a role in blood-organ barriers), two serine protease inhibitors (serpin a1d and serpin a1a), and two apolipoproteins (apoA2 and apoD). Figure 4.1 summarizes the major categories of proteins found in perilymph. The major family of proteins in perilymph was the group of protease inhibitors, which represented over 1/3rd of the total protein content in perilymph. The predominant type of protease inhibitors were the serine protease inhibitors or serpins (27.8%), followed by several cysteine protease inhibitors (HMW kininogen, cystatin, and GUGU beta, 5.6%). The broad spectrum protease inhibitors (alpha-2-macroglobulin and murinoglobulin) comprised the remaining (3.1%) protease inhibitors. Protease inhibitors bind to and inactivate proteases. While their specific role in the perilymph is unknown, a general role for these proteins is in mediating inflammation.

Table 4.1: Major proteins identified in mouse perilymph listed in descending order of the molar percentage in perilymph. For each peptide, a family or function is listed, though this categorization is arbitrary since most peptides can have multiple functions and families.

<u>Accession</u>	<u>Protein</u>	<u>Family or function</u>	<u>Molecular weight</u>	<u>Perilymph (mol%)</u>	<u>CSF (mol%)</u>
ALBU_MOUSE	albumin	ligand binding	68647	11.9%	9.9%
PTGDS_MOUSE	prostaglandin D synthase	enzyme	21052	6.3%	6.7%
A1AT4_MOUSE	serpin a1d	serpin	45969	5.5%	4.8%
APOA2_MOUSE	apoA2	apolipoprotein	11311	5.3%	3.5%
APOD_MOUSE	apoD	apolipoprotein	21515	4.8%	2.7%
Q3KQQ4_MOUSE	serpin a1a	serpin	45867	4.3%	3.8%
A1AT2_MOUSE	serpin a1b	serpin	45945	4.2%	3.7%
A1AT1_MOUSE	serpin a1a	serpin	45973	4.1%	3.7%
A1AT5_MOUSE	serpin a1e	serpin	45862	3.8%	3.4%
A2APX3_MOUSE	cystatin	cysteine protease inhibitor	11133	3.1%	6.9%
A1AT6_MOUSE	serpin a1f	serpin	45794	3.2%	2.8%
TRFE_MOUSE	serotransferrin	iron binding	76673	3.2%	2.8%
Q58EV2_MOUSE	apoA1	apolipoprotein	23007	3.0%	1.8%
PRDX2_MOUSE	peroxiredoxin	enzyme	21765	2.6%	4.0%
Q6GTX3_MOUSE	apoE	apolipoprotein	35830	2.5%	3.7%
CTF2_MOUSE	cardiotrophin 2	cell signaling	21986	2.5%	2.8%
SPA3K_MOUSE	serpin a3k	serpin	46850	2.1%	2.0%
ACTB_MOUSE	beta actin	actin	41709	2.0%	3.0%
Q6S9I1_MOUSE	hmw kininogen	cysteine protease inhibitor	53171	2.0%	1.8%
VTDB_MOUSE	vitamin D binding protein	ligand binding	53565	1.5%	1.3%
A0AUP0_MOUSE	ef hand C1	calcium signaling	27995	1.5%	2.0%
A2M_MOUSE	alpha 2 macroglobulin	I-39 protease inhibitor	165775	1.6%	0.8%
ESTN_MOUSE	liver carboxylesterase	enzyme	61133	1.5%	1.0%
MUG1_MOUSE	murinoglobulin	I-39 protease inhibitor	165192	1.5%	0.7%
CO3_MOUSE	complement C3		186364	1.3%	1.0%
Q9CS04_MOUSE	13 days embryo liver cDNA	transcription coactivator	15919	1.3%	1.2%
HEMO_MOUSE	hemopexin	heme transporter	51308	1.2%	1.2%
PLMN_MOUSE	plasminogen	enzyme peptidase S1	90722	1.1%	1.0%
A2A513_MOUSE	keratin 10	keratin	57006	1.0%	2.2%
A2NHM3_MOUSE	I f kappa		24149	1.1%	0.7%
Q8BWN0_MOUSE	monooxygenase	enzyme	13327	0.7%	1.5%
A1AG1_MOUSE	alpha 1 acid glycoprotein	ligand binding	23880	0.8%	0.8%
CAH2_MOUSE	carbonic anhydrase	enzyme	29014	0.7%	1.1%
B2RSI0_MOUSE	GTPase activator	enzyme activator	155179	0.7%	0.8%

FETUA_MOUSE	fetuin	cell signaling	37301	0.7%	0.7%
Q3TGJ9_MOUSE	gelsolin	actin binding	80798	0.5%	0.8%
Q6YJU1_MOUSE	GUGU beta	cysteine protease inhibitor	33857	0.5%	0.5%
KCD13_MOUSE	BTB (POZ) domain protein	transcription factor	36419	0.5%	0.2%
ANT3_MOUSE	serpin c1	serpin	51970	0.4%	0.5%
Q99K20_MOUSE	lactate dehydrogenase	enzyme	34481	0.4%	0.5%
CC113_MOUSE	coiled-coil domain-containing protein 113		44187	0.4%	0.4%
B2ZP54_MOUSE	phosphodiesterase	enzyme	98834	0.3%	0.7%
K2C1_MOUSE	keratin 1p	keratin	65565	0.3%	1.0%
A2RTA0_MOUSE	creatine kinase	enzyme	43017	0.3%	0.6%
A1L0X5_MOUSE	keratin 78	keratin	54739	0.3%	0.8%
K2C73_MOUSE	keratin 73	keratin	58874	0.3%	0.9%
Q9CUG7_MOUSE	adult male testis cDNA	transcription coactivator	53017	0.3%	0.5%
ENOB_MOUSE	beta enolase	enzyme	46995	0.3%	0.4%
CERU_MOUSE	ferroxidase	enzyme	121074	0.3%	0.2%
Q3UV17_MOUSE	keratin 2p	keratin	62805	0.2%	0.5%

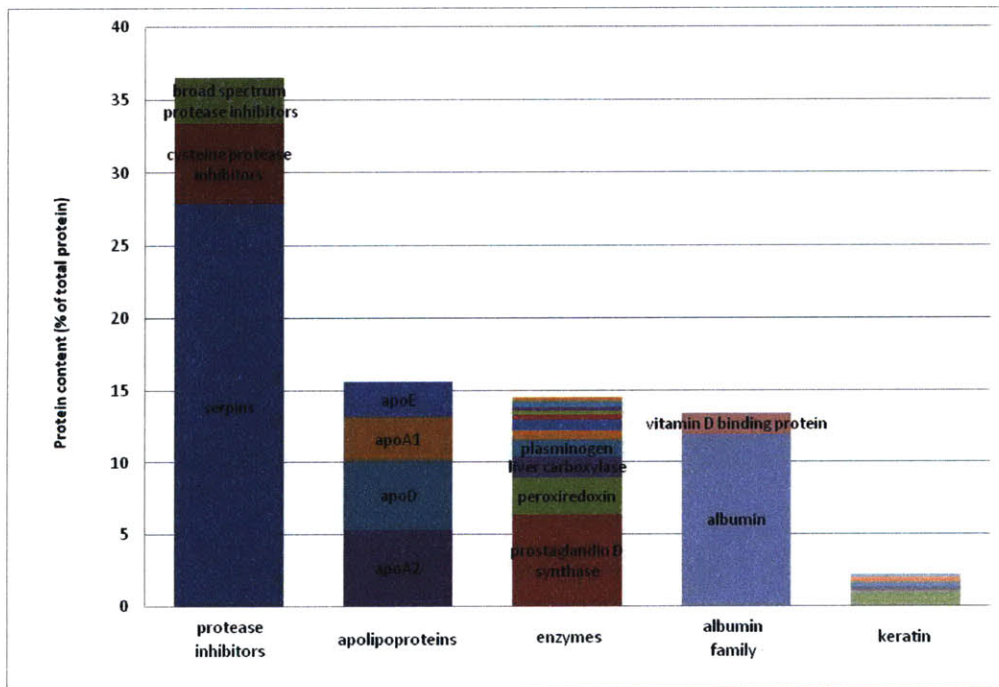


Figure 4.1: The most abundant protein families as percentage of total protein.

Enzymatic proteins represented another large family of proteins in perilymph, comprising over 14% of the total. These included prostaglandin D synthase, carboxylesterase, carbonic anhydrase,

lactate dehydrogenase, and several redox enzymes. Another major category of proteins in perilymph were the apolipoproteins, which act as lipid binders and transporters [14]. Apolipoprotein D, A1, and A2 were relatively concentrated in perilymph compared to CSF. Apolipoprotein D may have a role in maintenance and repair in the central and peripheral nervous systems.

A number of other proteins of potential interest to auditory biologists were identified. They did not meet the criteria for inclusion based on an automated probability analysis but were considered to be good identifications based on examination of individual spectra. These included cochlin, a secreted protein known to be involved in autosomal dominant nonsyndromal sensorineural hearing loss (DFNA9) [15], NF kappa B inhibitor, matrillin4, a protein involved in bone resorption, and malate dehydrogenase.

4.1.4 Discussion

4.1.4.1 Protein composition of perilymph

The results confirmed and extended the analysis of Thalmann and colleagues [4], which was based on a candidate approach with two-dimensional electrophoresis, and which until now has been the most extensive analysis of perilymph proteins. The current analysis found that while protein concentration in mouse perilymph was higher than that in CSF, the composition was similar. The data suggested protein concentration was 2.8 times higher in perilymph than in CSF, but this value should be taken only as an estimate, given that it is based on derived measures. The number of unique peptide fragments associated with each protein can be related to the quantity of protein injected, but is not a direct measure. The estimated perilymph/CSF ratio of 2.8 was low compared to analyses performed in other species. The ratio of total protein content in human perilymph to CSF has been reported to range between 4.3 and 5 [4, 5]. Moreover, Thalmann found a perilymph/CSF protein ratio of 5 in human and 12.5 in guinea pig [3, 4]. The total protein in perilymph and CSF in guinea pig [3] was 2.757 ± 0.238 and 0.219 ± 0.089 mg/mL \pm SD, respectively. Thalmann's electrophoretic analysis of human and guinea pig perilymph identified several of the major proteins found in this analysis including albumin, alpha-1 antitrypsins (serpina1), antichymotrypsin (serpina3k), and serotransferrin [3, 4]. These were also identified in Arrer et al.'s [6] study of human perilymph.

It was unlikely that there was significant contamination of the perilymph samples with CSF. Salt's [7] technique of collecting from the apical turn of the cochlea was modified and used, and only 0.5 μ L of fluid was collected. Flow out of the apical cochleostomy was not as robust in the mouse as in the guinea pig, suggesting that the cochlear aqueduct may be less patent in the mouse than in the guinea

pig. Minor contamination with red blood cells was suspected in both the CSF and perilymph samples since hemoglobin was detected in both, but a number of other major proteins known to be present in mouse plasma, including apolipoprotein B, fibronectin, complement C5, and complement C4 [16] were not detected. The sample was not spun before analysis, though no red color was observed in the fluid or in the dried protein. The extraordinarily high content of hemoglobin in red blood cells implies that even small amounts of contamination will be detected.

For any given protein, the estimates of differences between CSF and perilymph were based on the incorporation of iTRAQ reporter ions and were likely to be relatively accurate. Murinoglobulin, alpha-2 macroglobulin, and some apolipoproteins (apoD, apoA1, and apoA2) were found to be major proteins that were 5- to 6-fold higher in perilymph than in CSF. The results confirmed Thalmann et al.'s earlier work in the guinea pig [3], which found high relative levels of apolipoprotein D compared to plasma, and in human perilymph [17] compared to plasma and CSF. Alpha-2 macroglobulin and murinoglobulin are both members of the I-39 family of protease inhibitors and inhibit all four families of proteases. Apolipoproteins are transporter proteins that can carry a variety of ligands. A couple of transcription-related proteins, BTB (POZ) domain protein and TAF7-like RNA polymerase, and liver carboxylesterase were also found to be elevated around 5-fold in perilymph compared to CSF.

4.1.4.2 Implications for inner ear drug delivery

A concern with any implanted drug delivery device is the possibility of biofouling that can change the parameters of delivery over time. Protein adsorption to materials mediates the response of cells to the device, as well. Biofouling limits the usefulness of implanted biosensors and can influence the inflammatory process [1, 18]. Extensive research on protein response to various materials is ongoing [19-21]. Many studies use albumin, along with fibrinogen, as model proteins for understanding biofouling parameters [19-21]. Because perilymph has a large amount of albumin, designs for implantable devices should incorporate biofouling considerations.

One known source for biofouling is high-molecular-weight kininogen, which is present in perilymph and is a factor in coagulation and inflammation [22]. High-molecular-weight kininogen, produced in the liver, adsorbs to the surface of biomaterials that come in contact with blood in vivo [23].

Proteins found in perilymph may affect the metabolism and distribution of drugs delivered to the cochlea. Many proteins may bind to the drug molecules, making them unavailable to the target tissues. Albumin, alpha-1 acid glycoprotein, prostaglandin D synthase, and lipoproteins may act in this

way. Albumin tends to bind acidic ligands. Alpha-1 acid glycoprotein, found in relatively small quantities in perilymph, is the primary carrier for basic drugs. Apolipoproteins and prostaglandin D synthase bind ligands with hydrophobic characteristics [14].

Enzymes account for almost 15% of the protein in perilymph. Prostaglandin D synthase, found in relatively high concentrations in perilymph, is an enzyme which has, in addition to a variety of CNS functions, a role in maintaining the integrity of the blood-brain, blood-eye, and blood-testis barriers. A potential role in the blood-cochlear barrier is thus likely.

4.2 PROTEIN BIOFOULING

As discussed above, perilymph contains a large amount of protein, such as albumin, that has been shown to cause biofouling. The microfluidic system operates in direct communication with perilymph and is sensitive to changes in fluidic resistance which result from changes in channel dimensions. With channel diameters in the 50-75 μm range, biofouling is a significant concern. Fouling may affect flow characteristics and device performance.

4.2.1 Analysis

Sample calculations illustrate the effect of protein build-up on fluid flow. For example, a 7 mm long tube with a diameter of 50 μm has a fluidic resistance (R) of 0.110 psi/ $\mu\text{L}/\text{min}$ calculated from Equation 4.3.

$$R = \frac{128\mu L}{\pi D^4} \quad \text{Equation 4.3}$$

where μ is dynamic viscosity (1.00e-3 Pa*s for water), L is tube length, and D is tube diameter. This equation applies to steady, incompressible, laminar flow in a straight, smooth pipe. With pressure of 1 psi, volume flow rate (Q) is 9 $\mu\text{L}/\text{min}$ using Equation 4.4.

$$Q = \frac{P}{R} \quad \text{Equation 4.4}$$

where P is pressure. For a 3 μm reduction in diameter, the resulting resistance increased to 0.140 psi/ $\mu\text{L}/\text{min}$ and volume flow decreased to 7 $\mu\text{L}/\text{min}$ under constant pressure of 1 psi. Thus 6% decrease in tubing diameter resulted in 22% decrease in flow. With tubing diameter of 40 μm , the volume flow was 3.7 $\mu\text{L}/\text{min}$, or 40% of the original flow.

A calculation of the number of albumin molecules passing through the tube was done to check that layers on the order of a couple of μm were possible. An arbitrary layer thickness of $2.5 \mu\text{m}$ was used, and the number of albumin molecules required to create that layer was estimated. The results are shown in Table 4.2.

Table 4.2: Calculation of albumin molecules in deposited protein layer

Arbitrary layer thickness (μm)	2.5
Tubing length (m)	0.007
Albumin solution concentration (g/L)	2.76
Volume flow rate ($\mu\text{L}/\text{min}$)	7
Amount of albumin passing through tube (mg/day)	27.8
Albumin molecular weight (Da)	6.6e4
Number of albumin molecules passing (#/day)	2.5e17
Albumin diameter (nm) [24]	7.4
Number of albumin molecules in column (#)	169
Surface area of albumin (m^2)	1.7e-16
Surface area of inside of tube (m^2)	1.1e-6
Total albumin molecules in layer (#)	1.1e12

From this estimation, orders of magnitude more molecules pass through the tube each day than are necessary to form a micron-thick layer inside of the tubing. This would indicate that build-up of protein over several days to weeks would be enough to influence the tubing resistance and flow characteristics.

4.2.2 Method

A bench-top experiment was undertaken to compare protein build-up of various materials used in the drug delivery system. The test set-up was designed to expose the materials to the flow characteristics to which they would be exposed in the fully-operational device. These materials included stainless steel, polyetheretherketone (PEEK), polyimide (Kapton®), and fused silica. The dimensions of the material test sections were $50 \mu\text{m}$ in diameter and 7 mm in length, resulting in a fluidic resistance of $0.110 \text{ psi}/\mu\text{L}/\text{min}$. A protein solution of albumin in deionized water with a concentration matching the total perilymph protein concentration in guinea pig (2.76 g/L) was used as the flow medium and filled the test apparatus shown in Figure 4.2. The protein solution was used as a substitute for actual guinea pig perilymph which is limited in quantity to a few μL per cochlea. Albumin, along with immunoglobulin G (IgG) and fibrinogen, has been used as a model protein in numerous studies of biofouling [19, 21, 25,

26]. In this study, IgG and fibrinogen were not added to the solution as these two proteins were not identified in the mass-spectrometry analysis of perilymph. The liquid was maintained at a constant pressure head of 1 psi. Using Equation 4.4, the initial flow rate was 9 $\mu\text{L}/\text{min}$ which corresponded approximately to the maximum flow condition in the outlet cannula of a functioning device.

The test apparatus is diagramed below in Figure 4.2. The protein solution was maintained at 37°C to more closely mimic the internal temperature in the implanted situation. At intervals of 1 to 3 days, a flow sensor (Sensirion 1430, Staefa, Switzerland) was placed at the outlet of the various materials. The flow rate was recorded, and the fluidic resistance was determined from the recorded value and constant pressure. Flow continued uninterrupted over periods of weeks with repeated measurements. Fluidic resistance of measurement tubing was subtracted. Materials were also visually inspected using microscopy.

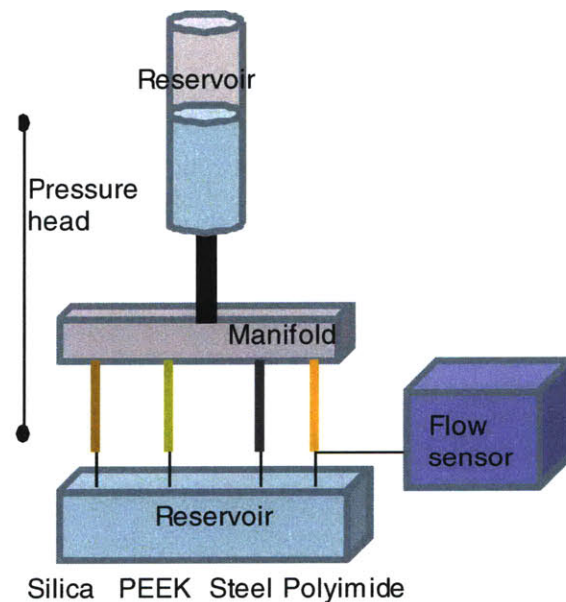


Figure 4.2: Diagram of protein biofouling test apparatus

4.2.3 Results

Results of testing indicated that all materials were prone to clogging. More than half of the tests of each type resulted in clogging within 10 days, as shown in Table 4.3. Clogging was defined as complete occlusion with no measurable flow rate.

Table 4.3: Material assessment of clogging

	# tests clogging within 10 days
Silica	4/6
PEEK	5/7
Steel	3/4
Polyimide	3/4

Graphs showing change in resistance of each material for a number of tests are shown below in Figure 4.3.

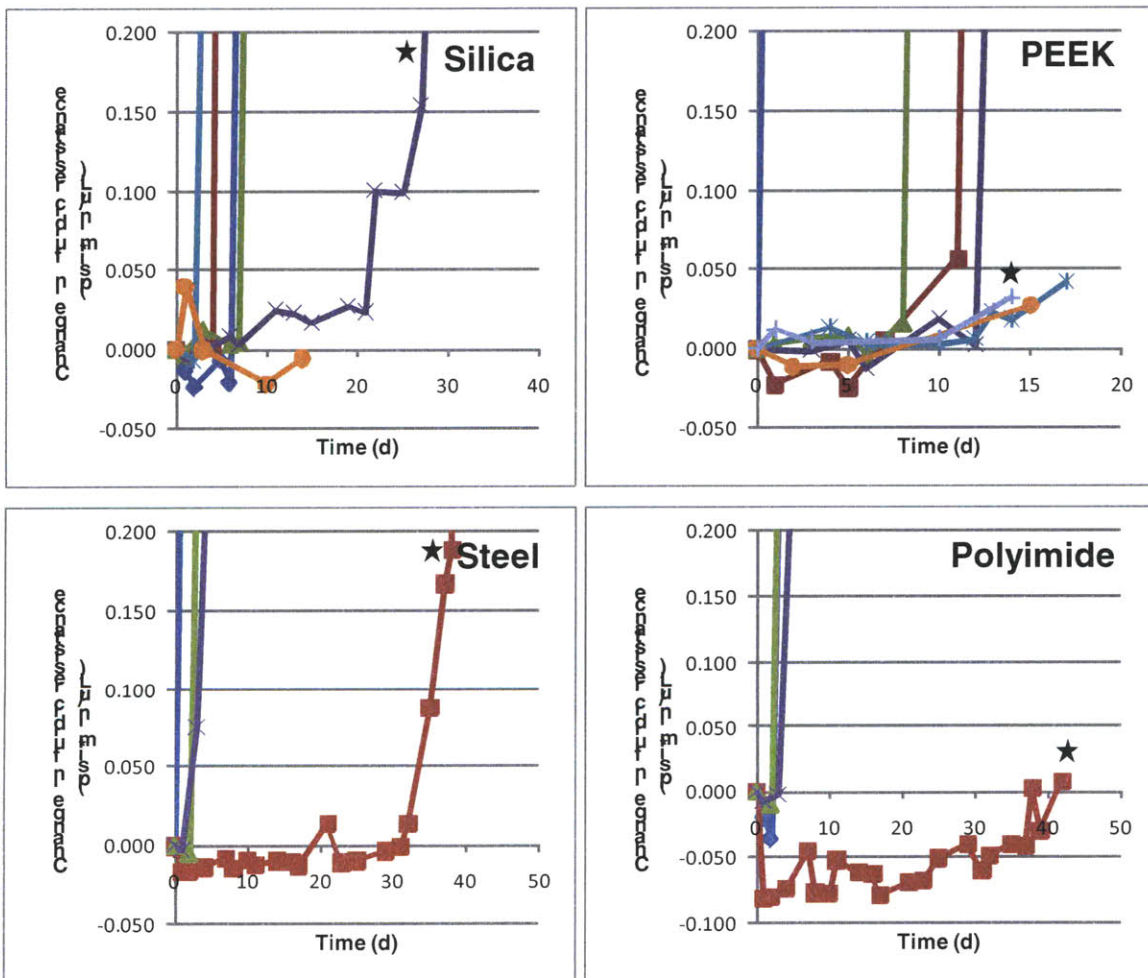


Figure 4.3: Change in fluidic resistance over time for four materials

Micrographs of material cross-sections for tests started in Figure 4.3 are shown below in Figure 4.4. These images were taken of the tubing after albumin solution flow for the number of days listed on

each image. Each tube was compared to a control tube of the same material which did not experience flow. In the top left image of Figure 4.4, the silica tube showed almost complete occlusion by protein, corresponding to the high resistance (>0.2 psi/ $\mu\text{L}/\text{min}$) shown in Figure 4.3. The diameter of the polyimide tubing (top right) decreased to result in a calculated difference in resistance of 0.06 psi/ $\mu\text{L}/\text{min}$. This corresponds to the graph above in Figure 4.3 showing approximate resistance difference of 0.04 psi/ $\mu\text{L}/\text{min}$. From the graph above (4.3), the steel tube was nearly occluded; however, the microscope in the image below (4.4) did not capture the interior of the tubing. Little difference is seen between the polyimide tube used in the experiment and the control tube. This corresponds to the minimal change in resistance reflected above (4.3).

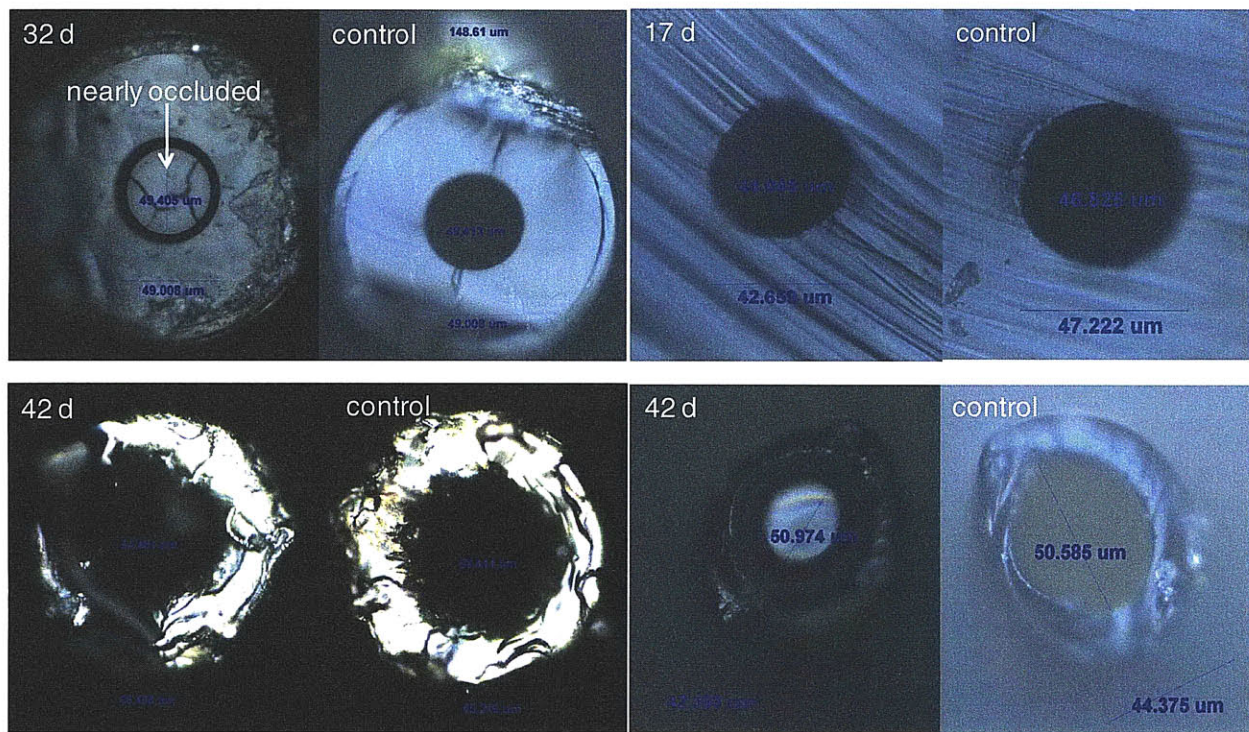


Figure 4.4: Micrograph images of materials (clockwise from top left, silica, PEEK, polyimide, steel) after albumin solution flow for the number of days labeled.

4.2.4 Discussion

This experiment was initially designed to assist in material selection for the next generation delivery device. However, a high likelihood of clogging in all 50 μm diameter tubes tested was discovered. Performance of the device components with small dimensions in any of these materials may be impacted by protein biofouling and clogging. It is important to remember that the flow rate achieved in this test was equivalent to that generated in the device during infusion into the inner ear.

The majority of each duty cycle has substantially lower flow rates. It is hypothesized that lower flow rates may allow greater protein build-up.

Various methods, both physical and chemical, may be explored to reduce biofouling and/or associated flow restrictions. Most simply, the largest dimensions that satisfy design constraints should be used. This may reduce the impact of increased fluidic resistance on flow characteristics. Sensors may be added in the device to monitor flow over time and adjust pumping to maintain desired delivery. Other design considerations may be employed such as multiple channels that may be used sequentially. When the sensor determines that biofouling has reached a critical level, flow can be diverted to an unused channel. The pump or other pressure source can be programmable to allow increased driving force to maintain desired flow characteristics even as biofouling continues to cause increases in resistance. Prior to loading the device, the drug and carrier should be carefully filtered to eliminate any particles that could clog the tubing.

Chemical methods of minimizing biofouling have been reported, as well. Poly (ethylene glycol) (PEG) films coated onto materials resist protein adsorption through steric repulsion. Popat et al. reported on a vapor deposition technique that yielded film thicknesses of approximately 20 Å. The surface coating was studied under stationary and flow conditions and decreased protein adsorption by 70-80% [27, 28]. Other chemical modifications including hyaluronic acid and N-(triethoxysilylpropyl)-O-polyethylene oxide urethane (TESP) coatings reduced biofouling [19, 29]. Oligomaltose coating was used to minimize nonspecific protein adsorption by steric hindrance. The variable saccharide lengths were designed to mimic the glycocalyx. Measured under flow conditions, this surface modification led to up to 90% reduction in biofouling.

As polyimide is a favored material for the device, studies on biofouling of fluorinated polyimide were useful. The material was cured at three different temperatures, 50, 150 and 250°C, and difference in protein adsorption with curing times of the polymer was investigated. The 250°C cured polyimide showed the least deposit of protein [30, 31].

Because this was an *in vitro* test, actual physiological activity in the guinea pig may not be accurately represented by this test. *In vivo* protein biofouling may be significantly different in time course and amount. This experiment was designed to begin to understand the role protein deposition may play in the device performance and guide material selection for future device revisions.

4.3 TISSUE BIOFOULING

In addition to protein biofouling, two other areas of concern for the implanted device exist. Biofouling due to cell migration and ingrowth of the device outlet in the cochlea and the effect of the device on surrounding tissue must be studied. Tissue ingrowth into and around the device outlet may increase fluidic resistance or occlude the implanted cannula. As the fluidic outlet was on the order of 50 μm in diameter, the studies described above showed reason for concern. Inflammation from a foreign body response to the implantation may result in damage to the fragile inner ear structures.

4.3.1 Introduction

Prior investigations have been reported in the context of electrodes for cochlear prostheses. Studies have shown that cells migrate along cochlear implants from the site of implantation and create new tissue growth [32]. Researchers report the presence of both fibrous tissue and new bone growth in both animal and human temporal bones [32-37]. In addition, the amount of ossification has been shown to be dependent on the site and method of implantation [37, 38]. In a study at the Temporal Bone Lab at the Massachusetts Eye and Ear Infirmary, a three-dimensional model was constructed by stacking sections of human temporal bones, and volume and distribution measurements of new bone were made. The total volume filled by new bone was 2-30%, with mean of 14% (SD 10%, n=7). Trauma of the insertion was seen as the primary influencing factor, accounting for 80% of the variance (Personal conversation with Peter Li of Temporal Bone Lab at MEEI 6/12/06). A universal observation was that the site of the cochleostomy showed the most bone growth. Bone cell migration may also be a concern with this novel device due to the similar surgical implantation method.

These electrodes have been placed in deaf ears so damage to fine structures in the cochlea has not been a concern. Minimizing surgical trauma and foreign body response will be of utmost importance as the devices will likely be implanted into hearing ears.

4.3.2 Histologic preparation

In this study, the device was implanted in the guinea pig for thirty days and was set to infuse every 3 min. The device was tested at 17 days by introducing DNQX into the system and testing guinea pig hearing. Threshold levels rose as expected due to the drug action. However, when tested again at 30 days, no hearing response to DNQX was shown. At that time, the cause of the failure could not be

determined but possible causes included occlusion inside of the cannula, failure of the pumping system, or tissue growth around the cochleostomy.

At the conclusion of the experiment, the delivery cannula was left in place, and the tubing connecting it to the device was cut. The animal was sacrificed with an overdose of sodium pentobarbital, and the inner ear was fixed, decalcified, sectioned, and mounted for histology.

The anesthetized guinea pig was perfused intracardially with 2.5% glutaraldehyde and 1.5% paraformaldehyde in a 0.1 M phosphate buffer. The whole head was kept in the same fixative at 4°C for 4 weeks. The bulla was dissected and decalcified in 0.4 M EDTA and 1% glutaraldehyde for an additional 4 weeks. After decalcification, the entire inner ear with bulla attached was washed in distilled water for 1 hr and soaked in 50% alcohol overnight. Dehydration in ethanol continued as follows: 70% for 1 day, 80% for 2 days, 95% for 2 days, and 100% for 3 days with alcohol changed daily. The sample was placed in 100% propylene oxide for 2 days. The inner ear was embedded in Araldite resin (Huntsman, Woodlands, TX) and sectioned in a plane perpendicular to the implanted cannula at 20 μm with a carbide steel knife. Sections were stained with epoxy tissue stain (Electron Microscopy Science #14950, Hatfield, PA), mounted with Permount (Science Co., Denver, CO) on microscope slides and coverslipped.

4.3.3 Results

The tissue was studied for evidence of inflammation and new bony tissue. The cannula was inspected to determine the degree of occlusion. By studying the series of sections with portions of the cannula, it became readily apparent that the end of the cannula was no longer located in the scala tympani, where it had been implanted. The cannula end was outside of the inner ear, and a tissue barrier between it and the scala had formed as shown in Figure 4.5. It is hypothesized that this occurred due to the body's natural defense of expelling the cannula at the cochleostomy site. Another explanation could be that the anchor site of the manifold holding the cannula (dental cement at the bulla) may have loosened and caused the cannula to move. Evidence of this has been seen in other chronic attempts. The anchor spot is in close proximity to the jaw, and constant motion from eating and drinking may cause slippage of the manifold.

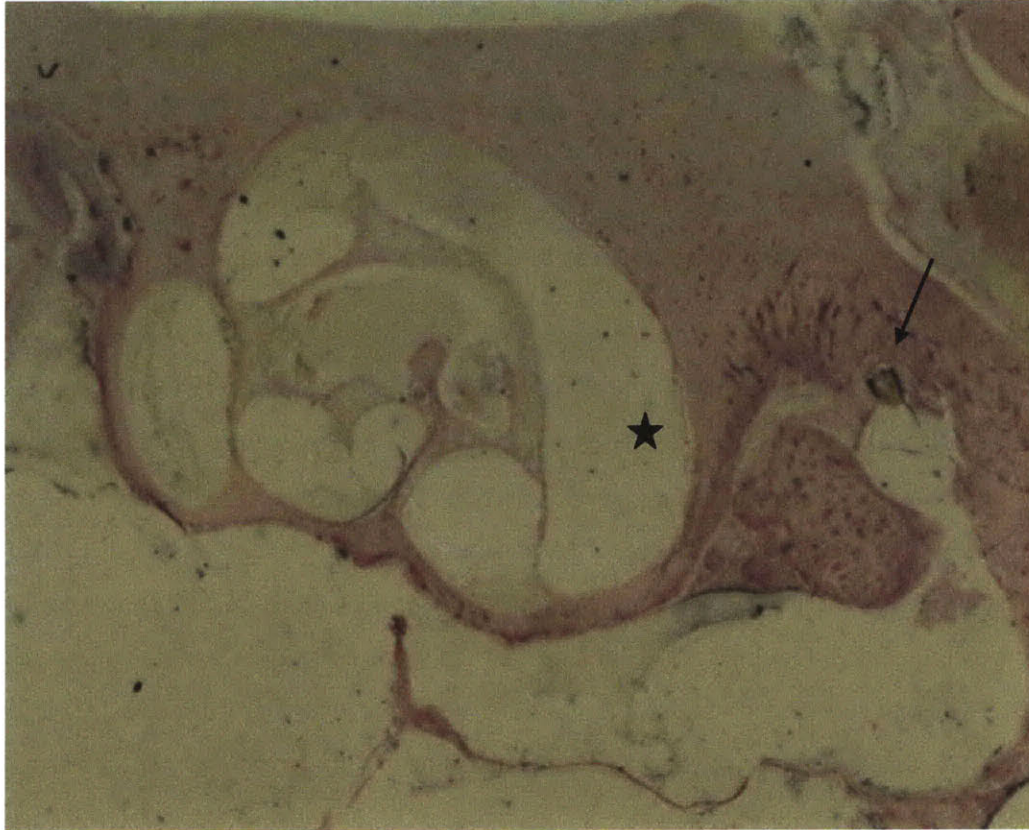


Figure 4.5: Histological slice of a guinea pig cochlea at 2x. The cannula (shown with the arrow) is not located in the basal turn of the scala tympani (shown with at star) where it was implanted.

The interior of the cannula was examined for tissue growth. If the inner diameter was diminished, the flow profile would have been altered. Every slice containing portions of the cannula was inspected, and no tissue growth was apparent inside the cannula. An example microscopic image is shown in Figure 4.6

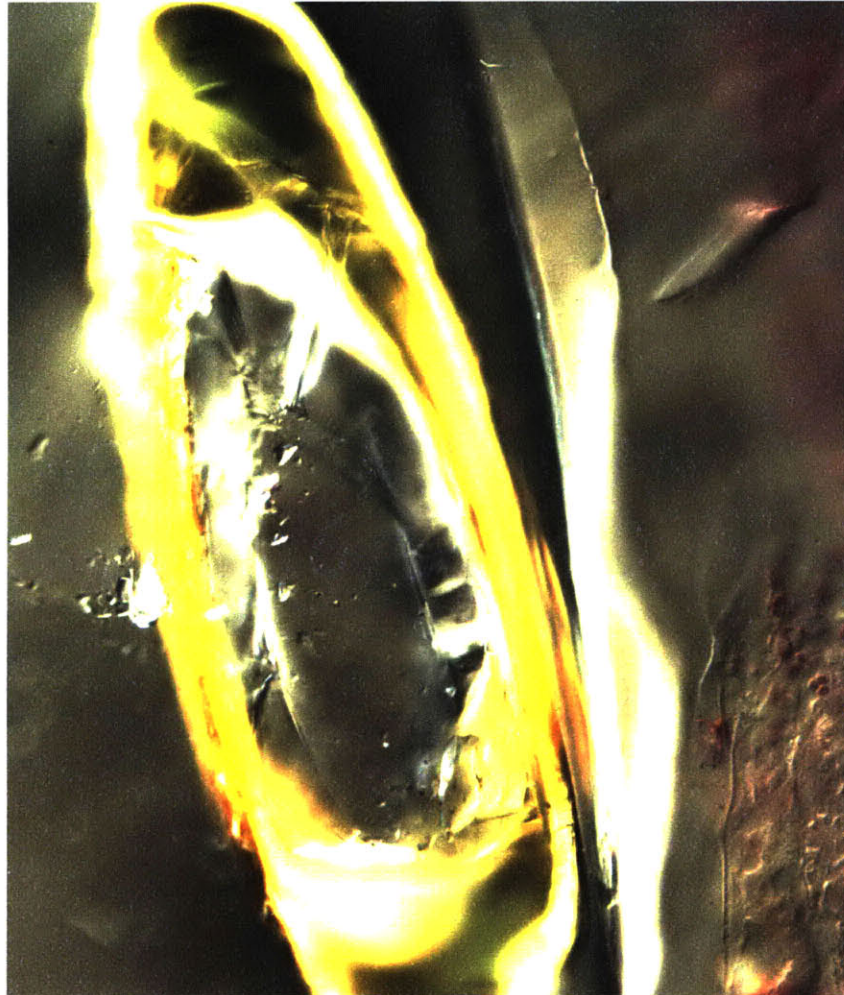


Figure 4.6: The inner diameter of the cannula shown at 20x. The cannula is composed of polyimide coated silica. The silica was cracked during the sectioning. Tissue was stained, as can be seen to the right of the cannula, and no tissue was visible inside the cannula.

Analysis of tissue response near the cannula showed no inflammation. New bone and fibrous tissue developed in the middle ear space, but there was no reaction in the inner ear as shown in Figures 4.7 and 4.8. The amount of growth in the middle ear did not pose a concern for hearing. This bone growth may have been a response to the initial drilling when the cannula was placed.

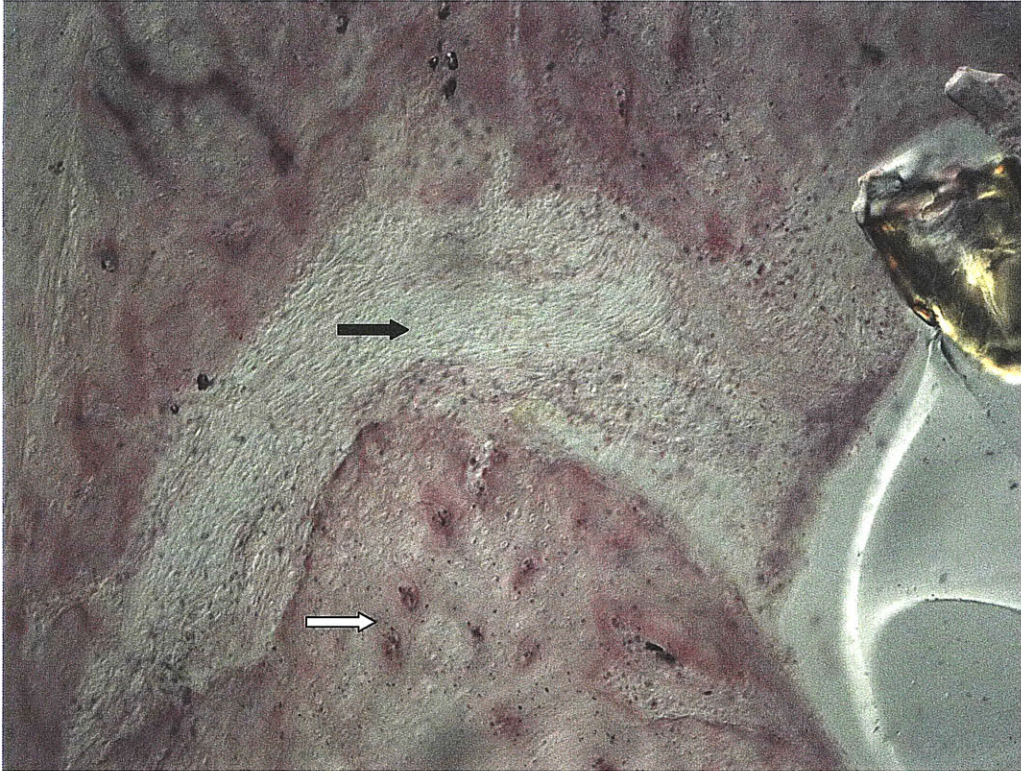


Figure 4.7: Same slice of guinea pig cochlea as shown in Figure 4.5 magnified to 10x. The white arrow shows a region of new bone growth in the middle ear near the cannula, and the black area shows an area of fibrous tissue. Over time, the fibrous tissue may be remodeled into bone.

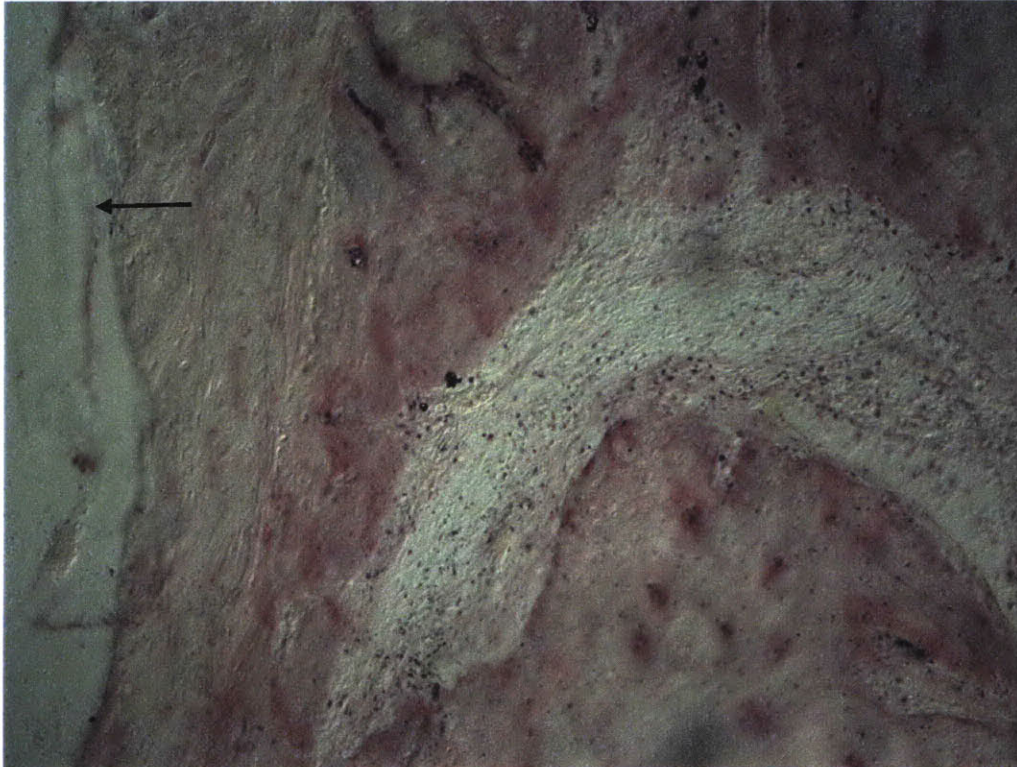


Figure 5.8: Same slice of guinea pig cochlea as shown in Figure 4.7 at 10x. The arrow shows the edge of the scala tympani. No new bone has developed inside the inner ear.

As discussed above, studies of patients with cochlear prostheses have shown new bone formation inside the scala tympani along the electrode. As such, bone growth in the inner ear was expected in this case. This observation leads to the uncertainty of whether the flow from the device reduces the likelihood of bone growth. If so, this knowledge could have significant impact on cochlear implants where much research is being conducted on using the devices in ears with residual hearing. If new bone formation could be minimized or eliminated, the cochlear implants would function more effectively, and hearing would be better preserved.

4.4 CONCLUSION

The protein composition of mouse perilymph was very similar to CSF, though proteins were on average 2.8 times more concentrated in perilymph than in CSF. Protease inhibitors comprised over $1/3^{\text{rd}}$ of the total protein content in perilymph, and more than half of these were serine protease inhibitors. Albumin was the single protein present in highest amounts.

Histological study of a chronically implanted cochlea showed no reaction to the cannula inside the cochlea. Additionally, no tissue build-up was observed within the cannula itself. While promising, these results must be further verified with additional animals and with longer implant periods.

Rights were reserved to reprint portions of this chapter from: Swan, E., et al., *Proteomics analysis of perilymph and cerebrospinal fluid in mouse*. *Laryngoscope*, 2009. **119**(5): p. 953-958.

4.5 REFERENCES

1. Babensee, et al., *Host response to tissue engineered devices*. *Advanced Drug Delivery Reviews*, 1998. **33**: p. 111-139.
2. Castner and Ratner, *Biomedical surface science: Foundations to frontiers*. *Surface Science*, 2002. **500**: p. 28-60.
3. Thalmann, I., et al., *Protein profiles of perilymph and endolymph of the guinea pig*. *Hear Res*, 1992. **63**: p. 37-42.
4. Thalmann, I., et al., *Protein profile of human perilymph: in search of markers for the diagnosis of perilymph fistula and other inner ear disease*. *Otolaryngol Head Neck Surg*, 1994. **111**(3): p. 273-280.
5. Paugh, Telian, and Disher, *Identification of perilymph proteins by two-dimensional gel electrophoresis*. *Otolaryngol - Head & Neck Surg*, 1991. **104**(4): p. 517-525.
6. Arrer, E., G. Oberascher, and H. Gibitz, *A map of cochlear perilymph protein based on high-resolution two-dimensional electrophoresis*. *Eur Arch Otorhinolaryngol*, 1990. **247**: p. 271-273.
7. Salt, A.N., S.A. Hale, and S.K. Plontke, *Perilymph sampling from the cochlear apex: a reliable method to obtain higher purity perilymph samples from the scala tympani*. *J Neurosci Methods*, 2006. **153**: p. 121-129.
8. Vogelweid and Kier, *A technique for the collection of cerebrospinal fluid from mice*. *Laboratory Animal Science*, 1988. **38**(1): p. 91-92.
9. Ross, P., et al., *Multiplexed protein quantitation in *Saccharomyces cerevisiae* using amine-reactive isobaric tagging reagents*. *Mol Cell Proteomics*, 2004. **3**(12): p. 1154-1169.
10. Elias, J. and S. Gygi, *Target-decoy search strategy for increased confidence in large-scale protein identifications by mass spectrometry*. *Nat Methods*, 2007. **4**(3): p. 207-214.
11. Ishihama, Y., et al., *Exponentially modified protein abundance index (emPAI) for estimation of absolute protein amount in proteomics by the number of sequenced peptides per protein*. *Mol Cell Proteomics*, 2005. **4**(9): p. 1265-1272.

12. Browne, C., H. Bennett, and S. Solomon, *The Isolation of Peptides by High-Performance Liquid Chromatography Using Predicted Elution Positions*. Anal Biochem, 1982. **124**: p. 201-208.
13. Urade, Y. and O. Hayaishi, *Biochemical, structural, genetic, physiological, and pathophysiological features of lipocalin-type prostaglandin D synthase*. Biochim Biophys Acta, 2000. **1482**(1-2): p. 259-71.
14. Goldstein, A., L. Aronow, and S. Kalman, *Principles of Drug action: the basis of pharmacology*. 2nd ed. 1974, New York: John Wiley and Sons.
15. Bhattacharya, S.K., *Focus on molecules: Cochlin*. Exp Eye Res, 2006. **82**(3): p. 355-356.
16. Lai, K., D. Kolippakkam, and L. Berretta, *Comprehensive and quantitative proteome profiling of the mouse liver and plasma*. Hepatology, 2008. **47**(3): p. 1043-1051.
17. Thalmann, et al., *Protein profile of human perilymph: in search of markers for the diagnosis of perilymph fistula and other inner ear disease*. Otolaryngol - Head & Neck Surg, 1994. **111**(3): p. 273-280.
18. Zhang, Wright, and Yang, *Materials and techniques for electrochemical biosensor design and construction*. Biosensors & Bioelectronics, 2000. **15**: p. 273-282.
19. Sasaki, et al., *Glial cell adhesion and protein adsorption on SAM coated semiconductor and glass surfaces of a microfluidic structure*. Proceedings of SPIE, 2001. **4265**: p. 152-163.
20. Richardson, R.R.J., J.A. Miller, and W.M. Reichert, *Polyimides as biomaterials: preliminary biocompatibility testing*. Biomaterials, 1993. **14**(8): p. 627-635.
21. Lim, et al., *Protein adsorption to planar electrochemical sensors and sensor materials*. Pure Appl Chem, 2004. **76**(4): p. 753-764.
22. Scharfstein, J., et al., *Kininogens coordinate adaptive immunity through the proteolytic release of bradykinin, an endogenous danger signal driving dendritic cell maturation*. Scand J Immunol, 2007. **66**(2-3): p. 128-136.
23. Yung, L., et al., *High-molecular-weight kininogen preadsorbed to glass surface markedly reduces neutrophil adhesion*. Biomaterials, 2000. **21**(4): p. 405-414.
24. Bisgaier, C.L., et al., *Distribution of apolipoprotein A-IV in human plasma*. J of Lipid Research, 1985. **26**: p. 11-25.
25. Peterson, S.L., et al., *Poly(dimethylsiloxane) thin films as biocompatible coatings for microfluidic devices: cell culture and flow studies with glial cells*. J Biomed Mater Res 2005. **72A**: p. 10-18.
26. Richardson, Miller, and Reichert, *Polyimides as biomaterials: preliminary biocompatibility testing*. Biomaterials, 1993. **14**(8): p. 627-635.

27. Popat, K.C. and T.A. Desai, *Poly(ethylene glycol) interfaces: an approach for enhanced performance of microfluidic systems*. *Biosensors & Bioelectronics*, 2004. **19**: p. 1037-1044.
28. Popat, K.C., et al., *Surface modification of nanoporous alumina surfaces with poly(ethylene glycol)*. *Langmuir*, 2004. **20**: p. 8035-8041.
29. Khademhosseini, et al., *Layer-by-layer deposition of hyaluronic acid and poly-L-lysine for patterned cell co-cultures*. *Biomaterials*, 2004. **25**: p. 3583-3592.
30. Kanno, M., et al., *Biocompatibility of fluorinated polyimide*. *J Biomed Mater Res*, 2002. **60**: p. 53-60.
31. Kawakami, H., et al., *Competitive plasma protein adsorption onto fluorinated polyimide surfaces*. *J Biomed Mater Res*, 2003. **67A**: p. 1393-1400.
32. Nadol, et al., *Histopathology of cochlear implants in humans*. "The Annals of Otolology, Rhinology, and Laryngology", 2001. **110**: p. 883-891.
33. Nadol and Eddington, *Histologic evaluation of the tissue seal and biologic response around cochlear implant electrodes in the human*. *Otology & Neurotology*, 2004. **25**: p. 257-262.
34. Schindler, *The cochlear histopathology of chronic intracochlear implantation*. *The Journal of Laryngology and Otology*, 1975. **40**: p. 445-457.
35. Zappia, et al., *Evaluation of the temporal bones of a multichannel cochlear implant patient*. "The Annals of Otolology, Rhinology, and Laryngology", 1991. **100**: p. 914-921.
36. Clark, et al., *Cochlear implantation: osteoneogenesis, electrode-tissue impedance and residual hearing*. "The Annals of Otolology, Rhinology, and Laryngology", 1995. **Supp 166**: p. 40-42.
37. Linthicum, F.H., et al., *Cochlear implant histopathology*. *Am J Otol*, 1991. **12(4)**: p. 245-311.
38. Chow, Seldon, and Clark, *Experimental animal model of intracochlear ossification in relation to cochlear implantation*. "The Annals of Otolology, Rhinology, and Laryngology", 1995. **Supp 166**: p. 42-45.

Supplemental table for perilymph protein analysis: Proteins that were identified with imposed criteria

<u>Accession</u>	<u>Protein</u>	<u>Molecular weight</u>	<u>Ratio of observed/observable peptides</u>	<u>emPAI</u>	<u>mol %</u>	<u>iTRAQ ratio 1*</u>	<u>iTRAQ ratio 2*</u>	<u>iTRAQ ratio 3*</u>	<u>Perilymph mol%</u>	<u>CSF mol%</u>
ALBU_MOUSE	albumin	68647	61/115	2.39	11.7%	2.08	5.56	2.50	11.9%	9.9%
PTGDS_MOUSE	prostaglandin D synthase	21052	9/25	1.29	6.3%	0.97	1.67	5.26	6.3%	6.7%
A1AT4_MOUSE	serpin a1d	45969	14/43	1.12	5.5%	2.04	5.00	2.56	5.5%	4.9%
APOA2_MOUSE	apoA2	11311	5/16	1.05	5.2%	2.56	7.14	3.03	5.3%	3.5%
APOD_MOUSE	apoD	21515	6/21	0.93	4.6%	1.61	2.38	11.11	4.8%	2.7%
Q3KQ4_MOUSE	serpin a1a	45867	12/44	0.87	4.3%	2.08	5.00	2.63	4.3%	3.8%
A1AT2_MOUSE	serpin a1b	45945	12/45	0.85	4.2%	2.04	5.00	2.56	4.2%	3.7%
A1AT1_MOUSE	serpin a1a	45973	11/42	0.83	4.1%	2.04	4.76	2.56	4.1%	3.7%
A1AT5_MOUSE	serpin a1e	45862	9/36	0.78	3.8%	1.96	5.00	2.44	3.9%	3.5%
A2APX3_MOUSE	cystatin	11133	4/17	0.72	3.5%	0.72	1.52	1.56	3.1%	6.9%
A1AT6_MOUSE	serpin a1f	45794	11/51	0.64	3.2%	2.04	5.00	2.56	3.2%	2.8%
TRFE_MOUSE	serotransferrin	76673	25/116	0.64	3.1%	1.96	4.76	3.03	3.2%	2.8%
Q58EV2_MOUSE	apoA1	23007	10/50	0.59	2.9%	2.94	8.33	2.86	3.0%	1.8%
PRDX2_MOUSE	peroxiredoxin	21765	5/26	0.56	2.7%	1.22	2.27	2.00	2.6%	4.0%
Q6GTX3_MOUSE	apoE	35830	11/59	0.54	2.6%	0.81	1.82	3.03	2.5%	3.7%
CTF2_MOUSE	cardiotrophin 2	21986	2/11	0.52	2.5%	1.47	4.35	1.72	2.5%	2.8%

SPA3K_MOUSE	serpin a3k	46850	8/51	0.44	2.1%	1.89	4.76	2.56	2.2%	2.0%
ACTB_MOUSE	beta actin	41709	9/58	0.43	2.1%	1.25	2.70	1.54	2.0%	3.0%
Q6S9I1_MOUSE	hmw kininogen	53171	9/62	0.40	1.9%	1.96	5.26	2.04	2.0%	1.8%
VTDB_MOUSE	vitamin D binding protein	53565	8/68	0.31	1.5%	2.08	5.26	2.70	1.6%	1.3%
A0AUP0_MOUSE	ef hand C1	27995	6/51	0.31	1.5%	1.25	3.45	1.64	1.5%	2.0%
A2M_MOUSE	alpha 2 macroglobulin	165775	19/163	0.31	1.5%	4.00	10.00	3.57	1.6%	0.8%
ESTN_MOUSE	liver carboxylesterase	61133	7/62	0.30	1.5%	2.86	6.67	2.78	1.5%	1.0%
MUG1_MOUSE	murinoglobulin	165192	18/162	0.29	1.4%	3.57	11.11	3.85	1.5%	0.7%
CO3_MOUSE	complement C3	186364	28/280	0.26	1.3%	2.17	5.88	2.38	1.3%	1.0%
Q9CS04_MOUSE	13 days embryo liver cDNA	15919	2/20	0.26	1.3%	2.00	4.35	2.27	1.3%	1.2%
HEMO_MOUSE	hemopexin	51308	7/73	0.25	1.2%	1.92	4.76	2.13	1.2%	1.2%
PLMN_MOUSE	plasminogen	90722	11/123	0.23	1.1%	1.82	5.26	2.38	1.1%	1.0%
A2A513_MOUSE	keratin 10	57006	6/68	0.23	1.1%	1.03	2.22	0.50	1.0%	2.2%
A2NHM3_MOUSE	If kappa	24149	3/36	0.21	1.0%	2.27	7.14	3.03	1.1%	0.7%
Q8BWN0_MOUSE	monooxygenase	13327	2/30	0.17	0.8%	0.83	1.82	1.47	0.7%	1.5%
A1AG1_MOUSE	alpha 1 acid glycoprotein	23880	2/30	0.17	0.8%	1.72	4.35	2.22	0.8%	0.8%
CAH2_MOUSE	carbonic anhydrase	29014	2/31	0.16	0.8%	1.32	2.17	2.04	0.7%	1.1%
B2RSI0_MOUSE	GTPase activator	155179	3/52	0.14	0.7%	1.79	3.70	1.96	0.7%	0.8%

FETUA_MOUSE	fetuin	37301	2/36	0.14	0.7%	1.56	5.00	1.82	0.7%	0.7%
Q3TGJ9_MOUSE	gelsolin	80798	5/105	0.12	0.6%	1.02	2.94	2.04	0.5%	0.8%
Q6YJU1_MOUSE	GUGU beta	33857	2/44	0.11	0.5%	2.04	4.55	2.22	0.5%	0.5%
KCD13_MOUSE	BTB (POZ) domain protein	36419	2/53	0.09	0.4%	3.33	11.11	3.13	0.5%	0.2%
ANT3_MOUSE	serpin c1	51970	3/81	0.09	0.4%	2.00	3.85	2.22	0.4%	0.5%
Q99K20_MOUSE	lactate dehydrogenase	34481	2/56	0.09	0.4%	1.54	2.94	1.89	0.4%	0.5%
CC113_MOUSE	coiled-coil domain-containing protein 113	44187	3/88	0.08	0.4%	1.72	4.76	2.13	0.4%	0.4%
B2ZP54_MOUSE	phosphodiesterase	98834	4/123	0.08	0.4%	0.74	1.64	2.08	0.4%	0.7%
K2C1_MOUSE	keratin 1p	65565	3/96	0.08	0.4%	1.22	1.08	0.23	0.3%	1.0%
A2RTA0_MOUSE	creatine kinase	43017	2/67	0.07	0.4%	1.23	2.56	0.79	0.3%	0.6%
A1L0X5_MOUSE	keratin 78	54739	3/107	0.07	0.3%	1.41	1.37	0.21	0.3%	0.8%
K2C73_MOUSE	keratin 73	58874	3/108	0.07	0.3%	1.14	1.05	0.23	0.3%	0.9%
Q9CUG7_MOUSE	adult male testis cDNA	53017	2/73	0.07	0.3%	1.30	2.04	1.69	0.30%	0.5%
ENOB_MOUSE	beta enolase	46995	2/78	0.06	0.3%	1.79	2.63	1.00	0.3%	0.4%
CERU_MOUSE	ferroxidase	121074	3/135	0.05	0.3%	1.89	4.55	3.57	0.3%	0.2%
Q3UV17_MOUSE	keratin 2p	62805	2/104	0.05	0.2%	1.61	1.20	0.32	0.2%	0.5%

*iTRAQ ratios 1-3 represent the ratios of the reporter ions of perilymph samples 1 through 3 to the reporter ion of the CSF.

5.0 MICROFLUIDIC COMPONENTS: FABRICATION AND TESTING

5.1 INTRODUCTION

Implantable drug delivery systems require integration of a delivery module with miniaturized electronics and power supply. Principal advantages of the MEMS-based (MicroElectroMechanical Systems) delivery system are the potential for miniaturization, full integration of pumps, sensors and control electronics, and the low cost of batch fabrication techniques for high-volume manufacturing. Device development has focused on systems constructed using micromachined polymer components for improved biocompatibility, advantageous mechanical properties and reduced cost. Two components of the microfluidic system, a manual 5-valve manifold and a fluidic capacitor, were fabricated using a versatile milling and lamination procedure. The process utilized laminate sheets of polyimide that were milled using a standard X-Y milling tool. The components were entirely compatible with and would permit integration into a complete delivery system including sensors, pumps, surface mounted electronics, and printed circuitry.

Many fabrication techniques have been used for producing microfluidic components and systems from polymers [1] including cast molding [2], embossing [3, 4], and other soft lithography techniques [5]. Generally, the devices created with these techniques have been for short-term use, and many cannot be seamlessly integrated with current electronics packaging.

Microfabrication using polyimide films provides a stable, versatile platform that can incorporate both fluidic and electronic elements. Because of its combination of chemical inertness, high temperature tolerance and robust mechanical properties, this material is routinely used in electronic circuitry and packaging. Polyimide films have also been used for polymer MEMS applications and biosensors [6-9].

Draper Laboratory has previously utilized polyimide in microfluidic applications. Laser-machining techniques were used to construct a closed loop flow controller with an anemometer-based flow sensor and electronically controlled microvalve [10]. Other laboratory capabilities include reactive ion etching to thin film adhesive and partial depth cutting of films using laser machining [11].

Although useful, fabrication with polyimide films using laser machining was too expensive for this project and required long lead times. Therefore, techniques for machining with an X-Y milling table were developed. The tools were inexpensive and immediately available for rapid prototyping and low-

volume production. Design changes were quickly incorporated. These tools achieved routing speeds of 60 in/min or higher and spindle speeds from 20 krpm to greater than 100 krpm (Quickcircuit, T-Tech, Norcross, GA). Positional accuracies of approximately 5 μm (lateral) and 10 μm (vertical) were typical. The availability of end mill diameters down to 100 μm provided the flexibility to machine a wide variety of microfluidic structures.

Two diaphragm-based polyimide microfluidic components, fluidic capacitors and manual screw valves, were developed using micromilling and lamination. The components were designed for integration into the MEMS-based device for chronic drug delivery to the inner ear [12]. The fluidic capacitors provided fluidic capacitance to filter the output of the pump. Tuning of these capacitive elements along with series resistance optimized volume flow and displacement into the cochlea. The pulsatile output was achieved, but the amplitude of flow rate fluctuations was reduced to prevent damage to delicate cochlear structures. The manual microvalves provided the required drug loading and purge functions with acceptably low leak rates [13].

The microfluidic components were seamlessly incorporated into the fluidic network used in animal studies. Both components significantly contributed to a reduction in size of the system and provided greater control over critical system variables. The valve and capacitor can be integrated into a versatile laminated polyimide fabrication platform along with other microfluidic and electronic components including flow sensing and control elements.

5.2 FABRICATION METHODS

5.2.1 Machining

The Quickcircuit 7000 (T-Tech, Norcross, GA) X-Y router table was used for machining. It had a 0 – 60 krpm variable spindle speed and a 0 – 60 in/min variable routing speed capability. Vertical position resolution (cut depth resolution) of the end mill was 10 μm . Double-edged clockwise-spinning stub end mills ranging from 100 to 375 μm in diameter were used. Conventional cutting (finished edge was to the left, relative to the direction of tool travel), as compared to climb cutting (edge to the right), yielded substantially better edge quality with less roughness. As a result, cutouts were routed in the clockwise direction, and channels were cut out one edge at a time, with some offset, rather than cut in a single pass as shown in Figure 5.1a. The films were placed on a sacrificial high-density fiberboard backer mounted on the router table for all cutting as shown in Figure 5.1b. The milling was done using a conservative spindle speed ranging from 10 to 20 krpm and material feed rates of 3 to 6 in/min.

Choosing the optimal parameters for machining of the polymer was complex [14]. The machining conditions were not necessarily optimized; however parametric studies varying spindle speed and feed rate were conducted and samples were evaluated. The general behavior was consistent with theory [14]: at high feed rates and low spindle speeds, cuts resulted in tears and poor edge quality, while at low feed rate to spindle speed ratios, excessive heating resulted, also leading to poor cuts.

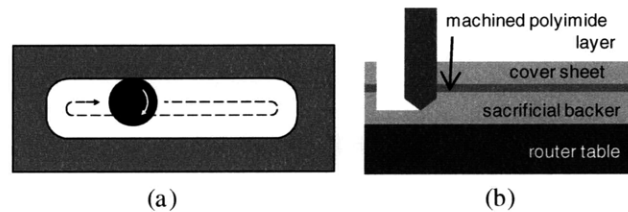


Figure 5.1: (a) Milling of a channel using only conventional cutting to avoid climb cutting. The solid arrow shows the top-view rotation of the tool; the dashed arrow shows the tool path. The finished part is shaded, while the through cut is shown in white. (b) Typical material stack used for machining single layer of polyimide (cover sheet required for thin layers only).

The components were developed using Kapton® polyimide films and R/flex®1000 Kapton®— adhesive laminate materials from Rogers Corporation. Specifically, Kapton® sheets with thickness of 1, 3, or 5 mil, Kapton® sheets with 0.5 or 1 mil thickness thermosetting adhesive, and stand-alone adhesive sheets of 1 mil thickness were used.

The typical machining procedure included the following. Alignment holes, typically 1/8 in diameter with 2.25 in spacing, were routed in a blank sheet. One of the holes was oblong in the direction of the axis of the two holes, permitting thermal expansion of the sheet during the lamination process but still providing repeatable placement on the routing table. The sheet was then repositioned onto mating alignment pins on the router table, and the pattern was milled through the full depth of the sheet and into the backer board as shown in Figure 5.1b. The sides of the sheet were taped down to improve part stability. To machine thin layers (1 mil thickness or less), the mounting procedure was modified. In addition to the description above, a second sacrificial layer of either 5 mil polyimide or medium tack tape was added on top of the layer to be machined. This provided sufficient mechanical rigidity to prevent bowing and/or tearing of the part during machining.

5.2.2 Cleaning

Parts were cleaned in a water-filled ultrasonic bath for 5 minutes. For sheets with adhesive, the adhesive backing layer was removed prior to placement in the bath. A nitrogen gun removed excess water, and a 30 min, 60 °C oven bake completed the drying process. Incomplete drying resulted in bubble formation in the adhesive layers and degradation of adhesion strength.

5.2.3 Lamination

The purpose-built laminator consisted of two chambers: a heated vacuum chamber in which the piece was placed and an upper high pressure chamber (420 kPaG maximum) which applied force to a movable 6 in diameter o-ring-sealed piston between the two chambers. In order to fabricate devices with free-standing diaphragms using a lamination process, it was necessary to minimize pressure differentials that can develop across the diaphragm during lamination due to trapped air. Otherwise, plastic deformation of the diaphragm may result. Using the same machining methods described above, additional sheets of polyimide were patterned with features that provided venting or pressure equilibration. In addition, a bleed valve may be used to control the pump-down speed in combination with vent channels.

The stack loaded for lamination contained multiple layers in addition to the active device layers. A 0.25 in thick aluminum base plate (typically 2.5 in square) with alignment pins of the same diameter and spacing as those used in the machining process provided the means for layer alignment. A 0.25 in thick aluminum top plate provided uniform pressure over the parts to be laminated. Multiple sheets of 5-mil polyimide were added to the stack as necessary to provide compliance to accommodate surface roughness and non-planarity in the base and top plates, improving pressure uniformity, and thus bond integrity. These extra layers were placed against the inner faces of the aluminum plates in the stack. As described above, additional layers of 5-mil polyimide with machined vent channels were used for pressure equilibration. These layers were placed immediately adjacent to the top and bottom active layers of the device. Figure 5.2 shows an example case of the overall stack. Note that inlet and outlet tubing may be positioned in milled grooves and included in the stack.

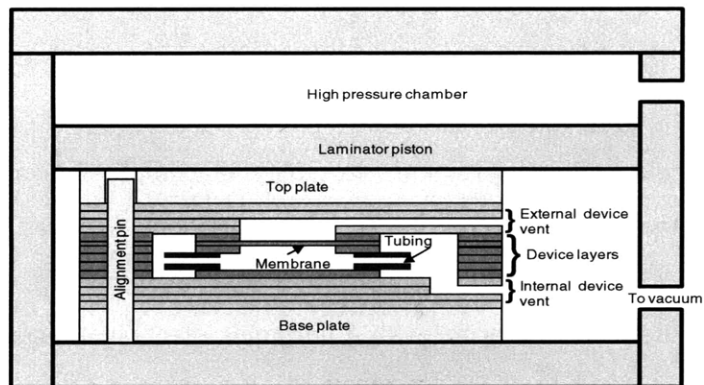


Figure 5.2: Cross section of example membrane capacitor shown in lamination chamber (not to scale).

Recommended lamination pressure for the adhesive was achieved by setting the upper chamber pressure appropriately. Specifically, the desired adhesive lamination pressure was scaled by the ratio of the laminated device area and the piston area to arrive at the required net laminator pressure (the gauge pressure of the upper chamber minus the vacuum level of the lamination chamber).

$$P_{set} = P_{vac} + P_{adh} \frac{A_{die}}{A_{piston}} \quad \text{Equation 5.1}$$

where P_{set} is the upper chamber pressure setpoint, P_{vac} is the vacuum level of the lower chamber, P_{adh} is the desired lamination pressure for the adhesive, and A_{die} and A_{piston} are the areas of the laminate stack and piston. The vacuum level P_{vac} was not used to achieve the desired P_{adh} because residual air in the lamination chamber resulted in bubble formation in the adhesive interfaces between polyimide layers. A vacuum level of less than 0.5 kPa was maintained. The lamination conditions, including lamination time and temperature, used for the process are shown in Table 5.1. Parameters were consistent with the manufacturer's recommendations for R/flex[®] 1000 of 1725–2760 kPa effective adhesive pressure.

Table 5.1: Lamination conditions

Vacuum level (kPa)	< 0.5
Over pressure (kPaG)	275
Laminate/piston area ratio ($A_{die}/A_{plunger}$)	0.2
Temperature ramp rate (°C/min)	5
Dwell time (min)	60
Dwell temperature (°C)	175
Effective adhesive pressure (P_{adh}) (kPa)	2000

5.2.4 Hybrid material components

The need to produce diaphragms with versatility in compliance and size motivated the development of hybrid material structures. Such implementations provided the freedom to use membranes with properties different from the polyimide used as the primary structural material of the microfluidic component. Besides a capacitor with a polyimide diaphragm, another capacitor with an inserted silicone (Specialty Silicone Products SSP-M823) diaphragm was fabricated. The router tool did not effectively cut the elastomer so biopsy punches were used to cut circular silicone diaphragms.

In addition to choice of diaphragm material, flexibility in the choice of material and configuration of inlet and outlet ports was useful. In-plane tubing ports were fabricated using stainless steel, polyimide, and polyetheretherketone (PEEK) tubing. Grooves with a width typically equal to the tubing diameter were milled in the stacked layers to prevent crushing of the tubing as shown in Figure 5.2.

5.2.5 Permeability reduction

Capacitor diaphragms were gold sputter-coated after lamination in order to reduce vapor loss through the thin membrane. Gold provided a good combination of ductility, corrosion resistance, and low water permeability. A thin adhesion-promoting layer of titanium or chromium (300 Å) was deposited prior to the gold deposition. Stress control of these materials was an important design consideration. Low stress gold films were achieved in a 6 in magnetron sputter system using an applied power of 600 W and an argon pressure of 0.4 Pa. Finally, film thickness was critical. Because both permeability and compliance were inverse functions of thickness, the design space for diaphragms with low permeability was limited. For example, a 1500 Å gold layer increased the tensile stiffness of a 1 mil polyimide membrane by 20%. An example of a fabricated fluidic capacitor with gold coating is shown in Figure 5.3.

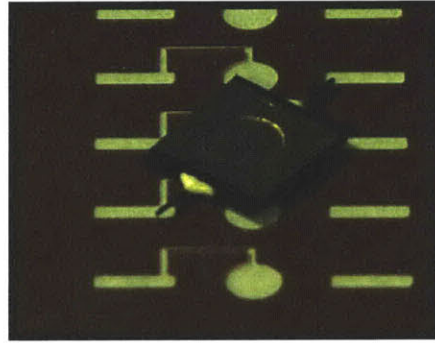


Figure 5.3: Gold-coated fluidic capacitor showing a partially fabricated device (background) and completed device (foreground)

5.3 MEMBRANE CAPACITOR

The microfluidic device relies on system capacitance and series resistors to adjust output flow from the pump for appropriate delivery to the ear. Early device iterations utilized long segments of compliant tubing to provide necessary system capacitance. In order to miniaturize the system and move to a more fully integrated circuit, the planar polyimide capacitor component was developed, as shown in Figures 5.4 and 5.5. Similar compliant structures have proven versatile in microfluidics for valving, pumping, and other uses [15, 16]. Compliant membrane structures have been previously described [15-17].

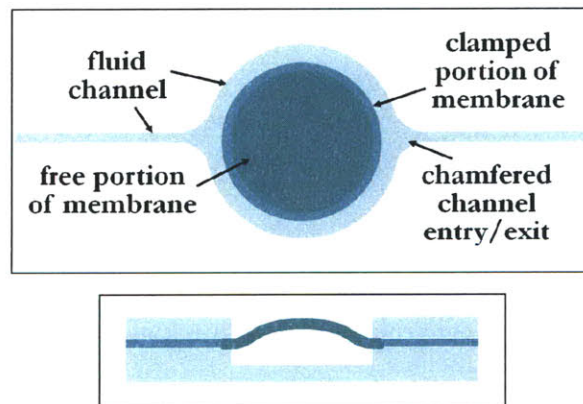


Figure 5.4: Depiction of fluidic capacitor with elastomer membrane. Top and side schematics of fluidic capacitor are shown.

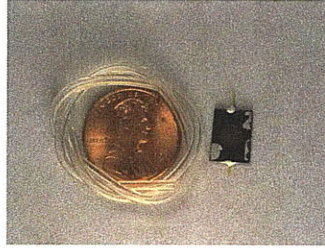
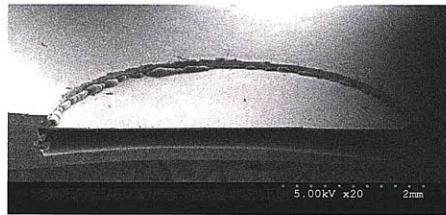
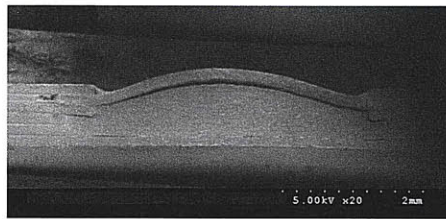


Figure 5.5: Microfabricated fluidic capacitor shown in size relation to penny and the compliant tubing it replaced.



(a)



(b)

Figure 5.6: Microfabricated fluidic capacitor elements. (a) 5mm diameter, 1 mil thickness polyimide, (b) 3.6mm diameter, 4 mil thickness silicone. Membrane reservoir was potted prior to sectioning to improve section cut quality.

Two example implementations of fluidic single-membrane capacitors, as shown in Figure 5.6, were described, and the predicted differential capacitance to measured values for different membrane diameters, thicknesses and materials were compared. In both cases, it was reasonable to assume a fully built in (fixed and held) boundary condition for model purposes. The relationship between maximum displacement and applied pressure for a circular diaphragm was then given approximately by

$$\frac{Pa^4}{Et^4} = \frac{(7-\nu)(z^3 - z_0^3)}{3(1-\nu)t^3} \quad \text{Equation 5.2}$$

where P was pressure, a was membrane radius, E was tensile modulus, t was membrane thickness, ν was the Poisson ratio, z was axial displacement, and z_0 was the displacement at zero applied pressure. The equation provided by Giovanni was modified [18] by neglecting the linear bending term of $16z/[3t(1-\nu^2)]$ and by introducing an offset displacement z_0 . This allowed approximate characterization of a membrane that was buckled and had a large displacement with no applied pressure. The offset displacement z_0 was either positive or negative and equal in magnitude for the two cases if the membrane had a symmetric buckling tendency. Total volume displacement (relative to the flat, unbuckled state) was estimated from

$$V = \frac{\pi a^2 z}{2} \quad \text{Equation 5.3}$$

where it was assumed that displacements were significantly greater than membrane thickness, and the membrane shape was approximately parabolic. For small displacements, where the membrane shape was approximately sinusoidal (both buckle amplitude and pressure-induced displacement were less than the diaphragm thickness), the denominator in Equation 5.3 was replaced by 1.68 and the linear term missing from Equation 5.2 was included.

An example membrane volume displacement plot is shown in Figure 5.7. The rapid change in volume at low pressures was indicative of buckling and a nearly symmetric function of pressure. The data was measured from a polyimide membrane that had been sputter-coated with 1500 Å of gold as a permeation barrier. The membrane had a zero-pressure buckle displacement of positive or negative 0.17 mm, as measured by a Keyence CCD Laser Displacement Sensor LK-031. Values of $E = 3.0$ GPa (thickness-weighted average of 2.5 GPa for Kapton® and 78 GPa for gold), $\nu = 0.3$, $t = 1$ mil, and $z_0 = \pm 0.17$ mm were used in Equation 5.2 to tabulate the displacement z as a function of applied pressure, and then Equation 5.3 was used to calculate the corresponding displacement volume shown as the model in the graph. The nonlinear displacement behavior resulted in a large differential capacitance at low pressure that decreased rapidly with increasing pressure amplitude as shown in Figure 5.8. The plots in the figure represented the pressure derivative taken numerically for the measured data of the displacement volume in Figure 5.7 and used no fit parameters. Also included in the figure was a best fit of the raw measured data. The fit had the form of the pressure derivative of the displacement described by Equation 5.2. The discrepancy between the model and fit of the measured data was believed to result from at least two factors including the lack of precision of measurement of membrane

displacement and the tendency of the buckled membrane to take on an asymmetric, non-parabolic shape at low pressures.

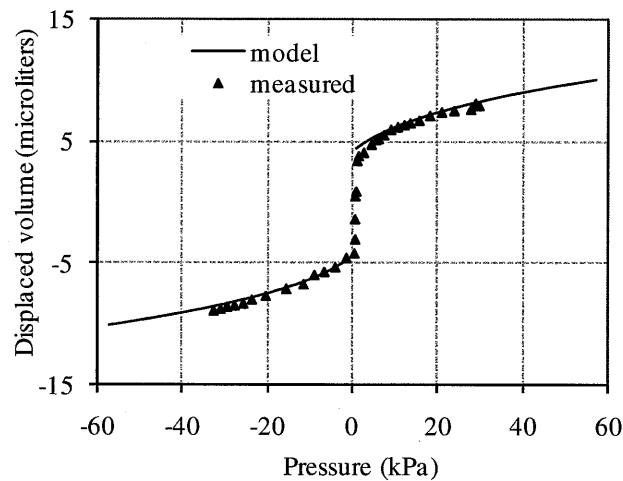


Figure 5.7: Polyimide capacitor membrane displacement volume as a function of applied fluid pressure. The membrane had a thickness of 1 mil and a diameter of 8 mm. The measured buckle displacement amplitude was 0.170 mm. The displacement volume was generated by a Harvard PHD2000 syringe pump, and the pressure was measured with an Entran Model EPX-V01 pressure transducer. The model used $z_0 = 0.17$ mm for $P < 0$ kPa and $z_0 = -0.17$ mm for $P > 0$ kPa.

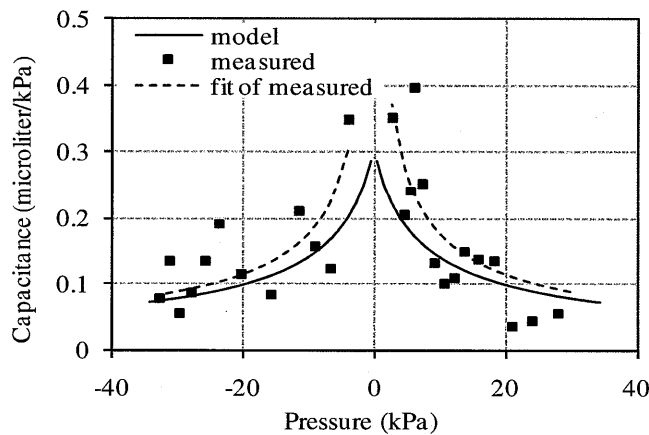


Figure 5.8: Polyimide membrane capacitance as a function of applied fluid pressure. The membrane had thickness of 1 mil and diameter of 8 mm. Buckle displacement amplitude was 0.17 mm.

As described above, the fabrication procedure provided a straightforward method for incorporating different membrane materials into the laminate device structure. Figure 5.9 illustrates the significant difference in volume displacement behavior versus pressure between the thin, high-modulus membrane (polyimide) and the thicker, lower-modulus material (silicone). As reference, for the

silicone membrane, a volume displacement of 0.63 μL occurred when the axial displacement equaled the diaphragm thickness of 4 mil. This is approximately where the membrane transitioned from bending mode to tensile mode expansion (the linear and cubic terms in the displacement versus pressure equation were equal when $z/t = 1.35$ for $\nu=0.3$). Approximately linear behavior was observed up to this displacement volume, which occurred at 3.5 kPa. This, not incidentally, was a reasonable upper bound of operating pressure range for some of the membrane capacitors in the system. The polyimide membrane, on the other hand, did not have a roughly linear displacement volume in this pressure range.

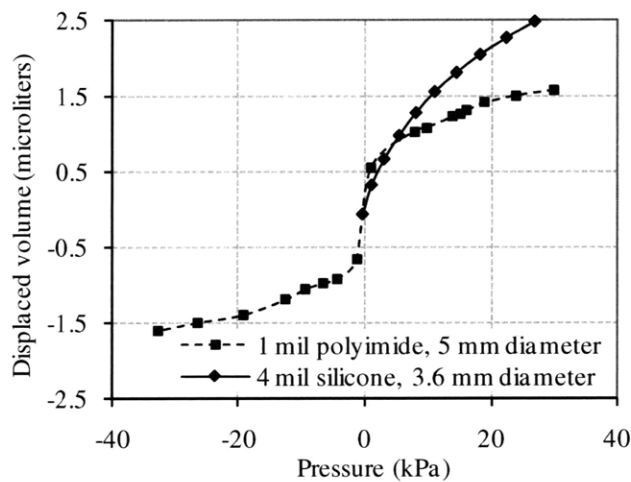


Figure 5.9: Comparison between 1 mil thick, 5 mm diameter polyimide and 4 mil thick, 3.6 mm diameter silicone membrane displacement volumes as a function of applied fluid pressure.

The above discussion illustrated the dependence of fluid capacitance on membrane material and thickness. Capacitance also showed predictable dependence on membrane diameter. Figure 5.10 shows measured small capacitance values (nominal pressure is 6.9 kPa) as a function of membrane diameter using the silicone membrane. The theoretical plot was generated by taking the pressure derivative of displacement as described by Equation 5.2 and then applying Equation 5.3 to obtain differential volume change as a function of pressure with membrane radius as a parameter. Relatively good agreement between measured values and the design model was demonstrated.

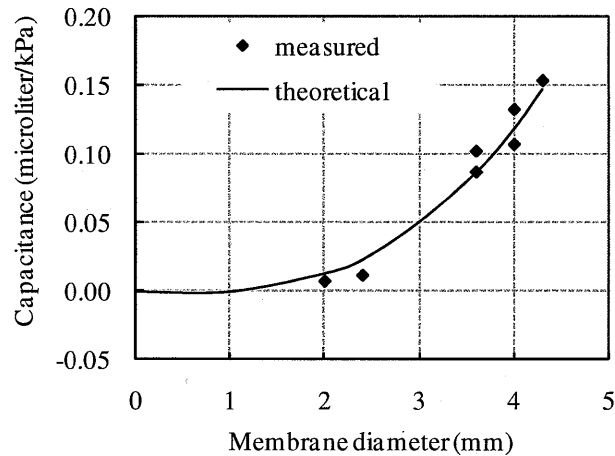


Figure 5.10: Measured versus theoretical capacitance as a function of membrane diameter. Membrane material was 4 mil-thick silicone.

5.4 MANUAL SCREW VALVE

In addition to fluid capacitors, manually-actuated screw valves were designed, built, and tested. Manual microfluidic screw valves were demonstrated by the Whitesides group [19], but the screw acted by direct compression on a silicone channel. Contrarily, this design used a laminate structure with a ring-shaped valve seat and a membrane, as shown in Figure 5.11. Axial displacement of the screw forced the membrane into contact with the valve seat and restricted flow between the inlet channel and the outlet channel. The inlet channel terminated at the inner diameter of the valve seat, and the outlet channel was in the form of a torus surrounding the valve seat. During fabrication, there were two valve seat cuts which defined the valve seat perimeter and the torus portion of the outlet channel. The first valve seat cut defined approximately 330 degrees of the seat perimeter. After lamination to the channel spacer layer, the second valve seat cut defined the remaining 30 degrees of the seat perimeter.

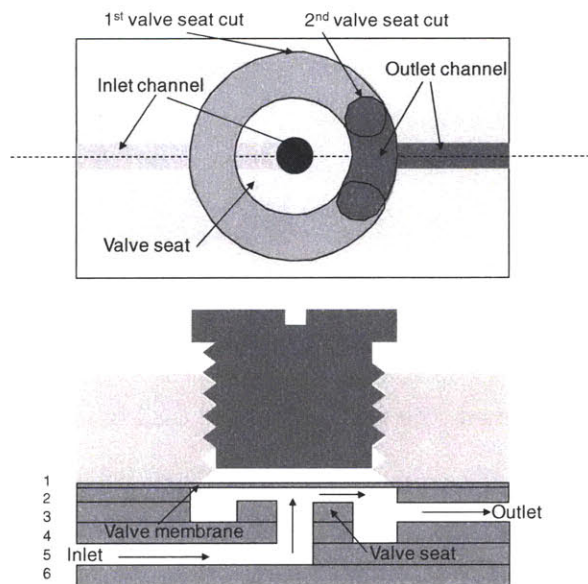


Figure 5.11: Depiction of normally-open screw valve. Top view (upper) and cross-section (lower). Layers 3 and 4 were laminated together between the 1st and 2nd valve seat cuts.

As with the microfluidic capacitors, these valves were built with different membrane materials and in configurations within a larger manifold of components. A 5-valve manifold was designed for functionality similar to that of a high performance liquid chromatography (HPLC) injection valve as shown in Figure 5.12 and was manufactured in a 1.5 cm x 1.5 cm die format with top and bottom aluminum plates as shown in Figure 5.13. Holes in the top plate aligned with valve seats. The holes were tapped to provide placement for the actuation screws. The bottom plate was used in high-pressure applications where large axial screw forces were applied, and coupling the plates with clamping bolts prevented delamination of the top plate from the laminate stack.



Figure 5.12: 5-valve manifold shown in size comparison to the HPLC valve it replaced.

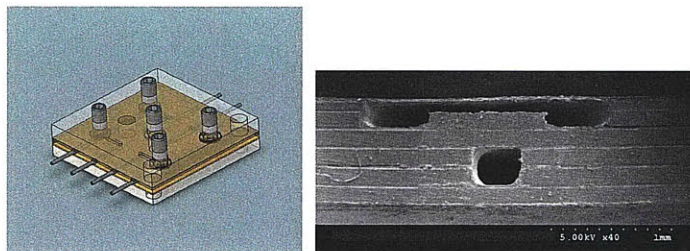


Figure 5.13: (left) Drawing of 5-valve manifold showing aluminum plates and screw actuators. (right) SEM cross-section of valve structure.

Two screw types were examined. The first was a steel 0-80 hex socket set screw with a cup point. The diameter of the cup point was matched to the nominal diameter of the valve seat. While this provided a very high effective pressure on the membrane during valve closure, it provided a relatively small contact area requiring precise alignment of the aluminum top plate to the polyimide stack. In addition, it generated wear on the outer surface of the membrane, severely limiting the cycle count of the valve. The second screw type was a nylon 0-80 slotted head screw with a flat tip. This generated approximately uniform pressure over the valve seat and significantly less wear on the membrane.

The manifold was useful for loading drugs into the fluidic network for animal testing and for filling and purging of the system, as shown in Figure 5.14. Without change to the wetted parts, the actuation mechanism could be altered for electronic control [10]. Given that the drug delivery system internal fluid volume was approximately 100 μL , and experiment duration could approach several months, low leak rates were required. Open-state resistance and closed-state leak rates for multiple polyimide-diaphragm valves using nylon screws to control water flow were measured and listed in Table 5.2. Open-state resistances were calculated from the slope of a linear fit of measured flow rate versus pressure set-point, with at least five different set-points ranging from 0 to 50 kPa. Closed-state leak rates were measured at a pressure set-point of 100 kPa. Flow rates in both cases were determined by measurement of linear displacement over time of a water segment traveling through fine-bore tubing attached to the output port of the valve under test.

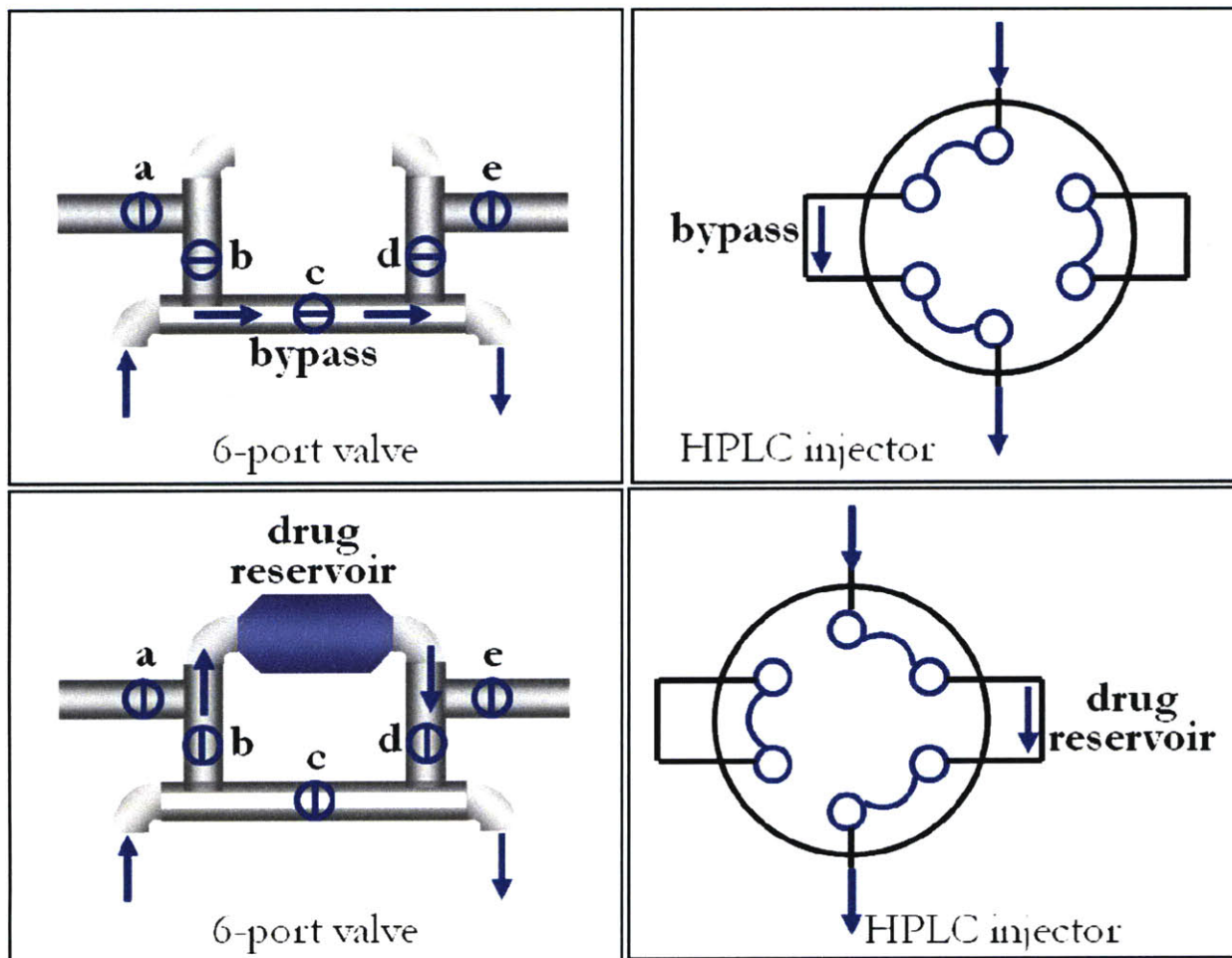


Figure 5.14: A functional comparison of the 5-valve manifold and a standard HPLC sample injector. The valve was manipulated in various configurations to allow for drug infusion, reservoir filling, or bypass. It also functioned as purge and refill ports.

Table 5.2: Measured valve characteristics using nylon screws

Leak rate at 100 kPa (1 in·ounce applied torque) ($\mu\text{L}/\text{min}$) [*]	0.015 – 0.040
Resistance in open position ($\text{kPa}\cdot\text{min}/\mu\text{L}$) [†]	0.028 - 0.065
Minimum resistance ratio, Closed:Open	> 38 000

^{*} - 3 valves tested, [†] - 5 valves tested

5.5 CONCLUSION

Diaphragm-based components were developed for a microfluidic drug delivery system using a set of versatile fabrication techniques suitable for rapid prototyping of laminate-based polymer microfluidic systems. The microfluidic components discussed were seamlessly incorporated into the fluidic network used in animal studies to deliver active compounds directly into the inner ear for up to a month. Both components significantly contributed to a reduction in size of the system and provided greater control over critical system variables. The valve and capacitor may be integrated into a versatile laminated polyimide fabrication platform along with other microfluidic and electronic components including flow sensing and control elements and should prove useful for a broad range of microfluidic applications.

Rights were reserved to reprint portions of this chapter from: Mescher, M., et al., *Fabrication methods and performance of low-permeability microfluidic components for a miniaturized wearable drug delivery system*. Journal of Microelectromechanical Systems, 2009. **18**(3): p. 501-510.

5.6 REFERENCES

1. Becker, H. and C. Gartner, *Polymer microfabrication methods for microfluidic analytical applications*. Electrophoresis, 2000. **21**(1): p. 12-26.
2. Jo, B.-H., et al., *Three-Dimensional Micro-Channel Fabrication in Polydimethylsiloxane (PDMS) Elastomer*. Journal of Microelectromechanical Systems, 2000. **9**(1): p. 76-81.
3. Martynova, L., et al., *Fabrication of plastic microfluidic channels by imprinting methods*. Analytical Chemistry, 1997. **69**(23): p. 4783-4789.
4. Becker, H. and U. Heim, *Hot embossing as a method for the fabrication of polymer high aspect ratio structures*. Sensors and Actuators A, 2000. **83**: p. 130-135.
5. Xia, Y. and G.M. Whitesides, *Soft Lithography*. Annual Review of Materials Science, 1998. **28**: p. 153-184.
6. Metz, S., R. Holzer, and P. Renaud, *Polyimide-based microfluidic devices*. Lab on a Chip, 2001. **1**: p. 29-34.
7. Metz, S., et al., *Polyimide microfluidic devices with integrated nanoporous filtration areas manufactured by micromachining and ion track technology*. Journal of Micromechanics and Microengineering, 2004. **14**(3): p. 324-331.

8. Zhang, G., V. Chu, and J. Conde, *Electrostatically actuated bilayer polyimide-based microresonators*. Journal of Micromechanics and Microengineering, 2007. **17**(4): p. 797-803.
9. Lindner, E., et al., *Flexible (Kapton-based) microsensors arrays of high stability for cardiovascular applications*. Journal of the Chemical Society, Faraday Transactions, 1993. **89**: p. 361-367.
10. Mescher, M.J., et al. *Surface mount microfluidic flow regulator on a polymer substrate*. in *Micro Total Analysis Systems (MicroTAS)*. 2003. Squaw Valley CA.
11. Dubé, C.E., J.O. Fiering, and M.J. Mescher. *A Si-based FPW sensor array system with polymer microfluidics integrated on a PCB*. in *Sensors, Proceedings of IEEE*. 2002. Orlando.
12. Chen, Z., et al., *Inner Ear drug delivery via a reciprocating perfusion system in the guinea pig*. J. Controlled Release, 2005. **110**(1): p. 1-19.
13. Fiering, J., et al., *Local drug delivery with a self-contained, programmable, microfluidic system*, Biomedical Microdevices, 2009. **11**(3): p. 571-578.
14. Kobayashi, A., *Machining of Plastics*. Reprinted from 1967 edition. ed. 1981, Huntington, NY: Robert E. Krieger Publishing Co., Inc. 287.
15. van Mullem, C.J., K.J. Gabriel, and H. Fujita. *Large deflection performance of surface micromachined corrugated diaphragms*. in *TRANSDUCERS*. 1991. San Francisco, CA.
16. Miles, R. and D.L. Schumann. *Thin-walled compliant plastic structures for meso-scale fluidic systems*. in *SPIE Conference Proceedings: Micro- and nanofabricated structures and devices for biomedical environmental applications II*. 1999. San Jose.
17. Yang, B., J. Metter, and Q. Lin. *Using compliant membranes for dynamic flow stabilization in microfluidic systems*. in *18th IEEE Int. Conf. on Micro Electro Mechanical Systems*. 2005.
18. Giovanni, M.D., *Flat and corrugated diaphragm design handbook*. 1982, New York: Marcel Dekker Inc.
19. Welbel, D.B., et al., *Torque-Actuated Valves for Microfluidics*. Analytical Chemistry, 2005. **77**(15): p. 4726-4733.

6.0 CONCLUSION

6.1 CONCLUDING REMARKS

Various biological aspects associated with long term drug delivery to the inner ear were investigated in this thesis. The concentration profile resulting from delivery within the cochlea was modeled using a lumped-parameter approach and implemented with electrical circuit simulator software. The model was validated by comparison to the analytical solution of the diffusion-only case. Additionally, a bench-top experiment using the device to deliver fluorescein into a glass tube was undertaken. The delivery profile showed agreement with the modeled results. Many weaknesses in modeling biological aspects such as protein binding and drug clearance limited the model's usefulness in predicting the drug concentration distribution in the cochlea. Future refinement of the model is needed to improve its capabilities. The effects of protein and tissue build-up on the flow parameters of the device were studied through bench-top flow testing and histology preparations after in vivo implantation. Characterization of the protein content of perilymph elucidated many individual proteins that likely will impact delivery of drugs into the cochlea. Device design and drug choices must be based on this knowledge. Finally, new microfluidic components were added to the delivery system to enhance performance and advance miniaturization methods. Through this research, both the impact of this device on the animal and the result of implantation on the device were more fully characterized.

6.2 FUTURE DIRECTIONS

6.2.1 Modeling

A number of improvements could be made in the model as it is further refined, but a better understanding of biological phenomena in the cochlea is needed. A dose-response curve for DNQX should be created with a broader range of concentrations measured. Also, a concentration that does not cause the hearing level to rise above measurable limits must be used. Together, this data will lead to a more accurate dose-response relationship from which to compare modeled and experimental results. In addition, studies of protein binding rates and clearance rates for the cochlea are needed. These values are drug-specific so numerous compounds will need to be studied. The measurements of aqueduct resistance and round window compliance were only reported for a small pressure range. Additional studies should be undertaken to expand this range to better understand the nonlinearity of

the anatomical structures. The nonlinearity can be incorporated into the circuit simulation using available elements in the software package.

6.2.2 Protein interactions

The protein flow study, though preliminary, showed the need to follow-up with more long-term studies of biofouling in vivo. This will be a major design consideration for future iterations of the device. After implantation for various lengths of time, the devices components should be inspected and tested for the degree of biofouling and resulting flow restrictions. Flow sensors will be incorporated into the system to allow for continuous monitoring of delivery profiles while the device is operating in animals. At the end of these experiments, additional histological examination of the cochlea is needed.

6.2.3 Microfluidic device components

As the device evolves, the components will be integrated into a full microscale delivery system on a single polyimide platform. The valves can be combined with an electrically-controlled actuator for automated control, and electrical circuitry can be integrated with the entire microfluidic device using similar microfabrication techniques.

While much progress was made on the specific aims, a great deal of work remains. Continued efforts on this delivery system will lead to a better understanding of device and biological interactions. More importantly, the inner ear delivery device may one day impact patient care if not in a form similar to the way it has been envisioned, at least by the insight that has been gained throughout its development.